NET SLIP AND LINKAGE PATTERNS OF THE SEVIER-TOROWEAP FAULT SYSTEM

by

Terrance A. Delisser

A Thesis Submitted to the Faculty of the

DEPARTMENT OF GEOSCIENCES

In Partial Fulfillment of the Requirements

For the Degree of

MASTER OF SCIENCE

In the Graduate College

THE UNIVERSITY OF ARIZONA

2021

THE UNIVERSITY OF ARIZONA
GRADUATE COLLEGE

As members of the Master's Committee, we certify that we have read the thesis prepared by: Terrance Delisser
titled: Net Slip and Linkage Patterns of the Sevier-Toroweap Fault System

and recommend that it be accepted as fulfilling the thesis requirement for the Master's Degree.

Amanda Hughes — Date: Aug 19, 2021

Roy Johnson — Date: Aug 19, 2021

Marc Sbar — Date: Aug 20, 2021

Final approval and acceptance of this thesis is contingent upon the candidate's submission of the final copies of the thesis to the Graduate College.

I hereby certify that I have read this thesis prepared under my direction and recommend that it be accepted as fulfilling the Master's requirement.

Amanda Hughes — Date: Aug 19, 2021
Thesis Committee Chair
Department of Geosciences

TABLE OF CONTENTS

ABSTRACT

The Sevier-Toroweap fault system is a 250+ km high-angle normal fault located in southern Utah and northern Airzona in the High Plateaus subprovince. It is one of three main normal faults that accommodate the strain concentrated on the boundary between the Basin and Range and Colorado Plateau in the Utah Transition Zone. As with all faults in the Transition Zone, the Sevier-Toroweap fault system trends N-S but has distinct bends in the fault trace that trend northwest or northeast. These characteristic changes in strike reflect the segmentation and growth history of the fault. Since fault linkage is reflected in a fault system's net slip distribution, this study characterizes the net slip distribution along the Sevier-Toroweap fault system reveals fault linkage patterns which can improve our understanding of how this fault formed, its extent, and geometric segmentation that could impact the potential seismic hazards associated with it.

Compiled surface geology and subsurface constraints were used to construct cross-sections using kinematic forward modeling techniques in order to evaluate the subsurface geometry of the fault and calculate displacement along the main trace of the fault system. Displacement constraints collected from these cross section, published USGS cross sections and maps, and other literature were compiled to produce distance vs. displacement plots. These plots demonstrate the segmentation of the Sevier-Toroweap fault system and help reduce uncertainty as to where the northern terminus of the fault system lies. The linkage history implied by variations in fault strike, locations of fault splays, and displacement gradients along strike suggest that there are three main segments of the fault, which are different than the fault sections commonly used to describe the fault in the existing literature. Additionally, the high displacements and lack of observed decrease in displacement at the northern extent of the mapped fault suggests that the northern terminus may extend over 100 km north of the

northernmost continuously mapped trace of the fault system and into the Marysvale volcanic field where it is thought to continue but be obscured due to outcrop conditions and geologic complexity within the volcanic system. In light of these new observations and constraints on displacement, fault linkage, and subsurface geometry, potential earthquake hazards associated with this fault are then evaluated.

INTRODUCTION

Many aspects of the geometry of fault systems provide insight into their role in accommodating strain in the crust; along-strike geometry and displacement variations reflect the growth and linkage history of faults, while their subsurface geometries demonstrate their trajectory through the brittle portion of the crust, both with implications for the size of earthquakes likely hosted on these faults. In this study, the net slip distribution and surface trace variability of the Sevier-Toroweap fault system is investigated to reveal fault linkage zones and patterns. The Sevier-Toroweap fault is an ideal case study as it displaces gently-dipping stratigraphy across the Colorado Plateau-Basin and Range Transition Zone, and it has several easily distinguishable broader segment boundaries.

Cross sections were also constructed at key locations within the fault segments to help to better constrain the geometry of the fault system at depth across its entire extent, which helps further evaluate and improve upon the existing estimates of slip on the fault. The determined overall net slip distribution and fault linkage patterns help build an understanding of the growth history and structural development of this long, geometrically segmented fault. Studying the net slip distribution of the Sevier-Toroweap fault system helps better constrain the nature of the fault at the northern extent of the fault system as it interacts with the Marysvale volcanic field (**Figure 1**). As discussed later in the geologic history section, the subsurface geometry of basin-and-range normal faults is widely contested; some studies prefer planar interpretations, while others prefer a listric fault interpretation at depth, and evidence for and against involvement of pre-existing detachments and reactivation is contested in some cases (West, 1992, Christie-Blickand others., 2007, Velasco and others, 2010, and references therein). In fault systems such as this, where subsurface constraints on the geometry are sparce, detailed compilation of geologic

constraints and kinematic model construction in this study are the only means by which the fault can be accurately characterized and some of these concepts can be evaluated. In the case of the Sevier-Toroweap fault system, characterized by relatively modest fault offset and well-constrained regional stratigraphic section, such an analysis allows concepts such as depth to detachment and variations in fault geometry evidenced by fault-related folding to be evaluated.

BACKGROUND

FAULT SYSTEM DESCRIPTION

The Sevier-Toroweap fault system is a long 250+ km N-NE trending high-angle normal fault with a hanging wall down to the west on the main strand and most splays. The fault system extends from the southern Grand Canyon region in Arizona northward into the Utah High Plateaus subprovince on the SW margin of the Colorado Plateau physiogeographic province (Hamblin, 1984). Within Arizona, the fault is referred to as the Toroweap fault and in Utah, the Sevier fault (Lund and others, 2008). The Sevier-Toroweap fault along with other faults such as the Hurricane and Paunsaugunt faults form the Transition Zone between the Colorado Plateau and Basin and Range, which is also referred to in many active tectonics contexts as the Intermountain Seismic Belt (ISB), as it hosts a significant concentration of the regional strain rates (Kreemer and others, 2012), seismicity (Smith and Sbar, 1974 and others) and seismic hazard (Haller and others, 2015) in the intermountain west. Although these faults are within the Transition Zone, they likely are geometrically similar to extensional faults in the Basin and Range further west, though they are less mature as they have accrued a lower magnitude of total displacement. Past studies have characterized four main sections of the fault: the Southern and Central Toroweap sections in Arizona, the Northern Toroweap section which crosses over the

Arizona/Utah border, and the Sevier section in Utah (**Figure 1**) (Pearthree, 1998; Black and others, 2003). These section boundaries serve as inferred seismogenic segment boundaries with individual rupture histories (Lund and others, 2008). The Sevier-Toroweap fault formed in Miocene time 12 to 15 million years ago as estimated by Davis (1999), and the growth and development of this fault over time involved the linkage of individual short normal faults to form longer composite faults. As with other faults in the Transition Zone, the Sevier-Toroweap fault generally strikes N-S but has distinct portions that strike either northwest or northeast. These changes in strike or bends along the fault trace in map view reveal potential linkage zones to be investigated.

FAULT LINKAGE REVIEW

As faults grow with progressive strain accumulation, they will often interfere with neighboring faults and eventually link up with them in a process known as fault linkage. Fault linkage describes the formation of longer continuous faults from the connection of smaller individual fault segments. These fault segments, almost parallel in strike, interact with each other through their stress and strain fields until they eventually link over time (Ferrill and Morris, 2001). Throughout the linkage process, the overall net slip distribution will change accordingly. Fault linkage has two main mechanical types: soft and hard linkage. Soft linkage describes two adjacent faults that have not physically linked but are displacing the same set of rock units in their vicinity as their stress fields interact with each other. In this type of linkage, a strain transfer zone, or relay ramp, develops between the fault segments. Hard linkage, on the other hand, describes the stage where faults have physically connected (Taylor and others, 2001; Schiefelbein, 2002).

There are four basic stages of fault linkage (t1 – t4 in **Figure 2**) described by many authors, including Peacock and Sanderson (1991,1994), Ferrill and Morris (2001), Fossen (2016) and others. The first two stages describe soft linkage. At t1, as two isolated underlapping faults grow toward each other, stress fields at their laterally-propagating tips begin to interact. During this stage, the propagation of fault tips slows down due to this interference. As a result, the displacement in the emerging linkage zone is increased. The faults at this stage are characterized as underlapping due to their fault tips extending past each other in the displacement direction. At t2, the faults tips have passed each other, and the faults are now overlapping. The overlapping of fault segments leads to the development of a strain transfer zone. A common result is a relay ramp fold structure that forms as the displacement on one fault tapers off as you move towards its terminus but transfers over to the adjacent fault. As deformation continues and the net slip distribution on each fault segment gradually merges, a cross fault will form (t3) to accommodate the stress change and increased strain within the transfer zone. At this stage of the linkage process, the fault segments are hard linked, and the relay ramp structure is breached. With increased displacement, the net slip distribution will gradually adjust to reflect the trend of a single fault (t4). What remains at the linkage zone is a is a geometric bend in the fault and a wide damage zone dependent on the mechanical properties of the rock medium. Therefore, as aforementioned, distinct geometric bends in the Sevier-Toroweap fault system will denote where linkage zones are and measuring the displacement distribution across these linkage zones can reveal the stage of linkage they are at and the relative linkage history.

DISPLACEMENT DISTRIBUTION

Fault linkage affects the overall displacement distribution in large faults (**Figure 2**). For a single fault segment, the displacement distribution along the strike of a fault has a characteristic

trend: maximum displacement in the center that tapers off towards the fault's tips (Barnett and others, 1987, Walsh and Watterson, 1987). This maximum can appear as a peak in the displacement trend or as a broader plateau which indicates displacement is more constant throughout the center (Fossen, 2016). On the other hand, for larger faults that have formed from the linkage of smaller segments, the overall displacement distribution will exhibit a combined trend influenced by each of the individual segments. What is commonly observed in the displacement distribution around linkage zones is two maxima, one for each segment, that may or may not be merged depending on the stage of linkage. Due to an increased displacement gradient at the linkage zone, each maximum is commonly shifted away from the center and more towards the adjacent fault tips.

FAULT ACTIVITY

INTRODUCTION

Fault activity along the Sevier-Toroweap fault system varies by fault section. The following sections review observations from previous studies that provide age constraints, timing of most recent surface displacements, and slip rates at specific locations along the fault system, which are useful in determining how slip varies throughout time, when different sections of the fault initiated, and the degree of seismic risk.

Southern Toroweap

There is a lack of detailed analyses in this section compared to the number of studies done in the Central Toroweap Section. In the Central Toroweap section, around the Colorado River, there is a 50 km Holocene rupture that occurred within alluvial fan deposits. The scarp from this rupture continues 10 km south which may allude to similar Quaternary activity in the

Southern Toroweap section despite there being no evidence of Holocene rupture in the section (Pearthree, 1998). Displacement of Quaternary deposits has not been documented and recent slip rates of the Toroweap fault in this section are unknown. However, Pearthree (1998) reported that the strong geomorphic expression of the fault in this section suggests that the most recent fault activity occurred in the late Quaternary.

Central Toroweap

Late Quaternary activity is recurrent in the Central Toroweap section and, notably, this section ruptured during the Holocene (Jackson, 1990; Pearthree, 1998). Karlstrom and others (2007) calculated late Quaternary fault displacement rates of the Sevier-Toroweap fault system by using $^{40}Ar/^{39}Ar$ dating of three offset basalt flows apart of the Uinkaret volcanic field. Measurements were made at Prospect Canyon and near Lava Falls, where the fault system intersects the Colorado River in Arizona. At Prospect Canyon, a net slip value of 52 m was calculated for a higher basalt flow across three associated fault strands. Using the mean Ar-Ar age of 518 ± 22 ka for this basalt, they calculated a displacement rate of 0.1 mm/yr. A lower basalt flow at Prospect Canyon was offset 60 m with a mean age of 568 ± 52 ka yielding a similar displacement rate of 0.106 mm/yr. A third basalt flow near Lava Falls was offset by 47 m, and had a mean Ar-Ar age of 487 ± 48 ka, yielding a displacement rate of 0.097 mm/yr. They thus interpreted that the average displacement rate of ~0.1 mm/yr in the past 600 ka was uniform throughout this time interval. They also noted that late Quaternary separation (e.g., 47 – 60 m from Karlstrom and others, 2007) makes up a significant portion of the total stratigraphic separation (e.g., 193 m from McKee and Schenk, 1942) measured in this area, suggesting that the Toroweap fault is one of the youngest and most active faults in the western Grand Canyon as

stated by Jackson (1990), and that these fault segments likely initiated far later than segments further to the north.

Northern Toroweap

Within the Northern Toroweap Section, Brumbaugh (2008) assessed the historical seismicity associated with movement along the Sevier-Toroweap fault system. From a dataset spanning 45 years (1959 – 2004), they identified three main cluster sets of epicenters within the vicinity of the fault zone. Within these sets, only one event greater than M_L 4.0 was identified, a M_L 4.40 earthquake in 1962. The P wave first motion-based fault plane solution calculated for this event indicated normal faulting on a fault plane sub parallel to the fault zone's trend. The dip of the fault plane solution (62˚ NE), however, appears to be antithetic to the main fault trace. In their concluding remarks, they noted that the spatial distribution of these cluster sets around the fault zone suggests that it is active.

Pearthree (1998) reported a single location along this fault segment where a fault scarp offsets alluvium near the Pipe Springs National Monument in Arizona, and, from this, calculated a vertical slip rate. This fault scarp is 3.5 m high and has a slope angle of 7.5˚ which Pearthree interpreted as recent fault activity dating back to the late Pleistocene (~50-150 ka). Displacement along this area of the fault yielded a 0.01 – 0.04 mm/yr slip rate.

Sevier

Within the Sevier section, historical earthquake activity has been recorded. From 1924 to 1927, a series of earthquakes with a Mercalli Intensity range of II to III were recorded around Long Valley at Orderville, Utah (Doelling and others, 1989). Magnitudes for these earthquakes

were not instrumentally derived. The 15 earthquakes that occurred in this locality during this time are all attributed to movement along a fault strand in the Sevier-Toroweap fault zone.

Paleoseismic activity of the Sevier-Toroweap fault zone has been evaluated through the dating of displaced Quarternary basalts in several locations. Quaternary basalt flows, 0.5 Ma in age, are displaced near Red Canyon in Garfield County, Utah (Lund and others, 2008). These lava flows erupted from vents and flowed eastward, depositing on the hanging wall and footwall side of the fault zone. Roughly 200 m of displacement in these dated basalts have been observed, from which Lund and others (2008) calculated a vertical slip rate of 0.4 mm/yr and recurrence interval of 5000 yrs for the late Pleistocene. At Rock Canyon, Biek and others (2015) used a displacement estimate of 237 – 344 m from Lund and others (2008) to calculate a vertical slip rate of 0.05 mm/yr for a 5 Ma Rock Canyon lava flow further south along the fault trace. They reported that this is a minimum rate and when considering the total displacement at this location, the slip rate cannot exceed 0.18 mm/yr. Near Black Mountain and the upper Long Valley area in Utah, the Sevier fault zone displaces Quaternary basalt lava flows (Doelling and others, 1989). The age of the basalts in this area, based on K-Ar radiometric dating, is 560,000 ± 60,000 years old (Best and others, 1980). Biek and others (2015) suggest that if the elevation difference between basalt flows at the top and base of Black Mountain solely represents displacement on the fault, then the vertical slip rate at this location is 0.4 mm/yr, which is similar to the slip rate calculated at Red Canyon.

Lund and others (2008) made note of the lack historical surface-rupturing earthquakes and scarps in unconsolidated sediments along the main trace of the Sevier fault, which has prevented any efforts to evaluate the paleoseismic history of this section through trenching efforts. The only scarps that have been identified were mapped in detail by Biek and others

(2015) in the hanging wall near a complexly faulted area of the fault zone east of Panguitch, Utah. Scarps in this area have formed in late Pleistocene fan alluvium. Given that this is the only known set of scarps in unconsolidated sediments within the Sevier section, the relative absence of scarps throughout the fault section is inconsistent with the previously mentioned slip rates, which suggests that late Quaternary activity decreased within this section of the fault (Biek and others, 2015), the slip rates are lower or equal to rates of erosion and burial of scarps (Lund and others, 2008), or that the fault is characterized by seismic events too small to create recognizable surface ruptures (~Mw 5-6, Bonilla, 1988, Wells and Coppersmith, 1994).

Summary

aleoseismic indicators and local seismicity suggest that fault slip rate, timing of initiation of slip, and timing of most recent slip varies throughout the fault system. **Table 1** provides a summary of the slip rates of the previously discussed paleoseismic indicators. Evidence of recent activity is apparent in all sections except the Southern Toroweap. In the Central Toroweap, Northern Toroweap and Sevier sections, evidence for Pleistocene activity comes in the form of alluvial scarps and offset basalt flows. Evidence of Holocene activity is found in the Central Toroweap, where Jackson, (1990) reported a 50 km-long Holocene rupture centered on the Colorado River. Additional evidence to be considered is seismicity clustering in the Northern Toroweap and Sevier sections (**Figure 3**). This striking pattern of seismicity along the Sevier-Toroweap fault as well as other major Transition Zone faults (primarily the Hurricane fault to the west and Paunsaugunt Fault to the east) defines the southern part of the Intermountain Seismic Belt that extends across the western United States (Smith and Arabasz, 1991 and others). In general, the evidence indicates that fault activity varies spatially and temporally but ultimately demonstrates that this is an active fault system.

GEOLOGIC HISTORY

Because primary constraints on the geometry and displacement on the Sevier-Toroweap fault derive from observed offsets of stratigraphic layers, a detailed understanding of the geologic history and controls on stratigraphic thickness are a necessary part of this study. The geologic history for the region the Sevier Toroweap fault passes through, encompassing an area of the Transition Zone spanning southwestern Utah and northwestern Arizona, can be traced backed to the early Proterozoic. It may be beneficial to begin the geologic history at this time as it marks the early beginnings of the Colorado Plateau, the geologic province which is flanked by the Sevier-Toroweap fault system along its southwestern margin. Near the end of the Paleoproterozoic, volcanic island arcs began migrating towards Northern America forming an intervening ocean basin where volcanics and sediments could be deposited. As the gap between the island arcs and North America closed, these basin deposits were compressed, deformed, and metamorphosed at depth. These rocks attached to the continent and formed the basement of the modern-day Colorado Plateau and nearby regions. These igneous and metamorphic basement rocks are commonly grouped together as Precambrian crystalline rocks (Blakey and Ranney, 2008). Subsequent erosion of Proterozoic highlands created a flat region for the alternating deposition and erosion of sedimentary units throughout the Mesoproterozoic to Neoproterozoic. The resulting thick assemblage of strata known as the Grand Canyon Supergroup represents the oldest sedimentary units of the Colorado Plateau. These strata lie outside the scope of this report and will not be discussed in detail within the stratigraphy section.

During the late Neoproterozoic, there was a rifting of the supercontinent Rodinia. In this event, Laurentia, the continental core making up North America, separated from a landmass consisting of Australia, Antarctica, and China to create a proto-Pacific Ocean and a passive

margin along the western edge of North America. The rifting event is responsible for the significant tilting of earlier Proterozoic sedimentary units, a characteristic that is not present in the mostly flat younger sedimentary units to be deposited later (Blakey and Ranney, 2008). The boundary that this event formed is known today as the Utah hingeline or Wasatch line. The hingeline serves as a major regional scale feature that separates thinner crust to the west, which was seaward at the time, from thicker crust to east. The hingeline plays an important role in controlling the distribution of strata throughout the region (Biek and others, 2015) as it delineates the margin of rapid Paleozoic subsidence to the west as well as a significant portion of the western margin of the Colorado Plateau.

During the early and middle Paleozoic, passive margin conditions along the western margin of the continent allowed for extensive deposition of marine sediments. Following the breakup of the supercontinent Rodinia, there was erosion and subsequent deposition along the western margin of Northern America. Rapid subsidence, flooding of the continent through marine transgression, and incremental growth of the proto-Pacific Ocean through sea-floor spreading created shallow to deep marine environments for these sediments to accumulate (Blakey and Ranney, 2008). Paleozoic strata in the region tend to thicken and have more deep-water facies to the west due to the accommodation space created by the subsiding marine basin as opposed to the shallower stable continental shelf that was located to the east (Biek and others, 2015).

Two orogenic events affected the deposition of Paleozoic and Early Mesozoic strata. During the late Devonian and Early Mississippian, the Antler Orogeny caused the accretion of intraoceanic volcanic arcs to the southwestern margin of North America (DeCelles, 2004). The erosion triggered from this orogenic event is a probable cause of the absence of Ordovician and

Silurian strata in the region. After this orogenic event, marine deposition resumed throughout Mississippian, Pennsylvanian and most of Permian time. In the late Permian, however, there was erosion and a halt in deposition associated with the Sonoma Orogeny which prevented late Permian and early Triassic rocks from entering the record. Both orogenic events brought the accretion of oceanic arcs to the western margin of North America which altered the landscape from a passive margin to a continental volcanic arc interior with mountain chains and volcanoes. The stratigraphic differences between the lower Triassic Moenkopi Formation and upper Triassic Chinle Formation (discussed further in later sections) highlights the end of shallow marine sedimentation and the beginning of deposition in an inland basin. Deposition within this inland basin region continued for the remainder of the Triassic and Early Jurassic (Biek and others, 2015).

In the Early Jurassic, a large portion of the western interior of North America entered the arid trade-winds latitudes as tectonic plates shifted (Biek and others, 2015). Simultaneously, mountains that were forming in present day California and Nevada created a rain shadow. The effect of these events was aeolian deposition to form a massive palaeodune field in the region (Milligan, 2012). This immense accumulation of wind-blown sand is recorded in the thick Navajo Sandstone unit that can be upwards of 600 m (Biek and others, 2015). The thickness achieved for this formation was possible due to basin subsidence caused by compressional deformation along the western edge of North America at the time.

The remainder of the Jurassic brought a variety of different depositional environments. During the middle Jurassic, deformation associated with the subduction of the Farallon plate underneath North America created the earliest shortening in what is now called the Sevier orogenic belt. Crustal flexure from the thrust wedge created a foredeep basin, fore-bulge high,

and a back-bulge basin to the east (DeCelles, 2004; Biek and others, 2015). The Elko Orogeny, centered to the NW of the area of interest produced this characteristic depositional pattern in the mid to late Jurassic throughout western Nevada and central Utah (Thorman and Peterson, 2003). Sea levels rise at the time allowed for the development of an inland sea within a foredeep basin associated with the Elko Orogeny. Shallow marine deposition in the inland sea occurred as the sea migrated southward along the western margin of North America. The middle Jurassic Carmel formation records the behavior of the seaway and the state of the foredeep basin. In general, the formation records a maximum incursion of the seaway as well as its alternating incursion and retreating periods. With these movements came a variety of environments for the region including sabkha, tidal flat, and sandy mud flat environments (Biek and others, 2015). Some of these environment types are recorded in the overlying Middle Jurassic Entrada Sandstone which ends the Jurassic period. Due to the migration of the forebulge high into southwest Utah, most of Utah was broadly uplifted which initiated a period of erosion and non-deposition that lasted from the end of the middle Jurassic to the middle of the Early Cretaceous. Since the Entrada Sandstone was removed west of the Paunsaugunt fault (Doelling, 2008), it is not discussed in the stratigraphy section.

The Cretaceous brought the deposition of several formations along the western margin of an epicontinental seaway. By the end of the Early Cretaceous, the landscape had become a broad alluvial plain. By the Late Cretaceous, however, migration of the Sevier orogenic belt associated with the Sevier Orogeny created a foredeep basin which collected sediment for several formations including the Dakota Formation, Tropic Shale, and Straight Cliffs Formation. Strata throughout this time record a variety of environments including an alluvial, brackish estuarine, lagoonal, open-marine, near shore, and coastal plain (Biek and others, 2015). Deposition of these

strata simultaneously took place during a global sea level rise and the maximum transgression and retreat of the Western Interior Seaway. This seaway formed as a result of crustal downwarping from the subduction taking place along the western edge of North America (Decelles, 2004). The Dakota Formation records the migration of the Western Interior Seaway while the Tropic shale records the maximum incursion. The Straight Cliffs formation, however, records a regressive sequence of marginal marine and shoreline beach sediments deposited after the seaway retreated (Biek and others, 2015). Above these formations lies the two final formations of the Cretaceous consisting of floodplain sediments of the Wahweap Formation and the prograding wedge of alluvial plain sediments that make up the Kaiparowits Formation. The latter formation records a period of rapid sedimentation into a subsiding basin and, as such, is thickest towards the Kaiparowits basin east of the Sevier-Toroweap fault zone.

Also, during the late Cretaceous, Paleozoic and Mesozoic rocks within the Colorado Plateau province were gently warped, folded, and uplifted as part of an east-northeast-west-southwest Laramide contractional regime (Billingsley and Wellmeyer, 2003). This tectonic regime, consisting of basement-cored uplifts (Tindall and Davis, 1999, Bump and Davis, 2003, and others) continued until the Eocene as a result of "flat slab" subduction of the Farallon Plate to the northeast (Dickinson and Snyder 1978, and others). Due to significant uplift, the majority of Mesozoic strata and some Paleozoic strata within the region have been eroded. Structurally, preexisting deep-seated Precambrian basement faults were reactivated as reverse faults within the metamorphic basement (Davis, 1978 and others). These faults displaced Paleozoic strata while folding of these strata above the faults produced monoclines (Huntoon, 1993; Billingsley and others, 2006a). The Toroweap and Moccasin Monoclines, in particular, span sections of the main fault trace of the Sevier-Toroweap fault system.

During the Early Tertiary (Paleocene – middle Eocene), a broad basin that developed in response to the Laramide orogeny allowed for the deposition of the colorful Claron Formation. Due to a subsequent erosion event after this formation was deposited, the margins of the basin or series of basins that this formation was deposited in is not fully understood (Anderson and Rowley, 1975; Goldstrand, 1990; Taylor, 1993; Biek and others, 2015). The formation records the end of the thin-skinned compressional deformation occurring throughout the region. Some evidence indicates that thrust faulting in the region continued into as late as lower Claron time (Anderson and Dinter, 2010). As a result of Laramide-induced erosion of Mesozoic strata throughout the region, the Claron formation overlies a variety of Upper Cretaceous strata including the Straight Cliffs, Wahweap, and Kaiparowits Formations in the vicinity of the fault system (Gregory, 1951; Biek and others, 2015). As suggested from the lack of volcanic ash in this formation, there was a halt in volcanism in the region in addition to the "flat slab" subduction that was taking place at the time of deposition. This lack of volcanism may have continued with the deposition of the following unit, the Conglomerate of Boat Mesa, which is known to lack volcanic clasts (Biek and others, 2015).

During the Late Eocene to Miocene came the deposition of strata that more clearly indicated widespread volcanism occurring throughout the western interior of North America. The landscape in the region during this time is referred to as the Great Basin altiplano which was a region of higher elevation that accumulated an array of ash-flow tuffs referred to as the Great Basin ash-flow tuff province (Best and others, 1989; Best and Christiansen, 1991; Henry, 2008; Best and others, 2013; Biek and others, 2015).This ash flow province was the result of a middle Cenozoic ignimbrite flare up described by Best and others (2009). Volcanism in the region from this time extended across multiple southwestern states and was sourced from numerous eruptive

centers including 42 calderas that produced over 200 large eruptions (Best and others, 2013; Biek and others, 2015). The Indian Peak and Caliente caldera complexes, in particular, produced over 50 large eruptions which ejected rocks across southwestern Utah and allowed for the deposition of volcanic formations such as the Wah Wah Springs strata in low lying areas of the Great Basin altiplano (Best and others, 2013).

A notable volcanic field the Sevier-Toroweap fault system intersects in southwestern Utah is the Marysvale volcanic field. The Marysvale volcanic field is located in southwestern Utah, in an area encompassing the central High Plateaus. The volcanic field emerged from a cluster of stratovolcanos and calderas and has had most of its notable volcanic activity in the Oligocene and early Miocene. The rocks in this field consists of predominately lava flows, volcanic mudflow breccia, and flow breccias (Stevens and others, 1984). The majority of Marysvale volcanic rocks along the northernmost traced extent of the Sevier-Toroweap fault system in **Figure 1** belong to the Mount Dutton Formation which is exposed along the southern flank of the volcanic field. The trace of the fault as it intersects the volcanic field is not fully understood as is discussed in the Northern Terminus section in the Discussion.

During the late Miocene, following the ignimbrite flare up, there was a change from Laramide compression to east-west extension. This extension came as result of the creation of the San Andreas Fault system as the Farallon plate's spreading ridge subducted under North America bringing the Pacific plate in direct contact with the North American plate changing the relative plate motion and imposing torsion on the North American continent (Dickinson, 2006). This initiated extensional deformation of the region that becomes the modern-day Basin and Range tectonic province. Accommodation of this extension is interpreted to often have involved reactivation of the Precambrian basement reverse faults as negative inversion structures which

displaced Paleozoic and Mesozoic strata (Billingsley and others, 2006a); regionally, thin-skinned thrusts and detachments of the Sevier appear also to have been reactivated in extension (Velasco and others, 2010), though the geometry and linkage of these thin-and thick-skinned systems, and the prevalence and style of reactivation is often debated (e.g., West, 1992, Christie-Blick and others, 2007). The sense of motion along the faults was reversed from reverse faulting on approximately north-south striking, west dipping thrust faults to down to the west normal faulting (Huntoon, 2003). Fault-adjacent structural observations suggest that in some cases the regional basement faults propagated past the vertical limits of the monoclines and produced fault scarps that generally trend north-south (Billingsley and Wellmeyer, 2003), while in other cases, the pre-existence of monoclinal folding is not evidenced in the geology.

During the late Cenozoic (Miocene and Pliocene), bimodal (rhyolitic and basaltic) volcanism occurred simultaneously with normal faulting leaving scattered basaltic flows throughout the region, with some displaced by the Sevier-Toroweap fault system and other faults of the ISB. Vents are present throughout the Grand Canyon region but do not seem to preferentially occur along the main traces of the late Cenozoic faults, indicating that magma more likely moved upward through parallel shallow fractures adjacent to the fault system that may have been created by Cenozoic extension (Billingsley and Wellmeyer, 2003).

During the late Pliocene and Quaternary, volcanism continued throughout the region and a notable volcanic field of this age that the Sevier-Toroweap fault system intersects is the Uinkaret volcanic field. This field is located in northwestern Arizona and caps the Uinkaret Plateau on the hanging wall of the Toroweap fault in the Central Toroweap section. The field has produced numerous basaltic lava flows and pyroclastic deposits dispersed across the region. Basalt flows including the basalt of Graham Ranch have flowed into Toroweap Valley which

parallels the Toroweap Fault. The age of volcanic eruptions in this field dates back to 3.6 Ma, in the second half of the Pliocene (Billingsley and others, 2001) and the cause of this basaltic magmatism along the margin of the Colorado Plateau is likely the result of lithospheric delamination induced mantle flow (e.g., Levander and others, 2011). The younger Quarternary basalt flows, which can be as young as 1 ka, are more widespread throughout this area, and have been displaced by the Toroweap fault. Strong N-S alignment of the vents in the Uinkaret suggest a genetic relationship between the magmatic pathways and second-order strain in the hanging-wall of the Toroweap Fault (see Discussion).

Also, during the Pliocene and Quaternary, continued extension produced new normal faults in between the older Precambrian faults. This led to the development of en echelon faults and graben structures along the main fault trace of the Sevier-Toroweap fault system (Billingsley and Wellmeyer, 2003). In general, normal faulting continues until this day as evidenced by displaced Tertiary and Quaternary units of varying ages, primarily basalt flows and alluvium (Jackson, 1990; Billingsley and Wellmeyer, 2003), seismicity, and geodetically-derived strain rates (as discussed in the previous section).

As of today, east-west extension continues in the region, specifically in the Basin and Range Province where the Earth's crust is being stretched and pulled apart, and this extension is accompanied by erosion. In the past 5 million years, rapid erosion due to drainage reorganization and likely recent, rapid uplift of the Colorado Plateau Province (Murray and others, 2016 and others), potentially due to lithospheric delamination (Levander and others, 2011), has helped to create the Grand Canyon (Young and Brennan, 1974, and others) and other deep incision into the rock units now exposed across the region. In contrast to the uplifted Colorado Plateau, where the gently warped, shallowly-dipping beds and igneous intrusions have been uplifted and eroded in a

broadly continuous manner (Bird, 1979; Morgan and Swanberg, 1985; Levander and others, 2011), the Basin and Range Province, displays a series of north-south trending faults that separate its thinner crust into blocks (Gilbert and Reynolds, 1973; Biek and others, 2015). The boundary between these two physiographic provinces, the Colorado Plateau-Basin and Range Transition Zone, in which is the Sevier-Toroweap fault, possesses characteristics of both provinces. The N-S trending faults in this zone step down from the elevated Colorado Plateau into the Basin and Range Province. In general, the Sevier-Toroweap fault system and other major transition zone faults have had significant structural control on how the landscape in this region has evolved.

STRATIGRAPHY

SEDIMENTARY ROCKS

Understanding and quantifying the amount of displacement along the Sevier-Tororweap fault system requires a detailed understanding of the Upper Paleozoic, Mesozoic, and Cenozoic stratigraphy. **Figure 4** shows a complete stratigraphic correlation chart of displaced units along the fault system's strike extent. The detailed constraints and extrapolations necessary to construct this regional characterization of variations in stratigraphic thicknesses summarized in **Figure 4** are described in detail in the Appendix, but the general trends are summarized briefly in this section. The Sevier-Toroweap fault system cuts exposed rocks ranging from Precambrian to Quaternary in age. These units have variable thickness as you move from south to north along the fault strike. As discussed in the Geologic History section, the stratigraphy reflects a change from a Paleozoic passive margin to a continental tectonically active setting. These rocks were

deformed by contractional structures in the Late Jurassic/Cretaceous and by extension and volcanism in the Cenozoic.

The Sevier-Toroweap fault system cuts through a region where stratigraphic layers are mostly sub-horizontal, and exposure of units is good. Within the regions containing the Toroweap sections of the fault system, the average regional dip is 1-2˚ ENE in most areas excluding the immediate vicinity of the fault (Billingsley and others, 2001; Billingsley and others, 2004). In the Sevier section, the strata commonly dip at 2 to 3 degrees (Cashion, 1961). Steeper dips are present in the vicinity of the fault zone. The stratigraphic units that are displaced and exposed by the Sevier-Toroweap fault system get progressively younger (with exception of units around the Colorado River) from south to north. In the Southern Toroweap section, the fault system predominately displaces exposed Lower Permian units. However, the northernmost section, the Sevier section, has exposures of displaced formations as young as Oligocene in age. It is possible that younger units may be displaced further north as the northern termination of the fault system, where geologic and outcrop conditions otherwise obscure the nature of the fault (see Discussion section on Northern Termination). The fault system is thought to terminate in Miocene volcanic rocks of the Marysvale volcanic field in the north and possibly be buried underneath (Lund and others, 2008).

Proterozoic and Cambrian formations displaced by the Sevier-Toroweap fault system include early Proterozoic intrusive and metamorphic basement rocks and the Lower to Middle Cambrian Tonto Group defined by Noble, 1922 consisting of, in ascending order, the Tapeats Sandstone, Bright Angel Shale, and Muav Limestone. The basement rocks are composed of granite plutons and stocks as well as pegmatite and aplite dikes (Ilg and others, 1996; Hawkins and others, 1996). Directly above the crystalline basement is a regional unconformity known as

the Great Unconformity, which separates lower Proterozoic rocks from overlying Paleozoic formations representing a 1.2-billion-year gap in missing time. The early Paleozoic Tonto Group represents the Cambrian Sauk marine transgressive sequence (Karlstrom and others, 2020) which has a westward thickening trend (Mckee, 1945; Billingsley & Wellmeyer, 2003).

The Middle Devonian to Upper Mississippian formations (excluding Upper Mississippian Supai Group formations) displaced by the Sevier-Toroweap fault system include the Temple Butte - Elbert Formation, Ouray Formation, Redwall Limestone, and Surprise Canyon Formation. These formations unconformably overlie the Tonto Group indicating a regional disconformity where Ordovician, Silurian, and most Lower and Middle Devonian rocks are removed from the Paleozoic section (Billingsley and others, 2000).

The Sevier-Toroweap fault system displaces the Upper Mississippian to lower Permian Supai Group consisting of, in ascending order, the Watahomigi Formation, Manakacha Formation, Wescogame Formation, and the Esplanade Sandstone. The Supai Group was originally a formation defined by distinctive red beds (Darton, 1910), and prominent breaks in the stratigraphic sequence at the top and base of the group (Noble, 1922). The four formations in the group were later defined by McKee (1982) using key conglomerate beds that separated red bed deposition. Due to difficulty in distinguishing the boundaries between the Wescogame, Watahomigi, and Manakacha Formations, these formations are often grouped on published USGS maps (Billingsley & Wellmeyer, 2003). These grouped formations will be referred to as "WMW, undivided" and will appear undivided in **Figure 4** and later cross sections. However, their individual unit descriptions and thickness trends are discussed separately within the Appendix.

Lower Permian formations (excluding the Esplanade Sandstone of the Supai Group) displaced by the Sevier-Toroweap fault system include, in ascending order, the Queantoweap-Cedar Mesa Sandstones, the Hermit Formation, Coconino Sandstone, Toroweap Formation, and Kaibab Formation. An unconformity is present at the base and top contacts of each formation that is characterized by erosion channels. The Kaibab Formation is the most exposed formation that forms the surface in the vicinity of the fault in the Southern and Central Toroweap sections as well as the southern half of the Northern Toroweap section. The Coconino is the thinnest formation in this time frame and eventually pinches out along strike toward the north. As such, this formation either does not appear or may be merged with the Hermit Formation in some northern cross sections discussed in subsequent sections.

The unconformably overlying Triassic formations displaced by the Sevier-Toroweap fault system include, in ascending order, the Moenkopi and Chinle Formations. At the base of Triassic strata is a regional unconformity (Billingsley and others, 2008). Triassic units appear in abundance in the north and as far south as halfway into the Northern Toroweap section as these formations, and younger ones, were mostly eroded away south of the Grand Canyon. Thin remnants of the Moenkopi Formation can be found on the Coconino Plateau in the Central Toroweap Section preserved within the Uinkaret Volcanic Field.

The unconformably overlying Jurassic formations displaced by the Sevier-Toroweap fault system include, in ascending order, the Moenave Formation, Kayenta Formation, Navajo Sandstone, Temple Cap Sandstone, and Carmel Formation. Older Jurassic units are exposed at the surface around the Utah-Arizona border and are exposed in abundance for the remainder of the Northern Toroweap section as well as ~20 km north into the Sevier Section. Near the state border, older Jurassic formations form the lower Vermillion Cliffs and the Navajo Sandstones

forms the upper part and caps the Moccasin and Moquith Mountains (Billingsley and others, 2004).

The unconformably overlying Cretaceous formations displaced by the Sevier-Toroweap fault system include, in ascending order, the undivided Dakota and Cedar Mountain Formations, Tropic Shale, Straight Cliffs Formation, Wahweap Formation, and Kaiparowits Formation. These formations are exposed in abundance within the southern half of the Sevier Section. Notably, the hardness variations in these Cretaceous Units create significant variations in topographic relief across the fault zone. Southwest of Glendale, Utah, the less resistant Tropic Shale in the hanging wall is juxtaposed against more resistant Jurassic units creating a large west-facing fault scarp with as much as 300 m of topographic relief (Cashion, 1961). The reverse occurs north of Glendale as Cretaceous shale units in the footwall are juxtaposed against more resistant Cretaceous and Tertiary units to the west creating a topographically higher hanging wall.

The unconformably overlying Tertiary formations displaced by the Sevier-Toroweap fault system include, in ascending order, the Claron Formation, Brian Head Formation, Wah Wah Springs Formation, and Mount Dutton Formation. These formations only appear in the Sevier Section and notably the Claron formation dominates the landscape in the vicinity of the fault zone in the northern half this section. The Mount Dutton Formation, the youngest formation, has widespread exposure on the southern flank of the Marysvale volcanic field at the furthest northern extent of the fault zone that can be confidently traced.

SURFICIAL DEPOSITS AND VOLCANIC ROCKS

A discussion of units younger than Oligocene in age displaced by the Sevier-Toroweap fault system is included in the Fault Activity section. This section discusses late Cenozoic units

that cover the fault and/or adjacent formations. These surficial deposits and volcanic rocks were only included in cross sections in this study if they were considerably thick. Regardless, these geologic units are important to document as they, where present, inhibit thickness constraints of underlying formations along certain portions of the fault system.

The Sevier-Toroweap fault system has a variety of surficial deposits along strike that consequently act as coverage. In the Southern Toroweap section, Pleistocene – Holocene alluvial fan deposits are the most prevalent deposits covering the proximity of the fault trace with minor fluvial valley-fill and landslide deposits of similar age (Billingsley and others, 2006a). Alluvial fan deposits can be tens of meters thick. In the Central Toroweap section, the most prevalent surficial deposits that cover the proximity of the fault trace are Pleistocene – Holocene alluvial fan deposits with minor floodplain and landslide deposits of similar age (Billingsley & Wellmeyer, 2003). Like in the Southern Toroweap section, alluvial fan deposits can be tens of meters thick. Coverage by volcanic rocks include Pleistocene basalt flows and pyroclastic deposits apart of the Uinkaret Volcanic Field (Billingsley and others, 2000). These volcanic rocks can be tens of meters thick. Basalt flows and surficial deposits in the northern part of this section cover remnant Mesozoic rocks (Billingsley & Wellmeyer, 2003). In the Northern Toroweap section, the most prevalent surficial deposits that cover the proximity of the fault trace include Pleistocene – Holocene alluvial fan deposits, with minor Pleistocene or Holocene alluvial terrace-gravel, stream channel, ponded sediment, valley-fill, dune sand, sand sheet, talus, and colluvial deposits (Billingsley and others, 2008; Billingsley and others, 2004; Doelling, 2008). Alluvial fan deposits are typically a few meters thick throughout the section except in the northern quarter where deposits can be tens of meters thick. Like in the Central Toroweap section, coverage by volcanic rocks include Pleistocene basalt flows and pyroclastic deposits.

These deposits form an eastern extension of the Uinkaret Volcanic Field and can be tens of meters thick (Billingsley and others, 2008). In the Sevier Section, the most prevalent surficial deposits that cover the proximity of the fault trace include Pleistocene - Holocene alluvial fan deposits with minor Miocene basin fill deposits and Pliocene, Pleistocene or Holocene alluvial gravel, stream alluvium, pediment alluvium, mass movement, talus, colluvium and Markagunt Megabreccia deposits (Doelling, 2008; Biek and others, 2015). Alluvial fan deposits can be tens of meters thick and fill the Sevier Valley directly adjacent of the fault trace in the hanging wall. Coverage by volcanic rocks include Pleistocene to Holocene Black Mountain basalt flows, and Miocene to Pliocene Rock Canyon basalt flows (Sable & Hereford, 2004; Biek and others, 2015). These volcanic rocks can be tens of meters thick. Based on geologic cross sections from Biek and others (2015) the valley fill across the northern half of the Sevier section can be 100s of meters thick which poses the greatest challenge in constraining units in the hanging wall.

STRUCTURE

Prominent structures in the southwestern margin of the Colorado Plateau physiogeographic province and Basin and Range-Colorado Plateau Transition Zone formed as a result of several major tectonic events discussed in the Geologic History section. Normal faults of the Transition Zone are characterized by main traces, splays, and second-order faults; however, other structures of note exist in the immediate vicinity of the main trace of the Sevier-Toroweap fault and are described here. Beginning in the late Miocene, east-west extension caused an inversion of Laramide and Sevier-associated reverse and thrust faults as normal faults as well as created hundreds of new normal faults which led to the development of more complex zones (Billingsley and others 2000). Since displacement and fault extension of these

predominantly west-dipping Cenozoic normal faults are greater than Laramide reverse offsets, fault blocks in the region step down to the west. The principal normal faults tend to form the boundaries of the major topographic plateaus in the region. The Sevier-Toroweap fault system and other major normal faults in the region generally have the downthrown hanging wall to the west and have developed extensional basins where Quaternary alluvium and basalt flows fill the fault-related basin accommodation and have been displaced along the fault traces themselves.

Aside from the normal faults of interest to this study, throughout the southern southwestern margin of the Colorado Plateau, other noteworthy structures include several north-, northwest-, and northeast-trending steeply-dipping normal faults as well as collinear monoclinal folds that dip to the east. Like the neighboring Aubrey and Hurricane monoclines, the Toroweap Monocline, found in Toroweap sections of the fault system, is interpreted to be a crustal-shortening structure that formed over Precambrian normal faults reactivated as reverse faults during Laramide time. As part of this contractional regime, these faults propagated upward while Paleozoic rocks were folded. At depth, the folded Paleozoic rocks in the Toroweap monocline are more steeply folded until they are overturned against the Toroweap Fault towards the base of the Paleozoic section (Billingsley and others, 2000). Post-Laramide extension in the late Miocene, Pliocene, and Pleistocene reactivated these reverse faults as normal faults which caused separation adjacent to or within these monoclines. Today, the Toroweap monocline consists of two segments; a northern segment that follows the Toroweap fault trace north of Diamond Creek and a southern stranded segment south of the Toroweap fault's southern termination (Billingsley and others, 2006a). The normal offset on the Toroweap fault may not have been able to continue to follow the trend of the structure toward the south due to the gap between these segments, interpreted to be related to the possible intersection of basements faults

in this location (Billingsley and others, 2000). Both segments have east dipping strata within the monoclinal limb as a result of east-northeast Laramide contraction (Huntoon, 2003).

Local folding of the stratigraphic layers occurs within the vicinity of the fault as well. Modest dips and folds with axial traces subparallel to the fault exist within the hanging walls of the normal faults, which reflects fault-related folding associated with slip over underlying bends in the faults. Additionally, due to gypsum dissolution in the Harrisburg member of the Kaibab Formation, more second-order warping of strata also occurs in localized areas (Billingsley and others, 2001). This effect is increased as you move upwards through Toroweap Valley, coincident with the outcrop expression of the Harrisburg member. Billingsley and others (2004) also report gentle warping of stratigraphy along the Uinkaret Plateau in the hanging wall of the fault. The layers are warped by small folds that trend N-S. This type may be due to compression during the Laramide (Huntoon, 2003), though some of the folding may be associated with extensional displacement on the underlying fault as well. As you move closer to the Arizona-Utah border in the Pipe Spring National Monument area, a significant west segment of the fault system extends northwestward and is followed along strike by the Moccasin Monocline. Strata in this monocline have a maximum dip of 10˚ which contributes to increased elevation in the near vicinity of the fault zone in the hanging wall.

The Sevier section also has interesting adjacent structural features. Apart from the regional N-NE trending normal faults that bound plateaus and gently warped sediments, there is structural overlap with features associated with the Sevier Orogeny. Moreover, the Paunsagunt thrust fault system contains several thrust faults that mainly reside on the Paunsagunt Plateau on the footwall side of the Sevier fault and are oriented nearly perpendicular to it. These unusual thrusts are suspected to have formed as a result of gravitational spreading of the Marysvale

volcanic field (Merle and others, 1993). One of these faults, the Ruby's Inn thrust fault, intersects the Sevier fault 3km SW of Wilson Peak and was recently mapped by Biek and others (2015) to extend west across the Markagunt Plateau. Notable features on the hanging wall side of the fault include deposits of the Markagunt Gravity Slide, a massive (4160 km^2) subaerial gravity slide and series of horst and graben structures along the Markagunt Plateau.

DISPLACEMENT GRADIENT

Displacement on the Sevier-Toroweap Fault System generally increases toward the north (Lund and others, 2008).This displacement gradient is generally lower than faults to the west of the structure within the easternmost Basin and Range, suggestive of the interpretation that the Sevier-Toroweap fault represents a similar structure at an early stage of fault system evolution. Local constraints on fault displacement, and interpretation of their patterns, are undertaken in this study, and so a detailed description of the existing published constraints at specific locations along the fault can be found in the Results section of this manuscript.

METHODS

DATA COMPILATION

The most time consuming, but essential, portion of this study, was the compilation and digitization of data from a wide range of published sources. Digital format data were used where available, and in other cases, maps were georeferenced and data were digitally extracted from them through digitization in MOVE. Map data included in this study included stratigraphic contacts, fault traces, and dip information obtained from USGS maps at the 30'-60'scale (Billingsley and Hampton, 2000;Billingsley and Workman, 2000; Billingsley and Wellmeyer,

2003; Sable and Hereford, 2004;Billingsley and others, 2006a, 2006b, 2008; Doelling, 2008, Biek and others, 2010, 2015), the 1:48000 scale (Billingsley and others, 2000, 2004; Billingsley and Priest, 2003), and the 7.5' (1:24,000) scale (Morris, 1957; Sable and Doelling, 1993; Billingsley, 1994, 1997; Sable, 1995; Kurlich and Anderson, 1997; Tilton and Sable, 2001; Doelling and others, 2002; Willis and others, 2002; Biek and others, 2007; Hayden, 2008, 2011, 2013; Hylland, 2010; Biek, 2013),. Subsurface constraints, including well top data obtained from the Utah Department of Natural Resources, Division of Oil, Gas and Mining, were also integrated into the same framework, as was a 30-m USGS 3DEPdigital elevation model . These digital data were all compiled into a common spatial reference frame and project, permitting completion of the subsequent portions of the study.

DISPLACEMENT VS. DISTANCE PLOTS DESCRIPTION

Displacement vs. distance plots or fault-displacement profiles show the cumulative displacement along the length of a fault. An idealized displacement vs. distance plot for each of the four stages described in the Fault Linkage Review sub-section within the Background is illustrated in **Figure 2**. For a single isolated fault that isn't underlapping with any nearby faults, a displacement vs. distance plot would show a symmetric hump-shaped profile where the maximum displacement is in the center of the fault and little to no displacement is seen at the fault tips. In stage t1 a displacement vs. distance plot of two underlapping faults would show two displacement profiles that are asymmetric towards each other. These displacement profiles will overlap and the portions of each profile in the overlap zone will be cumulatively added to form an aggregate displacement profile that represents the displacement along the relay ramp that has formed. The depression in the displacement profile will eventually flatten out over time with continued deformation. With enough deformation over time the displacement profile will

develop into that of a single fault, though the location of a local change in fault strike will often remain as a record of the prior location of a hard linkage.

For this study, a large number of displacement constraints were compiled from published geologic maps and other publications and were spatially referenced using ArcGIS and 3DMove, permitting construction of a detailed displacement vs. distance plot for the entire traced extent of the Sevier-Toroweap fault system. Separate profiles were made to show displacement in each fault section as well as to illuminate the details of the displacement variations at the two major segment boundaries located within the Fredonia 30’ x 60’ quadrangle geologic map (Billingsley and others, 2008). These plots heavily rely on the displacement measurements discussed in the Displacement Gradients subsection within the Results section as well as displacements calculated from constructed cross sections in this study, also described in the results section.

CROSS SECTION CONSTRUCTION

Six cross sections were produced throughout the Sevier-Toroweap fault system to constrain the fault geometry and determine displacement at key locations along the main fault trace (**Figure 5**). All map and well data used in cross section construction were compiled within the structural interpretation software MOVE as previously described and projected onto the cross section; the software was also used to model the footwall using strike and dip data, geologic contacts, formation outcrops, well top data, and extrapolated thickness values calculated using published thickness trends defined in USGS map pamphlets and described in the Appendix. The geometry of the fault and the hanging wall for individual cross sections was modelled using either the 2D structural interpretation software Structure Solver or the structural modelling program fbfFor (Connors and others, 2021), which both employ the same extensional fault-related folding method for relating fault geometry and slip to folding. The kinematic modelling

for construction of these cross sections is based on modeling extensional fault-related folding, or the relationship of folding in the hanging wall with fault geometry, displacement, and sedimentation rate, through conjugate inclined shear deformation (Dula, 1991, Xiao and Suppe, 1992, Connors and others, 2021, and others). Displacement across fault bends require the overlying material to fold during distributed shear processes so using the available geologic constraints to match the expected folding and structural relief allowed for modeling the fault geometry at depth. This kinematic modelling approach has been extensively and successfully employed to model subsurface geologic structures, particularly in cases well constrained by seismic reflection data (Xiao and Suppe, 1992, Shaw and others, 1997, and others), which demonstrates the validity of the method in modeling extensional systems, though it has only been utilized or implied in the interpretation of active tectonics evaluation of fault systems in a smaller number of cases, examples of conceptual or quantitative applications of this interpretation method to Basin and Range structures in the Western United States do exist (e.g., Kruger and others, 1995, DuRoss and Hylland, 2015, and others).

RESULTS

DISPLACEMENT GRADIENTS

Figure 5 shows the complied displacement locations across the Sevier-Toroweap Fault system. These displacement values came from a variety of sources including published USGS maps and cross sections, offsets calculated from structures contours, and literature. The amounts and sources of these displacement measurements are described in detail by fault section in subsequent paragraphs. Reported vertical displacements were converted to dip slip values using

an assumed 65˚ dip on the fault, based on a dip measurement of the fault system at an outcrop location from Karlstrom and others (2007). This dip value falls is typical for normal faults.

Southern Toroweap

Within the Southern Toroweap section, the Toroweap fault exhibits small displacement values (Wenrich and others, 1996). Within the Peach Springs 30’ x 60’ quadrangle, Billingsley and others (2006a) reported a collection of estimated dip-slip displacements along the trace of the fault. Measured displacement values from their mapping and cross section across the fault range from 60 to 290 m.

Central Toroweap

Displacement measurements in the Central Toroweap section have several sources. Within the Mount Trumbull 30’ x 60’ Quadrangle, Billingsley and Wellmeyer (2003) reported a collection of estimated separation displacements along the trace of the fault. Measured displacement values from their mapping and cross section across the fault range from 67 to 359 m. Billingsley and Hamblin (2001) reported a vertical separation of 198 m around 3.6 km N of Vulcan’s Throne and 67 m in the northern Toroweap Valley. This value was converted to 218 m. At the intersection of the Toroweap fault with the Colorado River, where Proterozoic units are exposed, Karlstrom and others (2007) report that there have been an array of displacement estimates ranging from 177 to 370 m. They use a value of 193 reported by McKee and Schenk (1943) based on Cambrian horizons which is the value that is used in this study at that location.

Northern Toroweap

Displacement measurements in the Northern Toroweap section have several sources. Within the Fredonia 30’ x 60’ Quadrangle, Billingsley and others (2008) reported a collection of

estimated vertical separation measurements along the trace of the fault. Measured displacement values from their mapping and cross section across the fault range from 26 to 259 m. This displacement range excluding the cross section slip value was converted to 29 to 286 m. In the SW corner of the map area, they report displacement values around 70 m. This value was converted to 77 m. The displacement remains under 100 m until a major splay area between the Little Hurricane and Sunshine Ridges that they describe as the connection of the Sevier and Toroweap faults. Near the Arizona/Utah border, they report a displacement of 366 m. This value was converted to 404 m. Near the border, on the Utah side, Hayden (2013) reported a vertical displacement of 500 m. This value was converted to 552 m. Within an area encompassing the Pipe Springs National Monument and Western Kaibab-Paiute Indian Reservation, Billingsley and others (2004) reported a collection of displacement measurements. Measured displacement values from their mapping and cross sections across the fault range from 45 to 805 m. This displacement range, excluding the cross section slip values, was converted to 50 to 805 m. Near Coral Pink Sand Dunes State Park, Anderson & Christenson (1989) reported an estimated throw of 475 m. This value was converted to 524. Due to a lack of data points for the remainder of the section the displacement profile appears constant at around 500 m of displacement for the remainder of the section.

Sevier

Displacement measurements in the Sevier section have several sources. Towards the beginning of the section, Anderson and Christenson (1989) reported a displacement of 450 m in the vicinity of Mount Carmel Junction. This value was converted to 497 m. Within the Mount Carmel 7.5-minute quadrangle, Hayden (2008) reported a displacement of 500 m east of Mount Carmel, Utah. Cashion (1961) however reported a maximum cumulative displacement of 610 m

within the same area. An average value of 555 m is used for this study. Between Orderville, Utah and Black Mountain, Schiefelbein (2002) reported a stratigraphic separation of 472 – 869 m in their fault linkage study. Within the 2004 Kanab 30’ x 60’ quadrangle (Sable and Hereford, 2004), a displacement of 841 m was calculated from their cross section located at the northern edge of the quadrangle. At Red Canyon, Lundin (1989) used seismic reflection data to estimate a throw of 900 m based upon offset of the basement rocks. This value was converted to 993 m. Within the Panguitch 30’ x 60’ quadrangle (Biek and others, 2015), cross sections along the northern and southern ends of the quadrangle give calculated displacements of ~1500 and 1450 m, respectively.

DISPLACEMENT-DISTANCE TRENDS

A displacement vs. distance plot was produced for each major section of the Sevier-Toroweap fault. Plots were also produced for areas where there is major apparent segmentation in the fault in the Fredonia 30’ x 60’ quadrangle including where the Sevier and Toroweap merge and where a long west segment branches off from the main trace near the Arizona/Utah border. In general, these plots are discussed in order from south to north along the fault trace.

For this section, the values used in the displacement vs. distance plots will strictly come from Displacement Gradients section. Several values reported in the Displacement Gradients section were cumulatively added with measurements on adjacent splays and as such those areas along-strike have higher displacement values on these plots. After subsequent descriptions of constructed cross sections in the next section, a modified displacement vs. distance plot of the entire Sevier-Toroweap fault is shown that incorporates the cumulative slip measured from the cross sections in this study.

Southern and Central Toroweap Sections

The displacement trend seen in both the Southern and Central Toroweap sections (**Figures 6** and **7**, respectively) is relatively simple and can be discussed together. The trend begins at ~60 m net slip in the Southern section and continually increases to 345 m towards the end of the section. At the beginning of the Central section, this trend continues to increase until a maximum of 359 m of net slip is reached at a distance of 37 km along the main fault trace. Following this maximum value, displacement begins to steadily taper out towards the northern end of this section. The trend across these two sections is mostly smooth because for much of the Toroweap portion of this fault zone, the trace is geometrically simple with few splays and or subparallel strands. The steady increase and tapering off of net slip across these two sections suggests that it is one main segment of the fault zone.

Northern Toroweap Section

The Northern Toroweap section contains two major two major splays in the fault and has an overall displacement trend (**Figure 8**) that isn't as simple as previous sections. This section begins with relatively low displacements below 100 m and steadily increases once the merge between the Sevier and Toroweap portions of the fault system is crossed at ~100 m along-strike distance. This further confirms a segment boundary here as slip from the previous two Toroweap sections of the fault is tapering off and being transferred to the linked Sevier strand. Across this segment boundary, the western Toroweap segment has a constant displacement of ~50 m before tapering out (**Figure 9**). The Sevier segment, however, shows a displacement minimum near the linkage zone, a gradual increase in displacement to a maximum displacement of 157 m at 110 m along-strike, and a decrease in displacement to 87 m adjacent to where the Toroweap segment tapers out. The cumulative displacement profile matches the shape of the Sevier segment. The

displacement trend after this major split in the fault increases until a section maximum of 805 m net slip is reached at a distance of 139 m along the fault (**Figure 8**). This maximum occurs right before the second major splay in the fault zone consisting of a western major splay and eastern main trace of the Sevier Fault. The displacement profiles of the western and eastern (main) strand (**Figure 10**) shows a minimum in the main segment and a maximum in the western segment at 144 m along-strike. The displacement of the western segment then tapers off and displacement of the main segment increases to 300 m and remains relatively constant until outside of this zone. This cumulative displacement profile matches that of the western segment and a high displacement profile for this major area of linkage suggests that this linkage zone is older relative to the Sevier/Toroweap merge. The section of the fault sitting between these two major splays may represent a second major segment. The displacement following the west and east (main) segment boundary quickly increases until it reaches 495 m at a distance of ~150 m along the fault trace. For the remainder of the section, displacement values remain relatively consistent around 500 m.

Sevier Section

The general displacement trend for the Sevier section (**Figure 11**) shows an increase to the highest displacement values seen throughout the fault system. Net slip values begin at ~500 m and rise to a maximum of 1513 m by the furthest northern extent of the fault trace that can be confidently traced from USGS maps. Looking at the overall trend for this section, there are two apparent drops at along-strike distances of 214 and 249 km. It is hard to gauge how accurate these values are with no nearby datapoints of similar values. The former value came from a USGS cross section which is simplified fault geometry and lacks rigorous structural modelling techniques. The value at 249 km came from estimates from seismic reflection data that is

unspecified in the source material. Looking at the map view trace, there isn't any apparent strike change or geometry that would suggest that the displacement minimum in these locations correspond with linkage zones.

The Sevier section proved to be the hardest section to create a displacement vs distance plot for, requiring integration of data from multiple sources. There were limited cross sections on USGS maps covering this section and attempts to produce more cross sections were hindered due to the burial of many important units adjacent to the fault trace. Additionally, direct measurements of offset were not present on maps in this section unlike previous fault sections. As a result, of the limited data points that were used, there is uncertainty in the displacement trend for this section.

CROSS SECTIONS

A-A'

Cross section A-A' (**Figure 12**) is a ~25 km-long section that transects across a single main strand of the Sevier-Toroweap fault as well as the Hurricane Fault. The Sevier-Toroweap fault intersection is located 4 km north of the Prospect Point Graben near the halfway mark of the Southern Toroweap section. The fault trace, geologic contacts, and outcrop expressions used in this cross section were obtained from the Peach Springs and Mount Trumbull 30' x 60' quadrangles. In this section, the Toroweap fault modestly displaces the Paleozoic section which is entirely exposed. Regional dip information projected to the cross section was collected from the Peach Springs and Mount Trumbull 30' x 60' quadrangles as well as a geologic strip map of the Toroweap Fault from Jackson (1990). The cross section is near-perpendicular to the strike of the fault system to avoid apparent dip and to get a true sense of the fault geometry along strike.

The purpose of this cross section was to validate the estimated dip slip displacements of 60 – 345 m from Billingsley and others (2006a). Projected strike and dip information in the footwall suggest that stratigraphy here is mostly flat dipping 1-2˚ E consistently. For the hanging wall, the fault geometry that successfully matches the stratigraphy to the contacts and outcrop locations is a fault that has concave bends in the shallow subsurface and a convex bend at depth. A significant shallowing of the fault dip to near flat (2˚) at ~6 km depth is needed to effectively match the data constraints. In general, the Toroweap Fault in this section has dips ranging from 2 – 65˚. The maximum dip of 65 ˚ is at the surface whereas the shallowest dips are seen at depth. Using this geometry, a displacement of 392 m was calculated.

B-B'

Cross section B-B' (**Figure 13**) is a 24.2 km-long section that transects across a single strand of main Sevier-Toroweap that intersects the Colorado River 2 km south of Vulcan's Throne, Arizona. The fault trace, geologic contacts, and outcrop expressions used in this cross section were obtained from the Mount Trumbull and Grand Canyon 30' x 60' quadrangles. In this section, the Toroweap fault modestly displaces exposed Triassic, and Paleozoic. Strata. The exposed formations, in ascending order, include the Bright Angel Shale, Muav Limestone, Temple Butte – Elbert Formation, Redwall Limestone, WMW, undivided, Esplanade Sandstone, Hermit formation, Coconino Sandstone, Toroweap Formation, Kaibab Formation, and Moenkopi Formation. Regional dip information projected to the cross section was collected from the Mount Trumbull and Grand Canyon 30' x 60' quadrangles as well as geologic strip map of the Toroweap Fault from (Jackson, 1990). The cross section is near-perpendicular to the strike of the fault system to avoid apparent dip and to get a true sense of the fault geometry along strike.

The purpose of this cross section was to validate the calculated displacement of 193 m from McKee and Schenk (1942). Projected strike and dip information in the footwall suggest that stratigraphy here is mostly flat dipping 1-2˚ E. For the hanging wall, the fault geometry that successfully matches the stratigraphy to the contacts and outcrop locations is a fault that has concave bends in the shallow subsurface and convex bends at depth. This helped produce an anticline structure in the hanging wall near the fault that creates a good fit with geologic contacts. This section passes through several unnamed faults in the hanging wall. I include one to the left that has significant slip to better match the contacts near the western edge of the section. The Toroweap Fault in this section has dips ranging from 38 – 65˚ The maximum dip of 65 ˚ is at the surface which matches a measurement made by Karlstrom and others (2007). From the surface the fault shallows at depth to 38˚ across it's concave bends and then steepens to a dip of 50˚ in it's convex bend. Using this geometry, a displacement of 370 m was calculated.

C-C'

Cross section C-C' (**Figure 14**) is a 41.5 km-long section that transects across a single strand of main Sevier-Toroweap in the northern Toroweap Valley. The fault trace, geologic contacts, and outcrop expressions used in this cross section were obtained from the Littlefield, Mount Trumbull and Grand Canyon 30' x 60' quadrangles. In this section, the Kaibab is displaced tens of meters across the fault zone. Thin eroded remnants of the Moenkopi Formation and Paleozoic units on the far ends of the section help to constrain this portion of the fault that has minimal slip. The exposed formations, in ascending order, include the Coconino Sandstone, Toroweap Formation, Kaibab Formation, and Moenkopi Formation. Regional dip information projected to the cross section was collected from the Littlefield, Mount Trumbull, and Grand Canyon 30' x 60' quadrangles as well as geologic maps of the Toroweap Fault from (Jackson,

1990). The cross section is near-perpendicular to the strike of the fault system to avoid apparent dip and to get a true sense of the fault geometry along strike.

The purpose of this cross section was to validate the minimal displacement of 67 m from Billingsley and Wellmeyer (2003). Projected strike and dip information in the footwall suggest that stratigraphy here is mostly flat dipping (<1˚) For the hanging wall, the fault geometry that successfully matches the stratigraphy to the contacts and outcrop locations is a fault that has a concave bend in the shallow subsurface followed by a convex bend and then another concave bend at depth. Similar to cross section B-B', this helped produce an anticline structure in the hanging wall near the fault that creates a good fit with geologic contacts. The Toroweap Fault in this section has dips ranging from 20 – 65˚ The maximum dip of 65 ˚ is near the surface and the minimum dip (20˚) is at the deepest bend of the fault geometry. Using this fault geometry, a slip of 67 m like reported was achieved.

D-D'

Cross section D-D' (**Figure 15**) is a 29.9 km-long section that transects across a single strand of main Sevier-Toroweap fault trace near the halfway point of the Sevier Section, 5 km northeast of Mt. Carmel Junction, Utah. The fault intersection lies 10 km north of Clay Flat, the location of the boundary between the Northern Toroweap and Sevier sections as well as a possible segment boundary proposed by Lund and others (2008). The fault trace, geologic contacts, and outcrop expressions used in this cross section were obtained from the Kanab 30' x 60' quadrangle. In this section, exposed Jurassic formations in the footwall are juxtaposed against Cretaceous formations in the hanging wall. The exposed formations, in ascending order, include the Navajo Sandstone, Temple Cap Sandstone, Carmel Formation, the undivided Dakota and Cedar Mountain Formations, Tropic Shale, and Straight Cliffs Formation. Regional dip

information projected to the cross section was collected from a geologic map of the Zion Park region (Gregory,1950) as well as various surrounding USGS 7.5-minute quadrangles. The cross section is near-perpendicular to the strike of the fault system to avoid apparent dip and to get a true sense of the fault geometry along strike.

The purpose of this cross section was to validate the calculated displacement from structure contours and the reported local displacement range of 450 – 610 from literature. Projected strike and dip information in the footwall suggest that stratigraphy here is mostly flat (<1˚). Additional constraints for the footwall include thicknesses of Permian and Triassic units from formation tops in the Federal 41-11 well. For the hanging wall, the fault geometry that successfully matches the stratigraphy to the contacts and outcrop locations is listric. The fault dips at 70 degrees near the surface and shallows to 22 degrees at depth. Using this geometry, a displacement of 680 m was calculated.

E-E'

Cross section E-E' (**Figure 16**) is a 17.5 km-long cross section that transects a single strand of main Sevier-Toroweap fault trace near the halfway point of the Sevier Section, 1.3 km southwest of Alton, Utah. The fault trace, geologic contacts, and outcrop expressions used in this cross section were obtained from the Kanab 30' x 60' quadrangle. In this section, exposed Cretaceous formations in the footwall are juxtaposed against Tertiary formations in the hanging wall. The exposed formations, in ascending order, include the undivided Dakota and Cedar Mountain Formations, Tropic Shale, Straight Cliffs Formation, Claron Formation and Brian Head Formation. Regional dip information projected to the cross section was collected from a geologic map of the Zion Park region (Gregory,1950) as well as various surrounding 7.5'

quadrangle USGS maps. The cross section is near-perpendicular to the strike of the fault system to avoid apparent dip and get a true sense of the fault geometry along strike.

The purpose of this cross section was to validate the the displacement minima of 841 m at an along strike distance of 214 km. Constraining the footwall and hanging geometry along this section required utilizing very subtle changes in dip. Few contacts are exposed in the footwall due to extensive coverage of surficial deposits. To overcome this, layers were folded according to projecting dips while also honoring the outcrop expressions. Overall, the regional stratigraphy in the footwall is gently folded towards the eastern edge of the cross section and flattens out westward to near horizontal. The resulting model has a listric geometry with four bends shallowing gradually to as little as 45 degrees. The measured slip on the fault is around 1300 m which suggests slip on the Sevier fault in this area may be even higher than the 840 m of slip predicted by structure contours to the top of the Carmel Formation.

F-F'

Cross section F-F'(**Figure 17**) is an 18.1 km-long section that transects a single strand of main Sevier-Toroweap fault trace near three fourths of the way north into the Sevier Section, 3 km north of Red Canyon, Utah. The fault trace, geologic contacts, outcrop expressions, and regional dip information used in this cross section were obtained from the Panguitch 30' x 60' quadrangle. In this section, within the vicinity of the fault exposed Tertiary Claron Formation lies in the footwall. No formations are exposed at the surface in the hanging wall due to extensive valley fill in Hatch Valley. The exposed footwall formations, in ascending order, include the Claron Formation, and Brian Head Formation. Apparent dip in this section is negligible.

The purpose of this cross section was to validate the reported Red Canyon vertical displacement of 900 m by Lundin (1989) (converted to 993 m in this study). Projected strike and dip information in the footwall suggest that stratigraphy here is dipping at ~2˚. Additional constraints for the footwall include geologic contacts that delineate the top of the Claron Formation at the eastern edge of the section. For the hanging wall, the main constraints used in place of exposed geologic contacts were well tops of the Carmel and Dakota Formations from the Dixie Unit 1-19 and Panguitch 1 wells. The fault geometry that successfully matches the stratigraphy to the contacts and outcrop locations is listric with several bends. The fault dips at 70˚ near the surface and shallows to 30˚ gradually degrees at depth. Using this geometry, a displacement of 2100 m was calculated.

Summary Of Cross Section Results

Cross section construction demonstrates that the Sevier-Toroweap fault is consistent with a normal fault geometry that generally decreases in dip with depth in the crust, creating a rollover fault-related fold geometry in the hanging wall that is required by the dipping beds and stratigraphic contact-related constraints observed in the surface geology in the hanging wall and in the stratigraphic elevations of formation tops observed in wells. While the fault in all cases becomes more shallowly dipping with depth, it is apparent due to the persistently lower structural elevation of stratigraphic layers in the hanging wall relative to their regional elevations in the footwall that the fault maintains some dip as it cuts through the lower portion of the crust, and therefore appears to cut the full brittle portion of the crust down to a depth of at least 15-20 km, based on area-depth and structural relief (Groshong, 1994 and references therein). Additionally, it is notable that the displacements on the fault inferred from from 5 out of the 6 cross sections are systematically higher than those reported in previous publications (**Figure 18**).

Cross sections E and F, which were placed in the proximity of questionable displacement minimum measurements provided a more confident assessment of the displacement in these areas of the gradient. In general, the rigorous nature of the stratigraphic thickness variations and quantitative cross section construction methods employed in this study demonstrate the value in undertaking such an effort, as these more carefully constrained displacement estimates refine our understanding of the fault system, with implications for its potential hazards.

DISCUSSION

FAULT SEGMENTS OF THE SEVIER-TOROWEAP FAULT SYSTEM

The segmentation of normal faults is known to place a first-order control on the potential magnitude of earthquakes hosted on these faults, as the irregular geometry of the fault at the sites of hard linkages have been documented to have limited the size of paleoseismic ruptures on similarly segmented (but better studied) faults such as the Wasatch Fault in northern and central Utah (Machette and others, 1991, DuRoss and others, 2016), with considerable implications for the potential maximum magnitude of earthquakes and seismic hazard posed by these structures (Valentini and others, 2020). Therefore, accurate description of the segmentation of the fault is essential. Though the fault had been previously described, from south to north, as the Southern Toroweap, Central Toroweap, Northern Toroweap, and Sevier sections (as depicted in **Figures 1** and **19**), analysis of the displacement gradients, along-strike variations in strike of the main fault strand, and sites of abundant second-order faulting associated with the breaching of relay ramps at previous segment boundaries suggests a modified description of the segments that is more aligned with their physical segmentation and linkage history.

Three segments were identified in this study: a Southern, Central, and Northern Segment as shown in a map-view comparison of these refined segments with previously characterized segments from past studies (**Figure 19**). The Southern Segment has a smooth profile of low displacements (**Figure 20**). Based on the shape of the segment's along-strike displacement profile, which matches that of a single fault, it is likely that the Southern and Central Toroweap sections collectively make up this 100 km segment. The next segment to the north, the Central Segment, is located within the bounds of the Northern Toroweap section and has intermediate displacement. This segment is around half the length of the Northern Toroweap section and is bounded by two areas of the fault that exhibit significant splays. The final segment, the Northern Segment, has the highest displacement values observed for the fault system. The displacement for this segment does not taper off at the northern traced extent of the fault which suggests that it is longer than 122 km based on displacement-distance relationships for faults. In general, from a map view perspective, it is apparent that the segment boundaries from this study more-so align with zones of the fault that that have a hard-linked geometry (**Figure 19**). Additionally, plotting these segment boundaries along the displacement gradient (**Figure 20**) shows that the redefined segment boundaries coincide with displacement minima observed at linkage zones. Unlike the previously characterized segments, these redefined segment boundaries reveal the relative timing of fault linkage. The northern boundary of the Central Segment has a greater displacement minimum than its southern segment boundary which indicates that this segment had already linked with the Northern Segment prior to linking with the Southern Segment.

NORTHERN TERMINUS

As aforementioned, the Sevier-Toroweap fault zone can be confidently traced all the way northward from southwestern Arizona to the southern Marysvale volcanic field in southwestern

Utah, but there is uncertainty in how far north into the volcanic field the fault extends. However, the displacement-distance analysis previously described would suggest that the fault likely cannot terminate where it is currently mapped but may extend tens of kilometers farther north. Davis (1999) notes that once the fault system bisects the volcanic field, the fault loses its distinct trace. The fault is likely buried underneath volcanic rocks, or the complexity of the faulting within the volcanic system and outcrop conditions conspire to make positive identification of the main trace of the Sevier fault uncertain. In this section the extent to which the Sevier-Toroweap fault system may bisect the volcanic field is investigated by first reviewing available evidence of its northern continuation and then extrapolating the displacement gradient further north to make an approximation as to how far this fault extends.

Evidence of Northern Continuation

There are various sources that provide evidence for the potential northern continuation of the Sevier-Toroweap fault zone considerably north of the southern Marysvale volcanic field. The fault system appears to follow the same structural trend as fault-bounded basins throughout the volcanic field and may potentially connect with a normal fault system as far north as Richfield, Utah (Hecker, 1993; Biek and others, 2015). It is also suggested in other studies to connect to the eastern bounding fault in Circleville Valley. Some geologic mapping also interprets the main trace of the Sevier fault extending northward as far as Richfield (Steven and others, 1990; Rowley and others, 2002) **(Figure 21)**. Considering seismic evidence, the same trend of clustered seismicity along the Northern Toroweap, and Sevier sections of the fault seems to trend consistently northward of the northern traced extent of the fault in this study, though with some suggestion of variability in its geometry through the region of Marysvale (**Figure 21**). Geologic mapping of these candidate northern extensions of the fault are often discontinuous or tentatively

linked given the extent of current mapping efforts; while some of this uncertainty may be due to the nature of the geologic outcrop exposure in the area, it may also reflect true discontinuity of the fault as it is expressed at the surface. In spite of discontinuous surface fault expression, however, the fault may be more continuous, particularly at depth, and thus still capable of propagating slip on earthquakes over a larger area than previously appreciated. This has been most recently demonstrated by instances in which previously mapped discontinuous surface traces of faults nevertheless hosted coseismic slip at depth on large, continuous, through-going rupture planes in moderate magnitude earthquakes, as in the Mw 7.3 Landers Earthquake in 1992 (Sieh and others, 1993) and Mw 6.4 and 7.1 Ridgecrest earthquake sequence in 2019 (Thompson Jobe and others, 2020). Revisiting the outcrop expression of the potential northern extensions of the Sevier fault is a worthy topic of future work.

Estimating the Extent of the Northern Segment

The displacements observed along the Northern Segment of the Sevier-Toroweap fault system, identified from the distance vs. displacement plot, demonstrates that the maxima of slip for the entire fault system (2100 m) exists at the along strike distance of 252 km (**Figure 20**). As there is no portion of the fault to the north along which the necessary decrease in displacement associated with a fault tip has yet been documented, as is required by the physical processes of normal fault growth outlined in previous sections, this would seem to imply that the fault may likely continue to the north of its currently mapped northern terminus. Extending this incomplete displacement profile over across a projected length will give us a minimal estimate of how far into the volcanic field the fault system is likely to extend.

To project the displacement profile, displacement-length relations during the growth of a fault had to be considered. The maximum displacement (D_{max}) of a fault has a power-law

relationship with horizontal fault length (L) represented by the equation $D_{max} = \gamma L^n$ (Fossen, 2016). The constant γ defines the mechanical properties of the rock material involved (Xu and others, 2005). For faults, D_{max} and L are proportional and linearly dependent and, as such, have a power law relationship with a slope of n=1 (Schultz and others, 2008). This power-law relationship is represented by straight lines in a logarithmic diagram of L plotted against D-max known as a displacement-length diagram. Plotting the estimated values for D_{max} and L for the northern segment will help determine if the displacement-length relationship is consistent with values for other faults studied.

As previously discussed in the Displacement vs. Distance Plots Description subsection in the Methods section, it is known that the maximum displacement is typically located halfway along the strike distance of a fault. The expected length of the Northern Segment is 204 km based on the 102 km half-length to the apparent maximum of 2100 m at an along-strike distance of 252 km. Plotting the expected length and maximum displacement on a displacement-length diagram with field data results for other studied faults (**Figure 22**) helps to validate this relationship as it falls within the trend of other faults. It is expected that the fault continues at least 77 km past the northern extent that was traced for this fault system. Following the trend of fault bounded basins and seismicity would extend the Northern Segment of the Sevier-Toroweap fault system though the Marysvale volcanic field, placing the terminus of the Northern Segment 12 km south of Richfield in the Sevier Valley.

Continuation of the plausible northern extension of the fault through the Marysvale volcanic field, and the geologic challenges associated with mapping the fault through this area, are demonstrated by the detailed mapping of the central portion of the Marysvale volcanic field by Rowley and others, (2002). From this mapping, several hints to the location of the main

strand of the Sevier fault through this area are in evidence, including the alignment of basins with quaternary fill along-strike with the previously mapped termination of the fault system in the eastern portion of the map area, and notable offset of distinguishable Tertiary volcanic units, such as mafic basalt flows of the Gunsight Flats and the Marysvale intracaldara series and folding of layers toward the fault in a graben and half-graben style geometry as illustrated in their cross section (though it is difficult to disambiguate fault slip-related tilting from primary variations in dip associated with the formation and collapse of the volcanic caldera system). Despite these hints, the geologic complexity of the volcanic system, characterized by rapid lateral variations in layer thicknesses and extensive faulting evidenced by the geologic map and cross section highlights the challenge associated with using geologic mapping-based arguments alone to interpret the Sevier fault through this region, demonstrating the need to rely upon other methods, such as the displacement gradient argument laid out herein.

EARTHQUAKE HAZARD ASSESSMENT

The Sevier-Toroweap fault system is a large, multi-segment normal fault, and one of only three across which the strain associated with the Intermountain Seismic Belt is distributed, and as such its seismic hazard potential and role in the regional accommodation of active deformation in the region should be evaluated. The fault system lies in the Intermountain Seismic Belt, a zone of substantial concentrated earthquake activity (Smith and Sbar, 1974). This zone is characterized by shallow (15-20 km focal depth) and diffuse seismicity with maximum earthquake magnitudes of 7.5 to 7.75 (Arabasz and Julander, 1986). Despite the fault system's location within the zone and having Quaternary fault scarps located along its fault trace, the Sevier-Toroweap fault has had no historical surface rupture (Lund and others 2008). Instead, what seismicity has been observed are primarily small, dense clusters of seismicity observed within several of the different

fault sections. Notable clustering is present in the hanging wall of the Northern Toroweap Section, near Red Canyon, and near Panguitch around a set of Quaternary scarps in the hanging wall as reported by Lund and others (2008). Seismicity within the Central and Southern Toroweap sections are limited and may be a result of a less extensive seismic network in Arizona than in Utah where far smaller diffuse events (M <3) are seen. Since seismicity varies along the fault system, and different potential segment boundaries can rupture independently, characterizing earthquake parameters for the identified potential segment boundaries in this study will aid in proper earthquake hazard assessment. For this study, maximum earthquake magnitude calculations for each of the identified potential fault segments are assessed.

The maximum magnitude of an earthquake that a fault may generate is a function of the area of the fault within the seismogenic brittle portion of the crust; this area is therefore a function of the thickness of the brittle crust, the dip and trajectory of the fault through the crust, and its strike length. The magnitude and area are related conceptually through assumptions of smoothly varying slip on an idealized elliptical fault, and through empirical relationships derived from global compilations of seismic sources (Wells and Coppersmith, 1994, data from which is integrated and expanded in Hanks and Bakun (2008)). We utilize the empirical relationships, characterized by the following equations, from Hanks and Bakun (2008):

$$M_w = 3.98 + \log(A) \text{ for } A \leq 537 \text{ km}^2 \quad (1)$$

$$M_w = 3.07 + (4/3)\log(A) \text{ for } A \geq 537 \text{ km}^2 \quad (2)$$

where M_w represents the earthquake magnitude and A represents the fault area in square kilometers, to estimate the maximum magnitude of events that could be hosted on the Sevier-Toroweap fault system. Because of the segmentation documented in previous sections of this study, single segment and multi-segment rupture scenarios are considered, as are the implications

of the potential northward extension of the fault beyond its mapped location. Fault areas are determined from geologic mapping of the trace length of the faults, fault dips as inferred from the previously described cross sections, and maximum thickness of the crust inferred from cross sections and regional maximum depth of seismicity (~20 km). From these areas, maximum magnitudes associated with each fault rupture scenario are outlined in **Table 2**. Furthermore, average displacement associated with such an event, d_{avg}, may be inferred from the following empirical scaling from Biasi and Weldon (2006):

$$Mw=6.92 + 1.14\log(d_{avg}) \quad (3)$$

Given the slip rate on the fault of (X), taken from values in **Table 1**, potential recurrence interval ranges for associated fault segments with these average displacements and associated maximum magnitudes may also be calculated, and these are reported in **Table 2.** These estimates highlight the seismogenic potential of such a large fault system in generating rare, but potentially large (M_w 7-8), earthquakes within the Intermountain Seismic Belt, which would have regional hazard implications. The magnitudes calculated in **Table 2** for one- and two- segment scenarios fall within the range of events that are observed in the Basin and Range such as, for example, the 1872 M_w 7.6 Owens Valley earthquake (Hough and Hutton, 2008), and the M_w 7.5 Sonora, Mexico, earthquake (Suter, 2015). The three-segment and full fault system rupture scenarios are unlikely considering earthquakes of those magnitude very rarely occur in the in the region. Additionally, historical ruptures for similar normal fault systems have only occurred on segments that are 102 km or less (Valentini and others, 2020). The historical data set they use to form this conclusion (from Wells, 2013) is limited and they note that it may not accurately constrain the maximum magnitude of events in the region. Even still, the magnitudes of the three segment and full fault system rupture scenarios require fault lengths well over 102 km. In general, the one and

two segment rupture scenarios are the most realistic scenarios when assessing seismic hazard. The similarly large and active Hurricane Fault system to the west and Paunsaugunt fault system to the east present similar seismic hazard potential, and so further detailed characterization of the relative partitioning of slip between these faults will prove beneficial in better understanding the seismic hazard in this region.

FAULTING AND VOLCANISM IN THE UINKARET FIELD

Though not the primary focus of this study, the process of map compilation and cross section construction undertaken in this study illuminated the relationship between the Toroweap segment of the fault and the alignment of volcanic vents in the Uinkaret volcanic field, which has been noted in the past but is revisited here for further discussion. Map data from the Mount Trumbull 30' x 60' (Billingsley and Wellmeyer, 2003, **Figure 23A**), demonstrate that the volcanic vents of the Uinkaret volcanic field are offset from, but aligned with, the main trace of the Toroweap fault in north of the Grand Canyon. The alignment of the trends of these features had been noted by previous authors (Dutton, 1882) and Koons (1945), but it was further noted that the vents lie aligned with, but between, the main faults, and are therefore independent (Best and Brimhall, 1970), despite the widely noted fact that both the faulting and volcanism are active at the same time. The applicability of inclined shear to interpreting the rollover geometry of the half-grabens that form overlying the Sevier-Toroweap fault due to extensional fault-related folding in the cross sections included in this study implies that the hanging wall of this fault system is strained in a distributed manner. Such strain may take the form of either distributed folding or, more commonly, second-order faulting (McClay, 1990, Xiao and Suppe, 1992 and others), which is often sub-parallel to the main strand of the fault. These second order faults are mapped in the excellent outcrop exposures along the Colorado River (Billingsley and

Wellmeyer, 2003, **Figure 23A**) and surely extend beyond those mapped locations along-strike throughout the hanging wall of the Toroweap fault. Such second-order normal faults, particularly in the position of a rollover, tend to have high dilation tendency and therefore fluid conductivity (for example, Siler and others, 2019) which may be further enhanced at this location due to stress field interference due to the close proximity of the Hurricane Fault. Such distributed normal faults in the hanging wall, and favorable dilatancy, have likely served to localize and provide conduits for the extrusive volcanism observed in the Uinkaret field (**Figure 23B**). Such relationships between fault geometry, hanging-wall strain and second-order faulting, and volcanic vent alignment is supported from past studies, although these relationships are widely interpreted/inferred. Some of these studies, which provide evidence for fault geometry controlling volcanism (Weaver and others, 1987; MacLeod and Sherrod, 1988; Parsons and Thompson, 1991; Casey and others, 2006; Valentine and Krogh, 2006; Ruch and others, 2010; Kokkalas and Aydin, 2013; Muirhead and others, 2015), are supportive of the general idea that faults provide conduits for magma traversal through the crust. Other studies, on the otherhand, argue that the regional tectonic stress state is the prevailing control on magma ascension (e.g., Heath and others, 2021). This makes sense considering the N-S orientation of the vents and Toroweap fault and the E-W extension inferred from geodesy for the area. However, for this study, I argue that because the Hurricane fault is in close proximity to the Toroweap fault, and the Hurricane fault has a significantly different strike, the local stress field in this area would be modified from the regional tectonic stress which suggests that the alignment of vents with the Toroweap fault in this area may be a reflection of a more local structural control.

CONCLUSIONS

The Sevier-Toroweap fault system is a long geometrically segmented fault located within the Colorado Plateau-Basin and Range Transition Zone. Growth and development of this fault over time involved linkage of shorter segments to form longer composite faults. Along-strike geometry and displacement variations of the fault system reflect its growth and linkage history while it's subsurface geometry helps demonstrate the fault's trajectory at depth, both of which are important in seismic hazard assessment. For this study the net slip distribution was investigated to reveal fault linkage zones and patterns. Additional, studying net slip distribution helped shed light on the nature of the fault systems as it interacts with the Marysvale volcanic field.

Displacement vs. distance plots were developed for each inferred segment boundary of the fault from past studies. Displacements values for these plots came from a culmination of displacement measurements from USGS maps and literature. Through rigorous data compilation of geologic constraints from published USGS maps and extrapolated thickness estimates of regional stratigraphic units, six cross sections were constructed at key locations within fault segments to help better constrain the geometry of the fault system at depth, which in effect, helped constrain estimates of slip. The Sevier-Toroweap fault is modeled in cross section view as a multi bend fault that shallows at depth. The high slip measurements from these cross sections suggest that displacement along the fault trace may be systematically higher than what has been previously reported.

Three major fault segments for the Sevier-Toroweap fault system were identified and characterized from variations in fault strike, locations of fault splays, and displacement gradients along strike. The Southern Segment extends for all of what had previously been described in the

literature as the Southern and Central Toroweap sections. The Central Segment is bounded by two major splays in the fault system in an area that was previously defined as the Northern Toroweap Section. The final segment, the Northern Segment, continues from this point and is proposed in this study to extend 77 km north of the northernmost currently mapped trace of the fault system. This would extend the trace of the fault through the Marysvale volcanic field where it is thought to continue but be obscured due to outcrop conditions and geologic complexity within the volcanic system.

Additional discussion topics were seismic hazard evaluation and the relationship of volcanism and faulting in the Uinkaret volcanic field. Seismic hazard evaluation was conducted by calculating the maximum magnitude and recurrence interval for each of the newly defined segments based on their segment length and fault area. Rupture scenarios were also done for multisegment ruptures. In general, one- and two- segment scenarios gave realistic magnitude estimates based on the historical earthquake activity in the basin and range as well as normal faulting in similar systems. The main conclusion from the discussion on volcanism and faulting in the Uinkaret volcanic field was that due to the differing strike of Hurricane fault as well as its proximity to the Toroweap fault within the volcanic field, the local stress field would be different from regional tectonic stresses suggesting that faults act as a primary control in vent alignment.

APPENDIX – DESCRIPTIONS AND EXTRAPOLATED THICKNESSES OF STRATAGRAPHIC UNITS

Tapeats Sandstone (lower to middle Cambrian) – At the base of the Tonto Group is the Tapeats Sandstone which consists of a massive cliff-forming sandstone. The thickness of this formation varies due to the topographic relief of the underlying Precambrian surface as well as changes in the shoreline during the transgressive sequence of the Tapeats sea (Metzger, 1961).

The Tapeats Sandstone has variable thicknesses in the region but is typically thinnest in areas where it pinches out against elevated Proterozoic formations (Billingsley and others, 2006a). Within the Peach Springs 30' x 60' Quadrangle, the exposed formation ranges in thickness from 0 to 60 m (Billingsley and others, 2006a). The average thickness of this formation near the fault on a cross section from Billingsley and others (2006a) is 56 m which is the value used for the formation in columns C1 and C2 in **Figure 4**. Within the Mount Trumbull 30' x 60' Quadrangle, the exposed formation ranges in thickness from 0 to 122 m (Billingsley and Wellmeyer, 2003). The average thickness of this formation near the fault on a cross section from Billingsley and others, (2003) is 80 m which is the value used for the formation in columns C3 and C4 in **Figure 4**. Within the Fredonia 30' x 60' Quadrangle (Billingsley and others, 2008), the formation is buried but a thickness range of 0 to 60 m is assumed based on exposures in the Grand Canyon (Billingsley and Workman, 2000). Using this information, thickness values of 49 and 43 m were calculated for columns C5 and C6 respectively in **Figure 4**. Within the Jarvis Peak Quadrangle in Washington County, Utah, the formation is 400 m thick in the northern and eastern Beaver Dam Mountains (Hammond, 1991). A much lower thickness of 88 m was obtained from the Tidewater Co Utah Fed A-1 Well in Kane County, Utah (Munger and others,

1965). Using this information, thickness values of 200, 160, and 138 m were calculated for columns C7, C8, and C9 respectively in **Figure 4.**

Bright Angel Shale (middle Cambrian) – Next in the Tonto Group is the gradationally overlying Bright Angel Shale, a slope forming shale and siltstone unit. This formation interlocks with the overlying Muav Limestone to form several tongues (Karlstrom and others, 2020). The gradational contact, facies changes, and intertonguing characteristics of this formation are what govern its thickness variations (Mckee & Resser, 1945). In general, the Formation thickens westward (Karlstrom and others, 2020).

The Bright Angle Shale has varying thickness trends across fault sections. Within the Peach Springs 30' x 60' Quadrangle, the exposed Bright Angel Shale ranges in thickness from 92 to 107 m (Billingsley and others, 2006a). Assuming a westward thickening trend, thickness values of 95 and 94 m were calculated for columns C1 and C2 respectively in **Figure 4**. Within the Mount Trumbull 30' x 60' Quadrangle, the exposed Bright Angel Shale has a reported thickness of 150 m but is expected to have variable thickness trends due to intertonguing relations (Billingsley and Wellmeyer, 2003). This thickness value is used for columns C3 and C4 (**Figure 4**). Within the Fredonia 30' x 60' Quadrangle (Billingsley and others, 2008), the formation is buried but a thickness range of 60 to 90 m is assumed based on exposures in the Grand Canyon (Billingsley and Workman, 2000). Assuming a westward thickening, thickness values of 84 and 82 m were calculated for columns C5 and C6, respectively. In Kane County, Utah, petroleum exploration wells reveal a westward thickening trend from the East Kaibab Monocline (98 m) to the eastern edge of the Coral Pink Bench and Canyonlands (105 m) as described in Doelling and others (1989). Using this trend, thickness values of 105 and 102 m were calculated for columns C7 and C8, respectively (**Figure 4**). In Garfield County, Utah,

Doelling (1975) estimated a westward thickening trend ranging from 82 to 103 m thick. Using this trend, a thickness value of 102 m was calculated for column C9 (**Figure 4**).

Muav Limestone (middle Cambrian) – the final formation in this sequence is the gradationally overlying Muav Limestone, a limestone and dolomite unit that forms resistant cliffs. This formation has a prominent westward thickening trend (Metzger, 1961).

The Muav Limestone has varying thickness trends across fault sections. Within the Peach Springs 30' x 60' Quadrangle, the exposed Muav Limestone ranges in thickness from 365 to 427 m and thickens westward (Billingsley and others, 2006a). Using this trend, thickness values of 379 and 372 m were calculated for columns C1 and C2 respectively in **Figure 4**. Within the Mount Trumbull 30' x 60' Quadrangle, the exposed Muav Limestone ranges in thickness from 185 to 425 m and thickens westward (Billingsley and Wellmeyer, 2003). Using this trend, thickness values of 202 and 194 m were calculated for columns C3 and C4, respectively (**Figure 4**). Within the Fredonia 30' x 60' Quadrangle (Billingsley and others, 2008), the formation is buried but a thickness range of 24 to 213 m and a westward thickening trend is assumed based on exposures in the Grand Canyon (Billingsley and Workman, 2000). Using this trend, thickness values of 178 and 160 m were calculated for columns C5 and C6, respectively (**Figure 4**). In Kane County, Utah, petroleum exploration wells reveal a westward thickening trend from the East Kaibab Monocline (341 m) to the eastern edge of the Coral Pink Bench and Canyonlands (375 m) as described in Doelling and others (1989). Using this trend, thickness values of 370, 374, and 353 meters were calculated for columns C7, C8, and C9, respectively (**Figure 4**).

Temple Butte - Elbert Formation (middle to upper Devonian) – The remnant uneroded Temple Butte - Elbert Formations, consists mostly of ledge-forming dolomite with some less resistant limestone. The formation generally thickens to the west and north (Heckert and Lucas,

2005). This increased thickening represents an advance to a paleogeographic shelf edge along the eastern flank of the Cordilleran miogeocline (Beus, 1989).

The Temple Butte - Elbert Formation has varying thickness trends across fault sections. Within the Peach Springs 30' x 60' Quadrangle, the exposed Temple Butte - Elbert Formation ranges in thickness from 122 to 140 m and thickens westward and northward (Billingsley and others, 2006a). Using this trend, thickness values of 126 and 124 m were calculated for columns C1 and C2 respectively in **Figure 4**. Within the Mount Trumbull 30' x 60' Quadrangle, the exposed Temple Butte - Elbert Formation ranges in thickness from 84 to 140 m and thickens westward (Billingsley and Wellmeyer, 2003). Using this trend, thickness values of 88 and 86 m were calculated for columns C3 and C4, respectively (**Figure 4**). Within the Fredonia 30' x 60' Quadrangle (Billingsley and others, 2008), the formation is buried but a thickness range of 24 to 106 m and a westward thickening trend is assumed based on exposures in the Grand Canyon (Billingsley and Workman, 2000). Using this trend, thickness values of 83 and 88 m were calculated for columns C5 and C6, respectively (**Figure 4**). Within Kane County, Utah, an isopach map of the formation (Doelling and others, 1989, p. 23) was used to calculate thicknesses of 127 and 61 m for columns C7 and C8, respectively (**Figure 4**). Within Garfield County, Utah, the formation is undifferentiated from the overlying Ouray formation as reported from several petroleum exploration wells (Doelling, 1975). An average combined thickness of 152 m is used for both formations in column C9 (**Figure 4**).

Ouray Formation (Late Devonian to Lower Mississippian) – The Ouray Formation in Utah consists of limestone, dolomite, and some shale. In southwest Kane County, the formation is eroded away as part of the Mississippian unconformity. In general, the formation thickens to the northeast (Doelling and others, 1989).

The Ouray Formation varies in thickness across the fault system. Within Kane County, Utah, the buried formation ranges in thickness 0 to 49 m and thickens to the northeast (Doelling and others, 1989). Using this trend, a thickness value of 15 m was calculated for column C8 (**Figure 4**). Within Garfield County, Utah, as stated previously, the Ouray and Temple Butte - Elbert Formations are reported undifferentiated in petroleum exploration wells (Doelling, 1975). An average combined thickness of 152 m is used for both formations in column C9 (**Figure 4**).

Redwall Limestone (Lower and Upper Mississippian) – The unconformably overlying Redwall Limestone is a multi-member formation consisting of mostly cliff-forming limestone. Dissolution of this limestone after it was deposited created a karst topography (Blakely and Middleton, 2012), which contributes to thickness variation in the formation. The formation, in general, thickens to the west and northwest.

Within the Peach Springs 30’ x 60’ Quadrangle, which covers the Southern Toroweap Section, the Redwall Limestone has a thickness trend defined by its members (Billingsley and others, 2006a). The Horeshoe Mesa Member has a thickness that ranges from 14 to 30 m and thickens westward. The Mooney Falls Member ranges in thickness from 92 to 122 m and thickens northwestward. The Thunder Springs Member ranges in thickness from 30 to 46 m and thickens westward. The final member, the Whitmore Wash Member has a consistent thickness of 24.5 m in the quadrangle. Using these individual trends, entire formation thicknesses of 178 and 177 m were calculated for columns C1 and C2 respectively in **Figure 4**.

For the Central and Northern Toroweap sections of the fault, the Redwall Limestone exhibits variable thickness trends. Within the Mount Trumbull 30’ x 60’ Quadrangle, the exposed Redwall Limestone ranges in thickness from 183 to 243 m and thickens westward (Billingsley and Wellmeyer, 2003). Using this trend, thickness values of 187 and 185 m were

calculated for columns C3 and C4, respectively (**Figure 4**). Within the Fredonia 30' x 60' Quadrangle, the Redwall Limestone has a thickness trend defined by its members (Billingsley and others, 2008). Although lateral thickness trends for each member are not defined in Billingsley and others (2008), it is expected that these members thicken west based on regional trends. The Horseshoe Mesa Member ranges in thickness from 14 to 30 m. The Mooney Falls member keeps a uniform thickness of 122 m. The Thunder Springs Member ranges in thickness from 30 to 46 m. The final member, the Whitmore Wash Member, keeps a uniform thickness of 24.5 m. Using this information, entire formation thicknesses of 216 and 210 m were calculated for columns C5 and C6, respectively (**Figure 4**).

For the Sevier section, the Redwall Limestone also exhibits variable thickness trends. In Kane County, Utah, which covers half of the Sevier section, petroleum exploration wells reveal a west and northwest thickening trend from the East Kaibab Monocline (188 m) to the eastern edge of the Coral Pink Bench and Canyonlands (285 m) as described in Doelling and others (1989). Using this trend, thickness values of 261 and 253 m were calculated for columns C7 and C8, respectively (**Figure 4**). In Garfield County, Utah, the formation has a thickness range of 152 to 366 m and thickens northwestward (Doelling, 1975). Using this trend, a thickness of 337 m was calculated for column C9 (**Figure 4**).

Surprise Canyon Formation (Upper Mississippian) – The final formation from this time frame is the Surprise Canyon Formation, a slope-forming siltstone and sandstone, with some dolomite, limestone, and conglomerate. This formation is not consistent throughout published cross sections and mostly appears in the karst dissolved depressions, paleochannels and paleovalleys of the Redwall Limestone. Due to its highly irregular deposition, this formation was not included in **Figure 4**.

The Surprise Canyon Formation has varying thickness trends across fault sections. Within the Peach Springs 30’ x 60’ Quadrangle (Billingsley and others 2006a) and Mount Trumbull 30’ x 60’ Quadrangle (Billingsley and Wellmeyer, 2003), which covers the Southern and Central Toroweap sections respectively, the Surprise Canyon Formation ranges in thickness from 0 to 122 m with accumulations that thicken westward.

Watahomigi Formation (Upper Mississpian to Lower Pennsylvanian) – The Watahomigi Formation is composed of ledge and slope-forming limestone, slope-forming siltstone, slope-forming mudstone, and conglomerate (Billingsley and others, 2006a). Limestone beds in this formation thin to the east, possibly because of a facies change from limestone to clay rich mudstone (Mckee, 1982). Regionally, this formation is progressively thinner to the east due to relief of the Redwall surface (Mckee, 1982).

The Watahomigi Formation has varying thickness trends across Arizona fault sections. Within the Peach Springs 30’ x 60’ Quadrangle, the Watahomigi Formation ranges in thickness from 30 to 60 m and thickens westward (Billingsley and others, 2006a). Using this trend, thickness values of 38 and 32 m were calculated for columns C1 and C2 respectively in **Figure 4**. Within the Mount Trumbull 30’ x 60’ Quadrangle, the exposed Watahomigi Formation ranges in thickness from 30 to 60 m and thickens westward towards the Grand Wash Cliffs (Billingsley and Wellmeyer, 2003). Using this trend, thickness values of 32 and 31 m were calculated for columns C3 and C4, respectively (**Figure 4**). Within the Fredonia 30’ x 60’ Quadrangle, the Watahomigi Formation ranges in thickness from 30 to 40 m (Billingsley and others, 2008) and is assumed to thicken westward based on regional trends. Using this trend, thickness values of 38 and 37 m were calculated for columns C5 and C6, respectively (**Figure 4**).

Manakacha Formation (Middle Pennsylvanian) – The unconformably overlying Manakacha Formation consists of cliff-forming sandstone, slope-forming siltstone, cliff and ledge-forming limestone, and slope-forming mudstone (Billingsley and others, 2006a). This formation is at its thickest in the eastern Grand Canyon and tends to thin in all directions from this point (Mckee, 1982).

The Manakacha Formation has consistent thickness throughout Arizona fault sections. Within the Peach Springs 30' x 60' Quadrangle (Billingsley and others, 2006a), Mount Trumbull 30' x 60' Quadrangle (Billingsley and Wellmeyer, 2003), and Fredonia 30' x 60' Quadrangle (Billingsley and others, 2008), the thickness of the Manakacha Formation is consistently reported as 55 m. This thickness value is used for columns C1 – C6 in **Figure 4**.

Wescogame Formation (Upper Pennsylvanian) – The unconformably overlying Wescogame Formation consists of cliff and slope-forming sandstone, dolomitic sandstone, slope-forming siltstone, slope-forming mudstone, and conglomerate (Billingsley and others, 2006a). The formation generally thickens to the southeast in the Grand Canyon region (Mckee, 1982).

The Wescogame Formation has varying thickness trends across Arizona fault sections. Within the Peach Springs 30' x 60' Quadrangle, the Wescogame Formation has a uniform thickness of 40 m (Billingsley and others, 2006a). This thickness value is used in columns C1 and C2 in **Figure 4**. Within the Mount Trumbull 30' x 60' Quadrangle, the exposed Wescogame Formation ranges in thickness from 40 to 64 m and thickens westward (Billingsley and Wellmeyer, 2003). Using this trend, thickness values of 42 and 41 m were calculated for columns C3 and C4, respectively (**Figure 4**). Within the Fredonia 30' x 60' Quadrangle, the

formation has an average thickness of 40 m (Billingsley and others, 2008). This thickness value is used in columns C5 and C6 (**Figure 4**).

Esplanade Sandstone (Lower Permian) – The uncomformably overlying final formation in this group, the Esplanade Sandstone has cliff and slope components composed of various sandstones, siltstones, gypsum, sandy limestone, and limestone pebble conglomerates (Billingsley and others, 2006a). This formation typically has a westward thickening trend but will thicken west, north, and northwest (Mckee, 1982).

The Esplanade Sandstone has varying thickness trends across Arizona fault sections. Within the Peach Springs 30' x 60' Quadrangle, the Esplanade Sandstone has a uniform thickness of 152 m (Billingsley and others, 2006a). This thickness value is used for columns C1 and C2 in **Figure 4**. Within the Mount Trumbull 30' x 60' Quadrangle, the exposed Esplanade Sandstone ranges in thickness from 107 to 167 m and thickens eastward (Billingsley and Wellmeyer, 2003). Using this trend, thickness values of 163 and 165 m were calculated for columns C3 and C4, respectively (**Figure 4**). Within the Fredonia 30' x 60' Quadrangle, the formation ranges in thickness from 122 to 137 m (Billingsley and others, 2008) and is assumed to thicken westward based on regional trends. Using this trend, thickness values of 134 and 133 m were calculated for columns C5 and C6, respectively (**Figure 4**).

Queantoweap (Lower Permian) – The Queantoweap Sandstone consists of ledge-forming sandstone, with some silty sandstone beds, and slope-forming gypsum (Billingsley and Workman, 2000). This formation is coeval to the Esplanade Sandstone and is located in northwestern Arizona and southwestern Utah. The unit regionally thickens west and northwestward (Blakey, 1988).

The Queantoweap Sandstone has varying thickness trends across the southern half of the Sevier section. In Kane County, Utah, the formation ranges in thickness from 183 m in the southwestern portion to 335 m in the eastern portion (Doelling and others, 1989). Using this trend, thickness values of 196 and 207 m were calculated for columns C7 and C8 respectively in **Figure 4**.

Cedar Mesa Sandstone (Lower Permian) – The Cedar Mesa Sandstone consists of ledge-forming sandstone, with some silty sandstone beds, and slope-forming gypsum (Billingsley and Workman, 2000). This formation is also coeval to the Esplanade Sandstone and is located in south central and southeastern Utah. Regionally, the formation is thickest in the northern half of Kane County and southern half of Garfield County and thins north and south of this area northwestward (Blakey, 1988).

The Cedar Mesa Sandstone has varying thicknesses trends across the northern half of the Sevier Section. Based on an isopach map of the area (Blakey, 1988, p. 131), a thickness value of 286 m was calculated for column C9 (**Figure 4**). C9 is located near an approximate depositional boundary for the formation as defined in Blakey, (1988). As a result, the formation may be absent from this area or significantly thinner than what is calculated.

Hermit Formation (Lower Permian) – The Hermit Formation is a siltstone and sandstone formation where the siltstone beds are weak and erosion prone. Sandstone beds in this formation thicken or thin laterally (Billingsley and others, 2006a) while the entire formation thins to the southeast (Blakey, 1990). Westward thickening in this formation is a result of a facies change from deltaic to marine-shoreline lithologies (Billingsley & Wellmeyer, 2003).

The Hermit Formation has varying thickness trends across fault sections. Within the Peach Springs 30’ x 60’ Quadrangle, the Hermit Formation ranges in thickness from 30 to 213 m

and thickens to the north, northwest, and northeast while thinning east, southeast, and south (Billingsley and others, 2006a). Using this trend, thickness values of 114 and 213 m were calculated for columns C1 and C2 respectively in **Figure 4**. Within the Mount Trumbull 30' x 60' Quadrangle, the exposed Hermit Formation ranges in thickness from 213 to 260 m and thickens westward towards the Grand Wash Cliffs (Billingsley and Wellmeyer,2003). Using this trend, thickness values of 216 and 215 m were calculated for columns for columns C3 and C4, respectively (**Figure 4**). Within the Fredonia 30' x 60' Quadrangle, the formation ranges in thickness from 150 to 340 m and thickens westward and northward (Billingsley and others, 2008). Using this trend, thickness values of 264 and 299 m were calculated for columns C5 and C6, respectively (**Figure 4**). Within Kane County, Utah, the formation ranges in thickness from 32 to 190 m and thickens southward and southwestward (Doelling and others, 1989). Using this trend, thickness values of 152 and 95 m were calculated for columns C7 and C8, respectively (**Figure 4**). Based on a regional isopach map of the Hermit formation (Baars, 1962, p. 188), a thickness value of 20 m was calculated for column C9 (**Figure 4**) in the northernmost Sevier section.

Coconino Sandstone (Lower Permian) – The unconformably overlying Coconino Sandstone is a quartz sandstone that forms resistant cliffs and slopes. This formation is widely exposed in Arizona but thins northwestward to a few meters around the Nevada and Utah borders (Reiche, 1938).

The Coconino Sandstone has varying thickness trends across fault sections. Within the Peach Springs 30' x 60' Quadrangle, the Coconino Sandstone ranges in thickness from 0 to 52 m and thickens to the southeast, east, and northeast and pinches out around the southern edge of the Shivwits Plateau (Billingsley and others, 2006a). Using this trend, thickness values of 39 and 45

m were calculated for columns C1 and C2 respectively in **Figure 4**. Within the Mount Trumbull 30’ x 60’ Quadrangle, the exposed Coconino Sandstone ranges in thickness from 3 to 47 m and thins westward (Billingsley and Wellmeyer, 2003). Using this trend, thickness values of 41 and 46 m were calculated for columns C3 and C4, respectively (**Figure 4**). Within the Fredonia 30’ x 60’ Quadrangle, the formation ranges in thickness from 0 to 52 m and thickens southeast of the fault trace while pinching out toward the northwest corner (Billingsley and others, 2008). Using this trend, thickness values of 10 and 8 m were calculated for columns C5 and C6, respectively (**Figure 4**). In Garfield County, Utah, wells in the southwestern portion have reported Coconino thicknesses of less than 8 m (Doelling and others, 1989). Since wells in area of the county are located in proximity to the fault trace, a thickness value of 8 m is used for column C7 (**Figure 4**). In the northern half of the county the formation is reported to be very thin or absent and in the north central portion it is less than 15 m (Doelling and others, 1989). Using this information, a thickness value of 2 m was calculated for column C8 (**Figure 4**).

Toroweap Formation (Lower Permian) – The unconformably overlying Toroweap Formation contains siltstone, sandstone, gypsum, limestone, and dolomite. Gypsum dissolution in the uppermost member of the formation (Woods Ranch Member) contributes to variable thickness trends (Billingsley and others, 2006a). In general, the Toroweap Formation thickens to the north, northwest, and west, while pinching out to the east and thinning south (Karlstrom and others, 1974). the formation thickens to the west based on an isopach map from Evans, (1971).

Within the Peach Springs 30’ x 60’ Quadrangle, which covers the Southern Toroweap Section, the exposed Toroweap Formation has a thickness trend defined by its members (Billingsley and others, 2006a). The Woods Ranch Member ranges in thickness from 18 to 30 m thick and thickens northward and northwestward. The Brady Canyon Member is 76 m thick

along the Coconino Plateau and 110 m thick along the Shivwits Plateau. The member thickens westward and northwestward. The final member, the Seligman Member, is 4.5 to 12 m thick and thickens northward and northwestward. Using these individual thickness trends, total formation thicknesses of 118 and 103 m were calculated for columns C1 and C2 respectively in **Figure 4**.

Within the Mount Trumbull 30' x 60' Quadrangle, which covers the Central Toroweap Section, the exposed Toroweap Formation has a thickness trend defined by its members (Billingsley and Wellmeyer, 2003). The Woods Ranch Member ranges in thickness from 18 to 60 m and thickens northward. The Brady Canyon Member has a thickness ranging from 40 to 137 m and thickens westward towards the Grand Wash Cliffs. The final member, the Seligman Member, has a thickness that ranges from 10 to 17 m and thickens northward. Using these individual thickness trends, total formation thicknesses of 93 and 113 m were calculated for columns C3 and C4, respectively (**Figure 4**).

Within the Fredonia 30' x 60' Quadrangle, which covers the majority of the Northern Toroweap section, the exposed Toroweap Formation has a thickness trend defined by its members (Billingsley and others, 2008). The Woods Ranch Member ranges in thickness from 49 to 81 m and has local variations in thickness due to gypsum dissolution. The Brady Canyon Member ranges in thickness from 30 to 70 m and thickens westward and southward. The final member, the Seligman Member, ranges in thickness from 6 to 51 m and thickens westward. Using these individual trends, total formation thicknesses of 137 and 194 m were calculated for columns C5 and C6, respectively (**Figure 4**).

For the remaining sections of the fault trace, the Toroweap formation has variable thickness trends. In Kane County, Utah, petroleum exploration wells reveal a westward thickening trend from the East Kaibab Monocline (101 m) to the eastern edge of the Coral Pink

Bench and Canyonlands (135 m) as described in Doelling and others (1989). Using this trend, thickness values of 135 and 129 m were calculated for columns C7 and C8, respectively (**Figure 4**). Within Garfield County, Utah, the formation is 122 m thick at Upper Valley oil field (Doelling and others, 1989). Using this thickness and the Coral Pink Bench and Canyonlands thickness (135 m), a thickness value of 128 m was calculated for column C9 (**Figure 4**).

Kaibab Formation (Lower Permian) – The final formation in the Paleozoic sequence, the unconformably overlying Kaibab Formation, contains slope-forming gypsum, siltstone, sandstone, limestone, chert breccia beds specific to the Toroweap Fault, and cliff-forming cherty limestone (Billingsley and others, 2006a). The formation thins to the east towards the paleo-coastline of a shallow sea as part of an eastward transgression (Mckee, 1938; Norton, 1990).

Within the Peach Springs 30' x 60' Quadrangle, which covers the Southern Toroweap Section, the Kaibab Formation has a thickness trend best defined by its members (Billingsley and others, 2006a). The upper member, the Harrisburg member, is 38 to 50 m thick and thickens eastward and northeastward. The lower member, the Fossil Mountain Member, ranges in thickness from 40 to 107 m. No specific thickness trends for this quadrangle were given but the member generally thickens westward while thinning eastward and northeastward (Hopkins and Thompson, 2003). Using these trends, total formation thicknesses of 102 and 96 m were calculated for columns C1 and C2 respectively in **Figure 4**.

Within the Mount Trumbull 30' x 60' Quadrangle, which covers the Central Toroweap section, the Kaibab Formation has a thickness trend best defined by its members. The upper member, the Harrisburg member, is 0 to 80 m thick in the north half of the quadrangle and removed by erosion along the southern edge of the Shivwits Plateau (Billingsley and Wellmeyer, 2003). Along the western edge of the adjacent Grand Canyon 30' x 60' Quadrangle, this member

is 80 m thick (Billingsley and Hampton, 2000). Using this information, it is assumed that the member is near 80 m thick along the entire fault trace in this section. The lower member, the Fossil Mountain Member, ranges in thickness from 70 to 120 m and is assumed to thin eastward across the Mount Trumbull 30’ x 60’ quadrangle. Using these individual trends, total formation thicknesses of 154 and 152 m were calculated for columns C3 and C4, respectively (**Figure 4**).

Within the Fredonia 30’ x 60’ Quadrangle, which covers the majority of the Northern Toroweap section, the Kaibab Formation has a thickness trend best defined by its members (Billingsley and others, 2008). The Harrisburg Member ranges in thickness from 30 to 52 m and thickens westward. The lower member, the Fossil Mountain Member, ranges in thickness from 61 to 80 m and thickens westward. Using these individual trends, a total formation thickness of 124 m was calculated for columns C5 and C6 (**Figure 4**).

For the remaining fault sections, the Kaibab formation displays variable thickness trends. Within the Kanab 30’ x 60’ Quadrangle, the formation is suspected to range in thickness from 45 to 155 m in the subsurface (Doelling, 2008). Using this trend, thickness values of 137 and 123 m were calculated for columns C7 and C8, respectively (**Figure 4**). In Garfield County, Utah, the formation is on average 16 m thick at the Circle Cliffs uplift thickening to 146 m along the western portion of the county (Doelling, 1975). Using this trend, a thickness value of 123 m was calculated for column C9 (**Figure 4**).

Moenkopi Formation (Lower to Middle Triassic) – The Moenkopi Formation, is a multi-member unit consisting of slope and ledge-forming siltstone, slope, ledge, and cliff-forming sandstone, cliff and ledge-forming limestone, and some dolomite, gypsum, and conglomerate (Billingsley and Wellmeyer, 2003). This formation is mostly eroded from the Toroweap

segments of the fault system. In general, the formation forms a wedge that thins to east (Mckee, 1954).

Within the Mount Trumbull 30’ x 60’ Quadrangle (Billingsley and Wellmeyer, 2003), the Moenkopi Formation is mostly eroded with scattered outcrops located beneath tertiary volcanic rocks. Only one complete section was identified, located in Hells Hollow, Arizona 15 km from the main fault trace. The complete section is 365 m. Due to formation being mostly absent around the fault trace, it was not included in columns C3 and C4 in **Figure 4**.

Within the Fredonia 30’ x 60’ Quadrangle (Billingsley and others, 2008), and Geologic map of the Pipe Spring National Monument and the Western Kaibab-Paiute Indian Reservation (Billingsley and others, 2004), which collectively cover the majority of the Northern Toroweap section, the Moenkopi Formation has a thickness trend best defined by its members. However, the complete formation generally thickens northwestward. Within the Fredonia area, the uppermost member, the Upper red member, has a uniform thickness of 49 m. The Shnabkaib Member has a thickness that ranges from 27 to 114 m and thickens northwestward. The Middle red member ranges in thickness from 55 to 92 m and thickens northeasterward. The Virgin Limestone Member ranges in thickness from 0 to 25 m and thickens westward and northward of Fredonia, Arizona. The Lower red member has a thickness that ranges from 36 to 76 m and is assumed to thicken northeastward based on the formation pinching out in the southwest corner of the quadrangle. The lowermost member, the Timpoweap Member, ranges in thickness from 0 to 30 m and thickens westward. Using these individual trends, a total formation thickness of 291 m was calculated for column C5 in **Figure 4**. Within the Pipe Spring National Monument area, the Upper and Middle red members follow the same trends defined in the Fredonia area. The Shnabkaib Member is 27 to 34 m thick and thickens northwestward. The Virgin Limestone

Member has a uniform thickness of 37 m. The lowermost members, the Lower red member and Timpoweap Member, have a combined thickness that ranges from 37 to 55 m and is assumed to thicken northwestward based on the total formation thickness trend in the Fredonia area. Using these individual trends, a total formation thickness of 247 m was calculated for column C6 (**Figure 4**).

For the remaining fault sections, the Moenkopi Formation exhibits variable thickness trends. Within Kane County, Utah, the Moenkopi Formation dramatically increases in thickness to the west from 45 m near the Colorado River to 365 m along the western edge of the county (Doelling and others, 1989). Using this trend, thickness values of 328 and 300 m were calculated for columns C7 and C8 respectively in **Figure 4**. Within Garfield County, Utah, the formation is 274 m thick at the Upper Valley oil field and 366 m thick in a well 6 miles west of Bryce Canyon (Doelling, 1975). Using this trend, a thickness value of 361 m was calculated for column C9 (**Figure 4**).

Chinle Formation (Upper Triassic) – The final Triassic unit, the unconformably overlying Chinle Formation, is a multi-member unit consisting of cliff-forming sandstone, siltstone, limestone, slope-forming claystone, siltstone, and some conglomerate with chert and quartz (Billingsley and others, 2008). This formation irregularly thickens to the south and east based on isopach map from Stewart and others (1972). Westward truncation of the Chinle Formation by overlying Jurassic formations explains westward thinning trends (Blakey and others, 1989).

Within the Fredonia 30’ x 60’ Quadrangle (Billingsley and others, 2008), and Geologic map of the Pipe Spring National Monument and the Western Kaibab-Paiute Indian Reservation (Billingsley and others, 2004), which collectively cover the majority of the Northern Toroweap

section, the Chinle Formation has a thickness trend best defined by its members. Within the Fredonia area, the uppermost member, the Owl Rock Member, ranges in thickness from 9 to 18 m thick and is assumed to thin westward and southwestward based on the thickness trends from Billingsley and others, (2004). The Petrified Forest Member ranges in thickness from 183 to 213 m and is assumed to thicken southward and eastward based on regional trends. The lowermost member, the Shinarump Member, ranges in thickness from 6 to 38 m and regional thickness trends are also assumed. Using these individual trends, a total formation thickness of 244 m was calculated for column C6 in **Figure 4**.

For the remaining fault sections, the Chinle Formation exhibits variable thickness trends. Within Kane County, Utah, the Chinle Formation ranges in thickness from 141 to 156 m in petroleum exploration wells along the southern half of the fault trace (Doelling and others, 1989). Using this information, the average value of 149 m was used as the thickness value for column C7 in **Figure 4**. Additionally, a formation thickness of 245 m was measured in a well on the eastern edge of the Paunsaugunt Plateau (Doelling and others, 1989). Using this thickness and the average thickness calculated for column C7 (eastern edge of Coral Pink Bench and Canyonlands), a thickness value of 198 m was calculated for column C8 (Figure 4). In Garfield County, Utah, the formation is thinnest at Poison Spring Canyon (91m) and thickens in all directions from this point to a maximum of 229 m (Doelling, 1975). Using this trend, a thickness value of 218 m was calculated for column C9 (**Figure 4**).

Moenave Formation (Lower Jurassic) – The Moenave Formation is a multi-member formation consisting of slope and ledge-forming sandstone, siltstone, mudstone, claystone with some dolomitic limestone and chert (Billingsley and others, 2008). This unit disconformably overlies the Chinle Formation (Stewart and others, 1972) and intertongues with the overlying

Kayenta Formation (Bazard and Butler, 1991). In general, this formation thickens west to northwest (Doelling and others, 1989).

Within the Fredonia 30' x 60' Quadrangle (Billingsley and others, 2008), and Geologic map of the Pipe Spring National Monument and the Western Kaibab-Paiute Indian Reservation (Billingsley and others, 2004), which collectively cover the majority of the Northern Toroweap section, the Moenave Formation has a thickness trend best defined by its members. Within the Fredonia area, the uppermost member, the Springdale Sandstone Member ranges in thickness from 36 to 60 m and thickens north and eastward. The Whitmore Point Member ranges in thickness from 12 to 24 m and thickens westward. Within the Pipe Spring National Monument area, the lowermost member, the Dinosaur Canyon Member, ranges in thickness from 36 to 61 m and thickens to the east. Using these individual trends, a total formation thickness of 119 m was calculated for column C6 in **Figure 4**.

In the southern half of the Sevier section, the Moenave Formation exhibits variable thickness trends. The Moenave Formation, including the now removed Springdale Sandstone Member, ranges in thickness from 100 to 150 m and is thickens west and southwestward (Sable and Hereford, 2004). The removed Springdale Sandstone Member, now reassigned to the Kayenta Formation, ranges in thickness from 27 to 60 m and thickens eastward. Using this information, thickness values of 104 and 90 m were calculated for columns C7 and C8 in **Figure 4**.

Wingate Sandstone (Lower Jurassic) – The Wingate Sandstone consists of a massive cliff-forming sandstone (Doelling and others, 1989). The formation has an intertonguing relationship with the coeval Moenave Formation. In general, the formation thickens eastward (Doelling and others, 1989; Clemmensen and others, 1989). It only appears within proximity to

the fault in Garfield County, Utah. Here, the formation ranges in thickness from 61 to 122 m (Doelling, 1975) and is assumed to thicken eastward based on regional trends. Using this trend, a thickness value of 65 m was calculated for C9 in **Figure 4**.

Kayenta Formation (Lower Jurassic) – The Kayenta Formation consists of slope-forming siltstone and mudstone, cliff-forming sandstone, and some conglomerate (Billingsley and others, 2008). This formation prominently intertongues with the overlying Navajo Sandstone (Bazard & Butler, 1991). The Tenney Canyon Tongue of this formation thickens westward while the Lamb Point Tongue of the Navajo Sandstone thickens eastward (Doelling and others, 1989; Doelling, 2008). Weak siltstone in this formation tends to fail, creating landslide debris consisting of the upper portion of this formation and the Navajo Sandstone above it. In general, the formation may thin eastward based on a restored cross section from Doelling and others (1989).

The Kayenta Formation has varying thickness trends across fault sections. Within the Geologic map of the Pipe Spring National Monument and the Western Kaibab-Paiute Indian Reservation, the Kayenta Formation is 82 m thick at Ed Lamb Point, Moquith Mountains, and 122 m thick at Potter Canyon, Arizona (Billingsley and others, 2004). Using this trend, a thickness value of 97 m was calculated for column C6 in **Figure 4**. Within the Kanab 30’ x 60’ Quadrangle, the formation is 35 – 45 m thick in the south-central portions and thickens to 200 m thick in the westernmost portion (Sable and Hereford, 2004). Using this trend, thickness values of 88 and 91 m were calculated for columns C7 and C8, respectively (**Figure 4**). In Garfield County, Utah the maximum thickness measured for this formation is 107 m (Doelling, 1975). 50 km west of the column C9 location, a 97 m thickness was measured in a petroleum exploration well. Using this information and assuming a westward thickening trend, a thickness value of 105 m was calculated for column C9 (**Figure 4**).

The prominent Tenney Canyon Tongue of the Kayenta Formation has its own individual thickness trends. Within the Geologic map of the Pipe Spring National Monument and the Western Kaibab-Paiute Indian Reservation, the Tenney Canyon Tongue has a measured thickness of 67 m which was used as the tongue's thickness in column C6 in **Figure 4**. Within Kane County, Utah, the Tenney Canyon Tongue is 35 m thick west of Johnson Canyon, Utah (Sable and Hereford, 2004) and 96 m thick in the Zion Canyon area (Doelling, 2008). Using this trend, thickness values of 61 and 35 m were used for columns C7 and C8, respectively (**Figure 4**).

Navajo Sandstone (Lower Jurassic) – The Navajo Sandstone consists of cliff-forming highly resistive quartz sandstone, and siltstone (Billingsley and others, 2008). White sandstone within this formation forms the White Cliffs of the Grand Staircase (Gregory, 1950). In general, this formation thickens from east to west (Doelling and others, 1989).

The Navajo Sandstone has varying thickness trends across fault sections. Within the Geologic map of the Pipe Spring National Monument and the Western Kaibab-Paiute Indian Reservation, the Navajo Sandstone is 457 m thick which is the value used in column C6 in **Figure 4**. The Navajo Sandstone has a thickness trend best described in terms of its main body and Lamb Point Tongue. Within the Kanab 30' x 60' Quadrangle, the formation ranges in thickness from 395 to 670 m and thickens westward (Doelling, 2008). Using this trend, thickness values of 578 and 515 m were calculated for columns C7 and C8, respectively (**Figure 4**). In southwest Utah, the formation is 427 m thick west of Escalante and 671 m at Zion National Park (Doelling, 1975). Using this trend, a thickness value of 512 m was calculated for column C9 (**Figure 4**).

The prominent Lamb Point Tongue of the Navajo Sandstone has its own individual thickness trends. Within the Geologic map of the Pipe Spring National Monument and the Western Kaibab-Paiute Indian Reservation, the Lamb Point Tongue has a thickness that ranges from 0 to 42 m. At Point Spring of Vermillion Cliffs near Kaibab, Arizona, the formation is 30 m thick which is the values used in column C6 in **Figure 4**. Within the Kanab 30' x 60' Quadrangle, the tongue is 150 m west of Johnson Canyon and 85 m in the Moquith Mountains area (Sable and Hereford, 2004). Using this trend, thickness values of 91 and 140 m were calculated for columns C7 and C8, respectively (**Figure 4**).

Temple Cap Sandstone (Middle Jurassic) – The Temple Cap Sandstone is a multi-member formation consisting of cliff-forming sandstone and siltstone (Doelling, 2008). The thickness variation of this formation is likely due to the irregular paleotopography that formed as part of the J-1 unconformity above the Navajo Sandstone (Doelling and others, 2013). In general, the formation thickens westward (Doelling and others, 1989; Doelling, 2008). It only appears within proximity to the fault in the Kanab 30' x 60' Quadrangle. Here, the formation ranges in thickness from 0 to 60 m and thickens westward. The formation is not present in the eastern half of the quadrangle. Using this information, a thickness value of 20 m was calculated for column C7 in **Figure 4**.

Carmel Formation (Middle Jurassic) – The final Jurassic formation in the sequence, the Carmel Formation, is a multi-member formation consisting of steep slope-forming silty sandstone and siltstone, gypsum that varies in thickness, weather-prone limestone, and minor amounts of mudstone and shale (Doelling, 2008). This formation overlies the Temple Cap in the hanging wall of the Sevier-Toroweap fault system but can overlie the Navajo Sandstone on the

foot wall, east of Johnson Canyon, Utah (Doelling and others, 1989). The formation tends to thin from west to east in the southwestern Colorado Plateau Region (Doelling and others, 2013).

Within the Kanab 30' x 60' Quadrangle, which covers the southern half of the Sevier section, the Carmel formation has specific thickness trends best described through its subunits (Doelling, 2008). The Judd Hollow Tongue ranges in thickness from 30 to 60 m and thickens westward. The Co-op Creek Limestone Member ranges in thickness from 15 to 80 m and thickens westward. The Crystal Creek Member ranges in thickness from 15 to 55 m and thickens westward. The Paria River Members ranges in thickness from 18 to 50 m and has an irregular thickness pattern based on gypsum dissolution but generally thickens eastward. The final member, the Winsor Member, ranges in thickness from 60 to 85 m and thickens eastward. Using these individual trends, total formation thicknesses of 247 and 228 m were calculated for columns C7 and C8 in **Figure 4**.

Within the Panguitch 30' x 60' Qudrangrale, which covers the northern half of the Sevier section, the Carmel Formation has specific thickness trends best described through its subunits, (Biek and others, 2015). The Winsor Member ranges is 75 m thick in Cedar Canyon and 15-45 m thick in the southeastern portion of the quadrangle. The Paria River Member is 53 m thick in Cedar Canyon and 44 – 120 m thick in the southeastern portion of the quadrangle. The Crystal Creek Member is 90 m thick in Cedar Canyon. This member thickens westward. The final member, the Co-op Creek Limestone Member is estimated to be 120 m thick in the quadrangle. Using these and previously mentioned Kanab area trends, a total formation thickness of 326 m was calculated for column C9 in **Figure 4**.

Dakota and Cedar Mountain Formations undivided. (Lower to Upper Creataceous) – The undivided Dakota and Cedar Mountain Formations are grouped together based on lithologic

similarity (Doelling, 2008). These formations consist of cliff, slope, and ledge-forming sandstone, shale, conglomerate, mudstone, coal, and marl (Biek and others, 2015). These formations, paired with the cliff-forming lithologies in the Straight Cliffs formation, form the Gray Cliffs of the Grand Staircase (Doelling, 2008). In general, these formations thicken to the west based on USGS maps covering the Sevier section (Doelling and others, 1989, Biek and others, 2015).

The undivided Dakota and Cedar Mountain Formations have varying thickness trends across fault sections. Within the Kanab 30' x 60' Quadrangle, the formations have a combined thickness of 60 to 270 m and thicken westward (Doelling, 2008). Using this trend, thickness values of 200 and 152 m were calculated for columns C7 and C8 respectively in **Figure 4**. Within the Panguitch 30' x 60' Quadrangle, the Dakota Formation ranges in thickness from 25 to 85 m across the Paunsaugunt Plateau and thickens westward (Biek and others, 2015). The Cedar Mountain formation only has one measurement of 18 m in Cedar Canyon and may or may not be present in the proximity to the fault. Using this information, a thickness value of 83 m was calculated for column C9 (**Figure 4**).

Tropic Shale (Upper Cretaceous) – The Tropic Shale consists of steep slope-forming marine shale and sandstone. This formation is known to intertongue with the underlying Dakota Formation (Eaton and others, 1987). In general, the formation is a wedge that thickens to the east and southeast (Doelling and others, 1989).

The Tropic Shale has varying thickness trends across fault sections. Within the Kanab 30' x 60' Quadrangle, the formation has a thickness that ranges from 90 to 300 m and generally increases to the east but often has an irregular thickness trend (Doelling, 2008). Using this trend, thickness values of 162 and 212 m were calculated for columns C7 and C8 respectively in

Figure 4. Within the Panguitch 30’ x 60’ Quadrangle, the Tropic Shale is 180 to 275 m in the southeast portion of the quadrangle and 12 m thick in the southwest portion. Using this trend, a thickness value of 167 m was calculated for column C9 (**Figure 4**).

Straight Cliffs Formation (Upper Cretaceous) – The Straight Cliffs Formation consists of ledge, cliff, and slope-forming sandstone, mudstone, and siltstone, with some claystone and coal (Doelling, 2008). This formation thickens dramatically to the east on the hanging wall of the Sevier-Toroweap fault system due to foredeep basin subsidence (Biek and others, 2015).

The Straight Cliffs Formation has varying thickness trends across fault sections. Within the Alton Quadrangle, the Straight Cliffs Formation is 365 m (Tilton and Sable, 2001) which is the value used in column C8 in **Figure 4**. Within the Panguitch 30’ x 60’ Quadrangle, the Straight Cliff Formation has a thickness trend that is best described through its members (Biek and others, 2015). The Drip Tank Member is 30 to 60 m thick on the Paunsaugunt Plateau and 41 m at First Left Hand Canyon southeast of Parowan, Utah. The John Henry Member is 275 to 300 m in Cedar Canyon and 240 to 335 m in Bryce Canyon National Park. The Smoky Hollow Member is 95 to 110 m at Cedar Canyon and 60 to 75 m at Bryce Canyon National Park. The Tibbet Canyon Member is 200 to 245 m on west edge of the Markagunt Plateau and 12 to 15 m on the east edge of the Paunsaugunt Plateau. Using these individual trends, a total formation thickness of 454 m was calculated for column C9 (**Figure 4**).

Wahweap Formation (Upper Cretaceous) – The Wahweap Formation is a multi-member formation consisting of slope and ledge-forming mudstone, claystone, sandstone, siltstone, and conglomerate (Doelling, 2008). The lower three members of this formation experience a dramatic thickening to the west across the Paunsaugunt Plateau on the footwall of the Sevier

Fault (Biek and others, 2015). On the hanging wall of the Sevier fault, the formation will gradually thicken west across the Markagunt Plateau.

Within the Kanab 30' x 60' Quadrangle, the Wahweap Formation has a thickness of 100 to 200 m south of the Paunsaugunt Plateau, and 245 to 300 m thick south of the Markagunt Plateau (Doelling, 2008). Using this trend, a thickness value of 173 m was calculated for column C8 in **Figure 4**.

Kaiparowits Formation (Upper Cretaceous) – The youngest formation in this timeframe, the Upper Cretaceous Kaiparowits Formation, consists of steep slope-forming sandstone, mudstone, and siltstone (Doelling, 2008). Current exposures of the formation form badland slopes due to weathering caused by the poor cementation of these lithologies (Biek and others, 2015). West of the Paunsaugunt fault the formation undergoes dramatic thinning and variable local thickness trends. East of the Paunsaugunt fault, this formation reaches its max thickness around the Kaiparowits Plateau (Doelling and others, 1989).

Within the Kanab 30' x 60' Quadrangle, the Kaiparowits Formation ranges in thickness from 0 to 75 m and thickens thins eastward to where it is nearly absent around the Paunsaugunt Plateau (Doelling, 2008). Using this trend, a thickness value of 15 m was calculated for column C8 in **Figure 4**.

Claron Formation (Paleocene to Eocene) – The Claron Formation is a multi-member unit that forms the Pink Cliffs of the Grand Staircase (Biek and others, 2012). The lithologies of this formation include mudstone, limestone, siltstone, sandstone, and minor conglomerate (Biek and others, 2015). Most of these units originate from fluvial and lacustrine deposits (Goldstrand, 1990). In general, the Claron Formation, is thicker west of the Sevier Fault in the western part of Kane County (Sable & Hereford, 2004), but can vary considerably more north.

Within the Kanab 30’ x 60’ Quadrangle, the Claron Formation has a thickness trend conveniently defined by its white and pink members (Sable & Hereford, 2004). The white member ranges in thickness from 20 to 40 m and thickens to the east while the pink member ranges in thickness from 150 m east of the Sevier fault to 250 m west of the fault trace. Using these individual trends, a total formation thickness of 255 m was calculated for column C8 in **Figure 4**.

Within the Panguitch 30’ x 60’ Quadrangle, the Claron Formation has a thickness trend conveniently defined by its white and pink members (Biek and others, 2015). The white member is 105 to 135 m across the Paunsaugunt and Markagunt Plateaus and 105 m thick in the southern Sevier Plateau. The pink member is 300 m thick at Cedar Breaks National Monument and 180 m thick at Bryce Canyon National Park. Using these individual trends, a total formation thickness of 313 m was calculated for column C9 in **Figure 4**.

Brian Head Formation (middle Eocene to lower Oligocene) – The Brian Head Formation is a volcaniclastic unit consisting of sandstone, conglomerate, mudstone, siltstone, volcanic mudflow breccia, ash flow tuff, and some limestone and chalcedony. The unit marks some of the earliest widespread volcanism within southwestern Utah. In general, the formation appears to thicken from west to east based on measured sections near Cedar Breaks National Monument, Utah, and the western flank of the Sevier Plateau (Sanjuan and others, 2017).

The Brian Head Formation has varying thickness trends across fault sections. Within the Kanab 30’ x 60’ Quadrangle, the Brian Head Formation has an exposed maximum thickness of 120 m (Sable and Hereford, 2004). which is used in column C8 in **Figure 4**. Within the Panguitch 30’ x 60’ Quadrangle, the Brian Head Formation is 300 m thick along the southwest

edge of the Sevier Plateau (Biek and others, 2015). This thickness value is used in column C9 (**Figure 4**).

Wah Wah Springs Formation (lower Oligocene) – The Wah Wah Springs Formation is a Great Basin ash-flow tuff consisting of crystal rich dacites and a unique abundance of hornblende. Near the Sevier fault, only distal deposits of this ash-flow tuff are present as the Indian Peak caldera complex, where this tuff originates from, is located over 100 km west (Biek and others, 2015). In general, the formation thickens from west to east across the Markagunt and Sevier Plateaus. The formation is only present near the fault within the Panguitch 30' x 60' Quadrangle. Here, the formation is 40 m thick in the Sevier Plateau (Biek and others, 2015) which is the value used in column C9 in **Figure 4**.

Mount Dutton Formation (upper Oligocene) – The final displaced Cenozoic formation, the upper Oligocene Mount Dutton Formation, consists of volcanic mudflow breccia, volcaniclastic conglomerate, and tuffaceous sandstone (Biek and others, 2015). This formation dominates the footwall of the Sevier-Toroweap fault system in the northernmost part of the Sevier section. The rocks in this formation form the southern flank of the Marysvale volcanic field (Biek and others, 2012). In general, this formation thickens north along the Sevier Plateau (Biek and others, 2015). The formation is only present near the fault within the Panguitch 30' x 60' Quadrangle. Here, the formation is 600 m thick along the southern edge of the Sevier Plateau and 2000 m thick in the Sevier Plateau north of the quadrangle (Biek and others, 2015). Using this trend, a thickness value of 1217 m was calculated for column C9 in **Figure 4**.

FIGURES AND TABLES

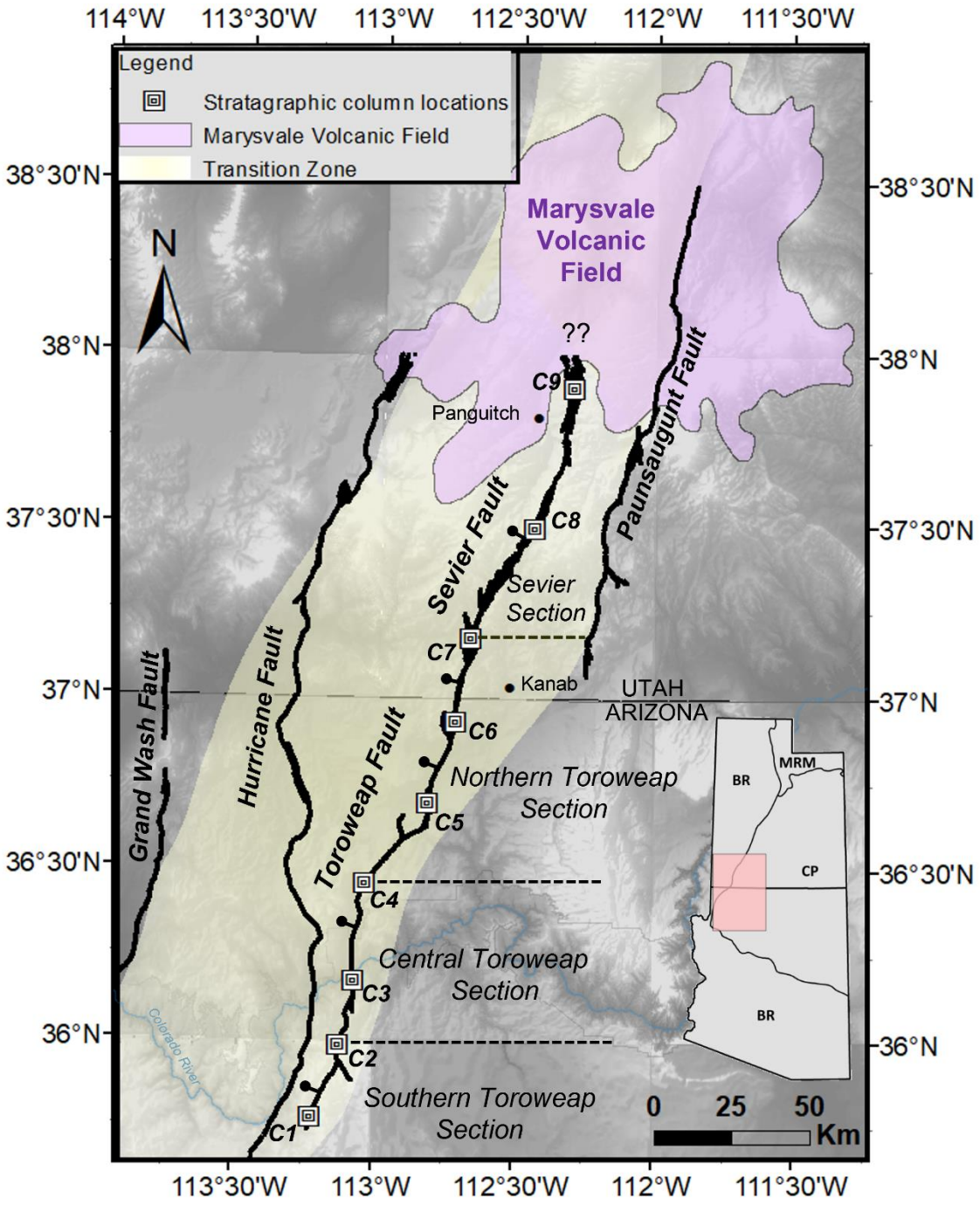

Figure 1: *Regional map of the Sevier-Toroweap fault system and other major normal faults apart of the Basin and Range – Colorado Plateau Transition Zone. Dashed lines indicate fault section boundaries defined in past studies (Pearthree, 1998; Black and others, 2003). Square symbols represent the locations of stratigraphic columns from the stratigraphic correlation chart in Figure 2. Question marks indicate uncertainty in the northern trace of the fault system as it interacts with the Marysvale volcanic field. The inset shows the regional map in relation to major physiographic provinces in Arizona and Utah (BR,*

Basin and Range; CP, Colorado Plateau; MRM; Middle Rocky Mountains). Figure significantly modified after Lund and others (2008). Marysvale volcanic field boundary after Best and others (2013).

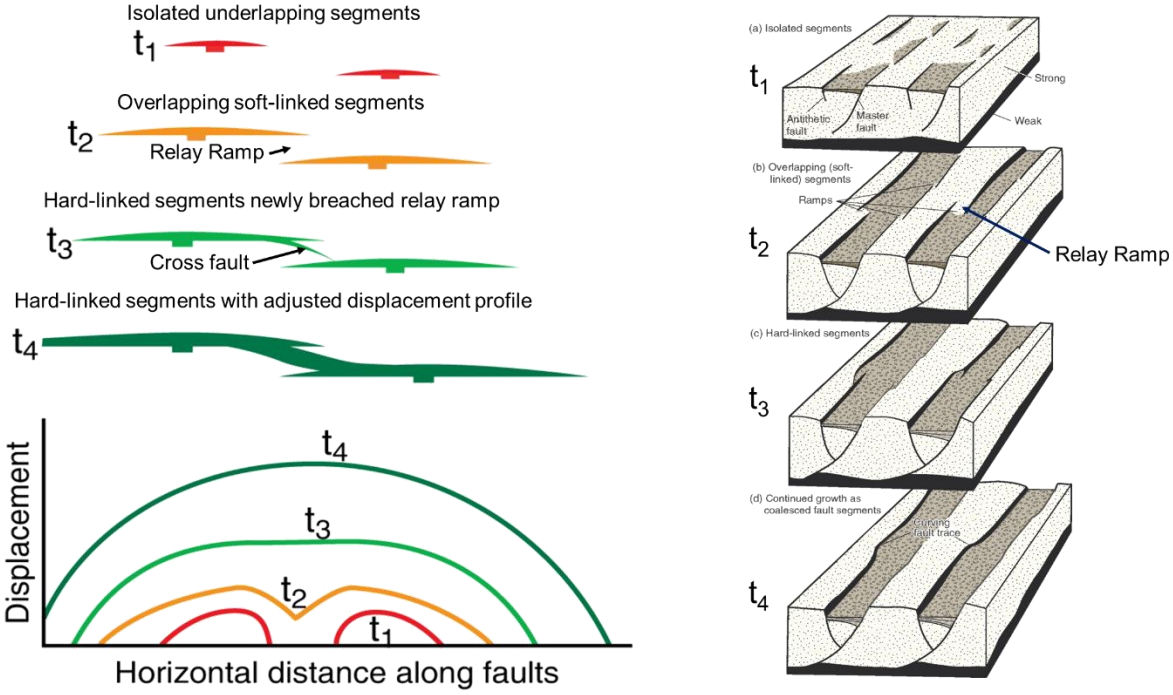

Figure 2: *Collection of diagrams displaying the stages of fault linkage with corresponding plot of "Displacement vs. Horizontal distance along faults" showing displacement distribution for each stage. Figures slightly modified from Fossen (2016).*

Table 1: *List of reported slip rates along the Sevier-Toroweap fault system from various sources.*

Slip Rates from Paleoseismic Indicators			
Location	**Type**	**Slip Rate (mm/yr)**	**Source**
Prospect Canyon/Lava Falls	Offset basalt flow	0.1	Karlstrom and others, 2007
Pipe Spring National Monument	Alluvial scarp	0.01 – 0.04	Pearthree, 1998
Black Mountain	Offset basalt flow	0.4	Biek and others, 2015
Rock Canyon	Offset basalt flow	0.05-0.18	Biek and others, 2015
Red Canyon	Offset basalt flow	0.4	Lund and others, 2008

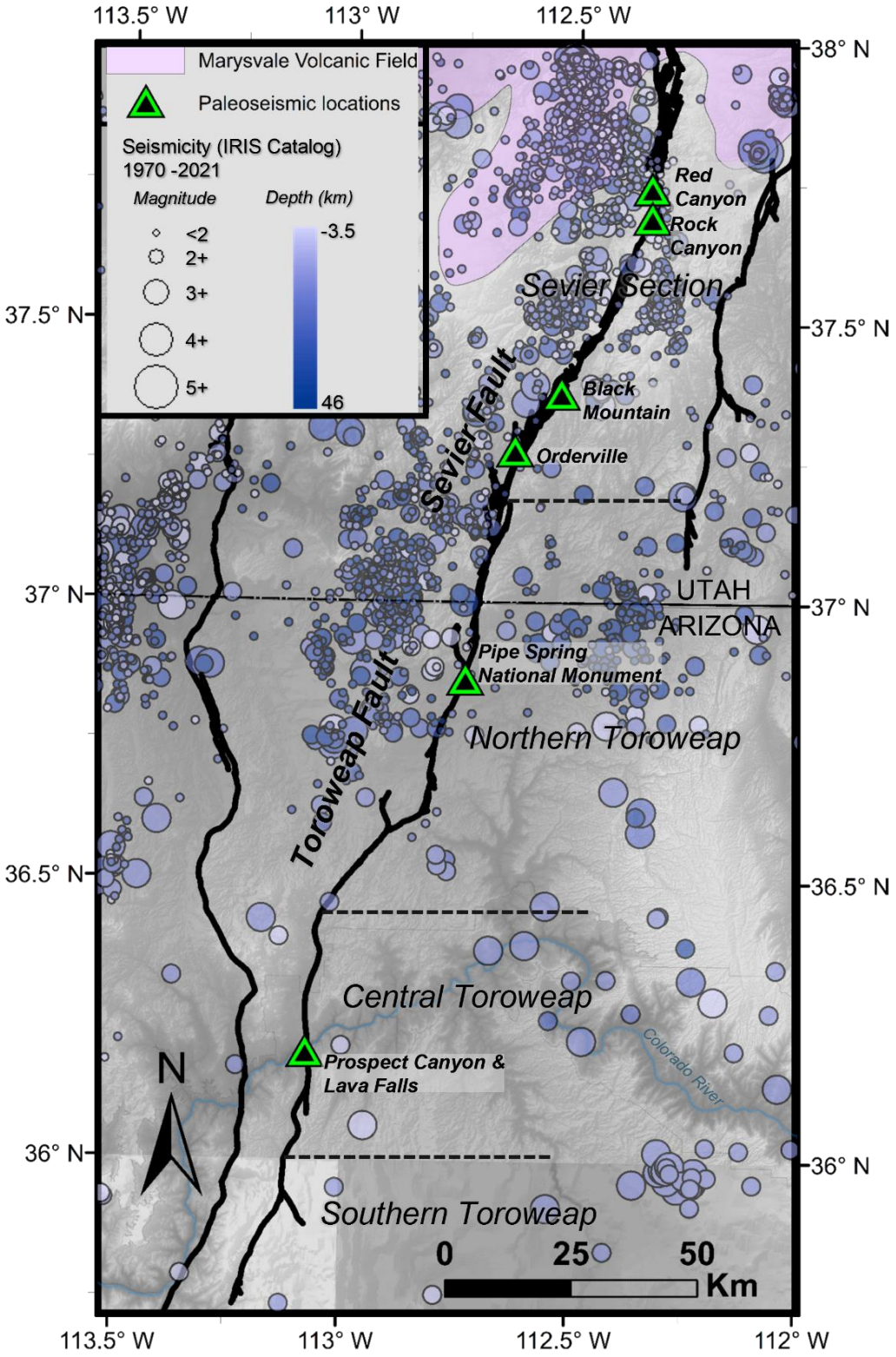

Figure 3: *Regional seismicity map for the Sevier-Toroweap fault system with seismicity and notable paleoseismic indicator locations plotted. A clustering of events is apparent in the Northern Toroweap and Sevier sections.*

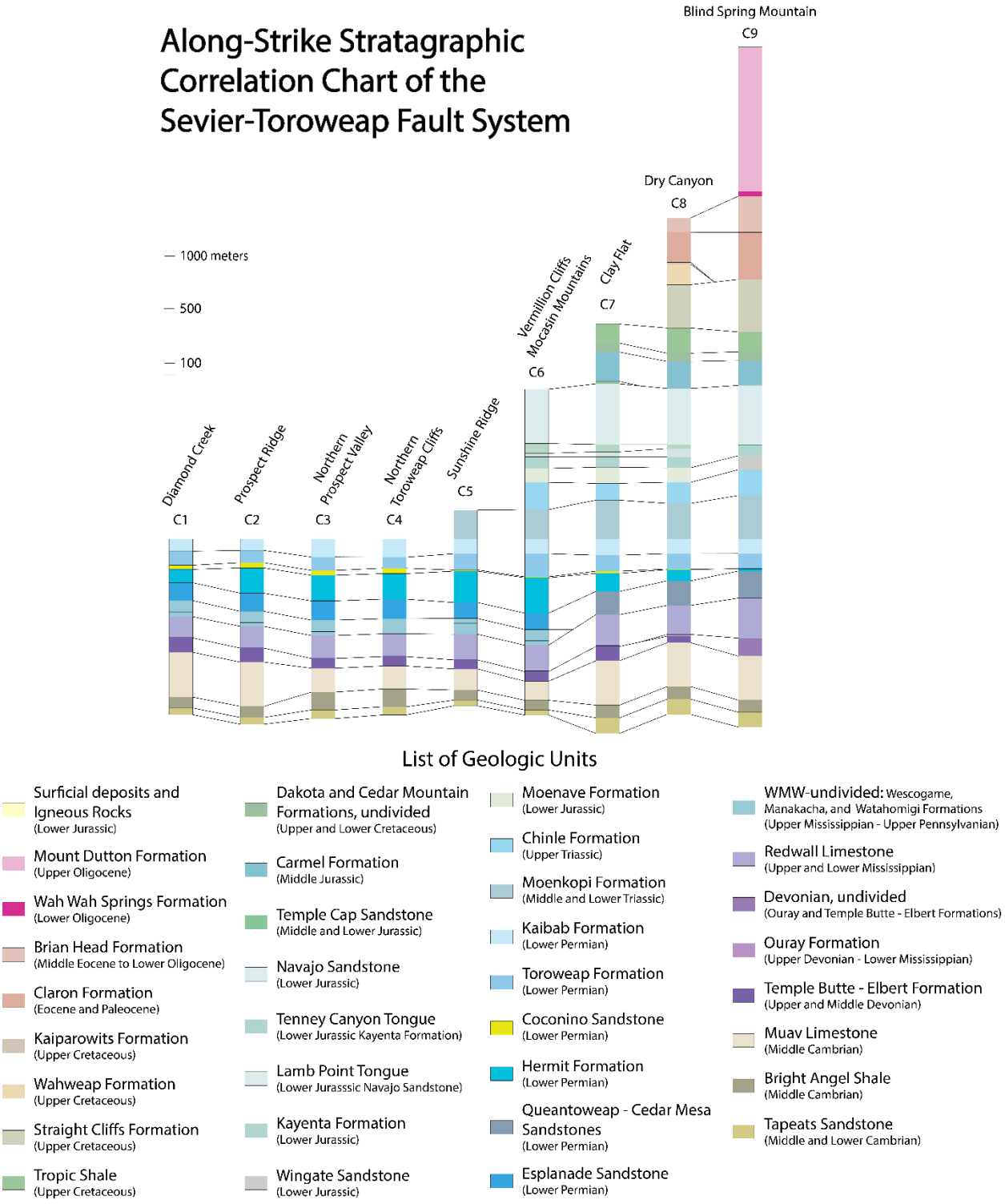

Figure 4*: Stratigraphic correlation chart of displaced formations along the strike of the Sevier-Toroweap fault system. The locations of columns C1 – C9 are indicated in Figure 1. The formation thciknesses in each column were calculated based on thickness trends described in the Appendix.*

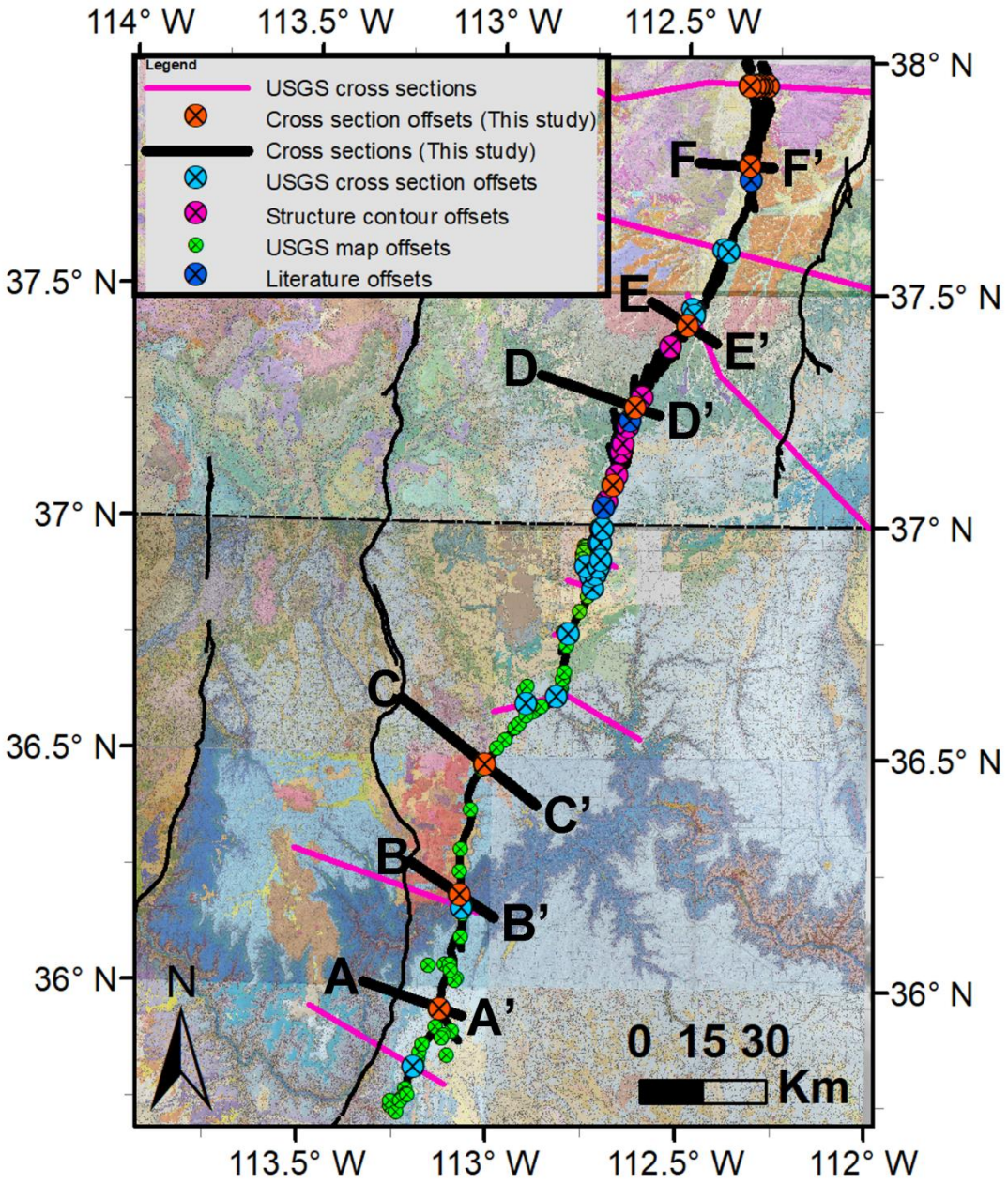

Figure 5: *Cross section locations and data compilation of displacement measurements from this study and values reported from literature. The main data sources for the displacement gradient and cross sections are the imaged USGS 30' x 60' quadrangle maps (Billingsley and Hampton, 2000; Billingsley and Workman, 2000; Billingsley and Wellmeyer, 2003; Sable and Hereford, 2004;Billingsley and others, 2006a, 2006b; 2008; Doelling, 2008, Biek and others, 2010, 2015).*

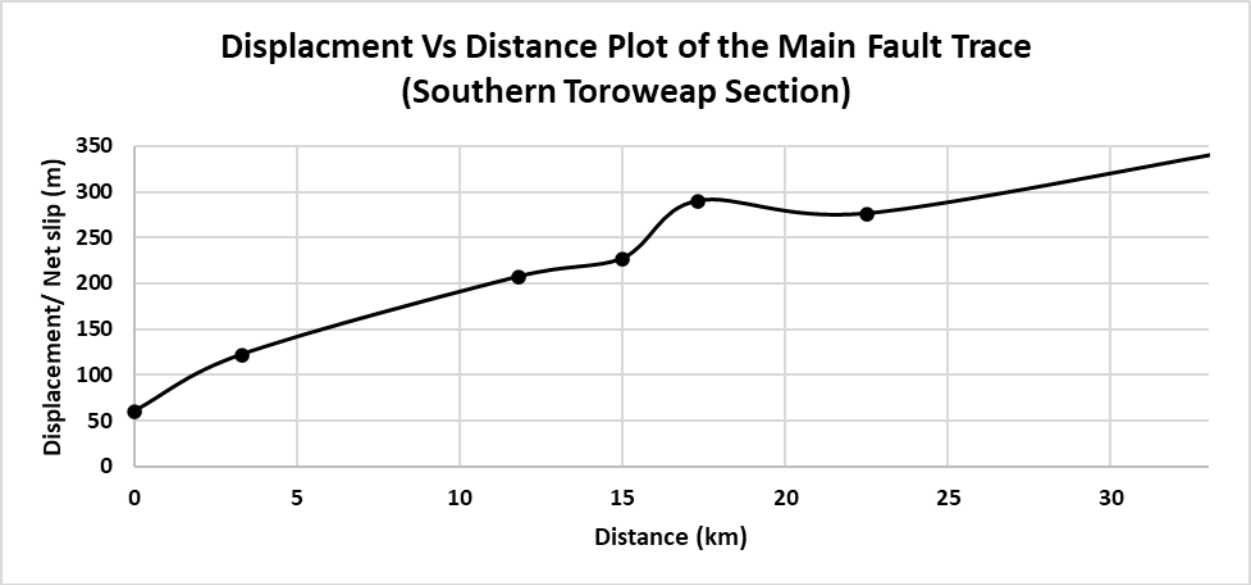

Figure 6: *Displacement vs. distance plot for the Southern Toroweap section.*

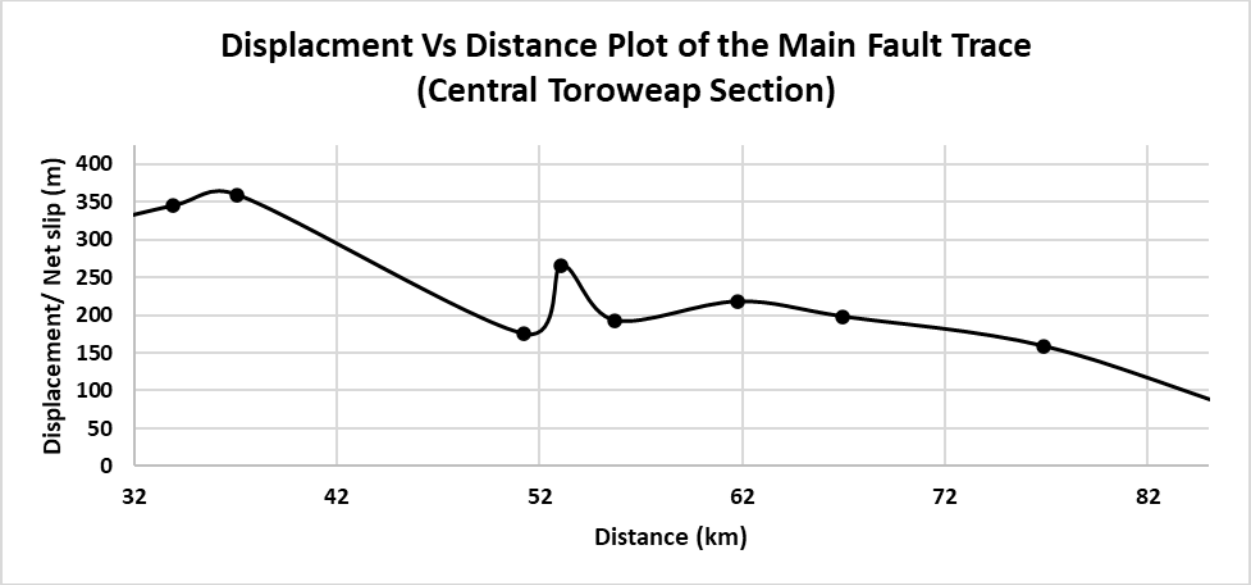

Figure 7: *Displacement vs. distance plot for the Central Toroweap section.*

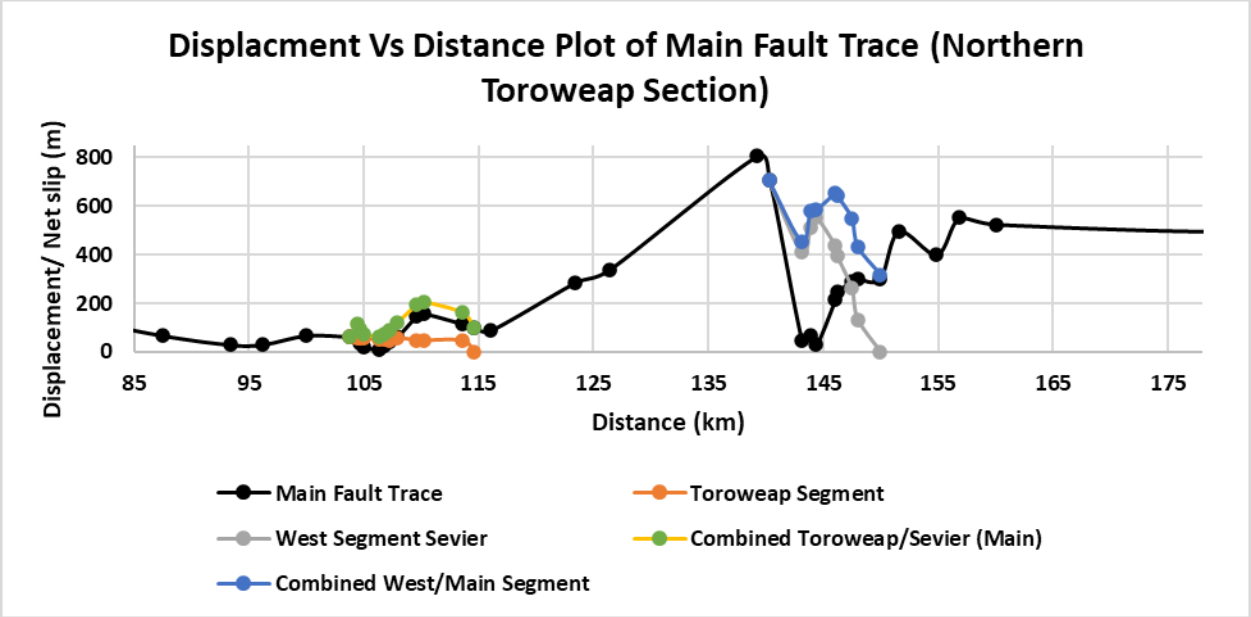

Figure 8: *Displacement vs. distance plot for the Northern Toroweap section. Individual and cumulative displacement profiles are shown across two potential segment boundaries where the fault has a prominent splay.*

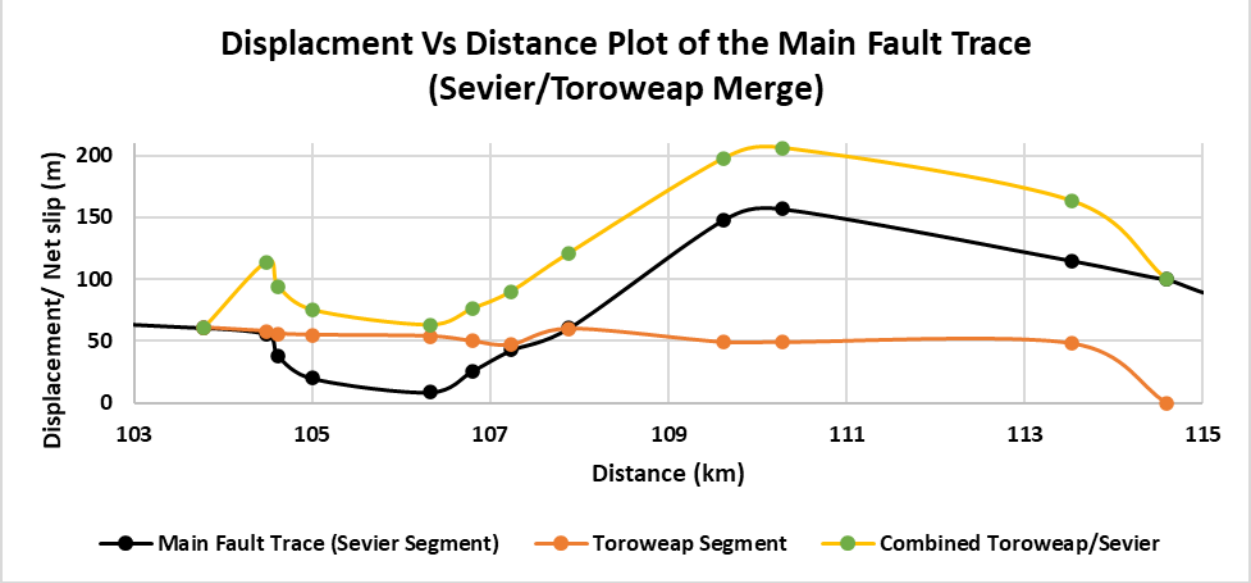

Figure 9: *Displacement vs. distance plot for the potential Sevier/Toroweap segment boundary. Individiual and cummulative displacement profiles for the western Toroweap segment and eastern main fault trace (Sevier segment) are shown.*

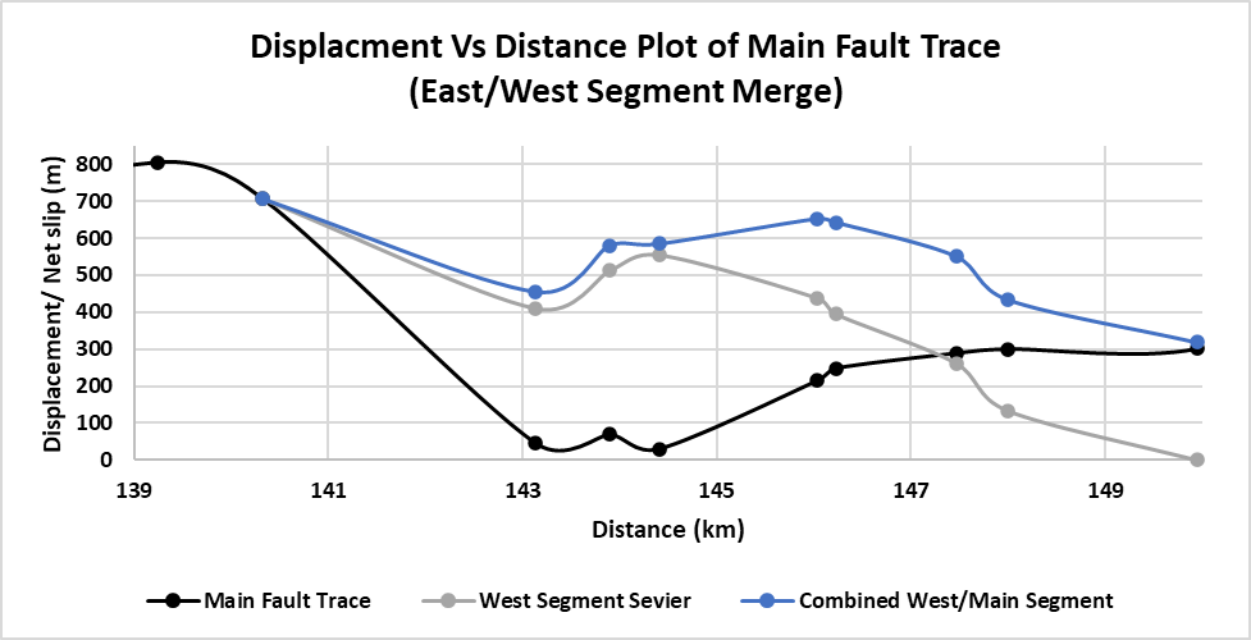

Figure 10: *Displacement vs. distance plot for the potental West Sevier/Main Sevier segment boundary. Individiual and cummulative displacement profiles for the western Sevier segment and eastern main fault trace (Main Sevier segment) are shown.*

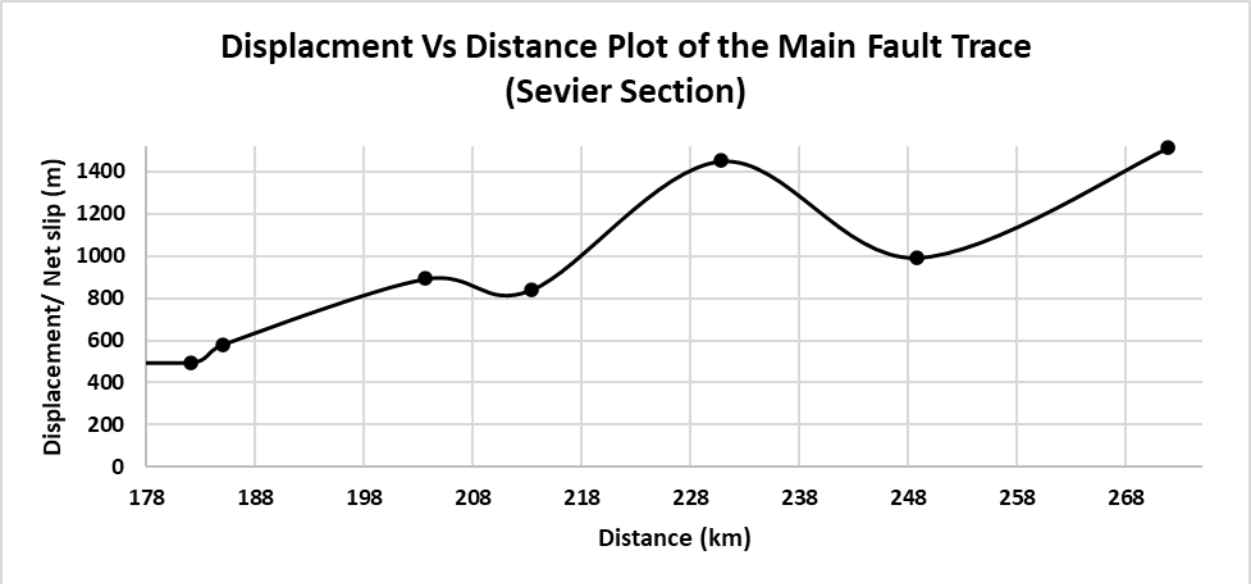

Figure 11: *Displacement vs. distance plot for the Sevier section.*

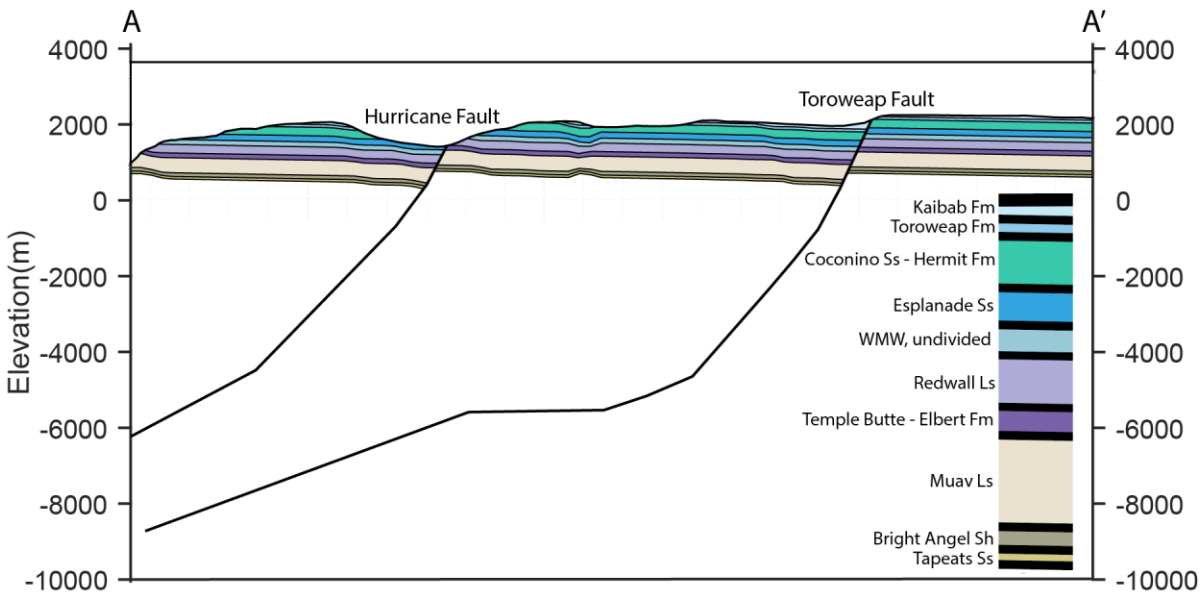

Figure 12: *Cross section A-A' within the Peach Springs and Mount Trumbull 30' x 60' quadrangles (Billingsley and others, 2006a; Billingsley and Wellmeyer, 2004) showing the modeled fault geomtry for a single main strand of the Sevier-Toroweap fault system. The fault intersection on this cross section is located at an along strike distance of 27 km.The measured displacement on the Sevier-Toroweap fault is 392 m.*

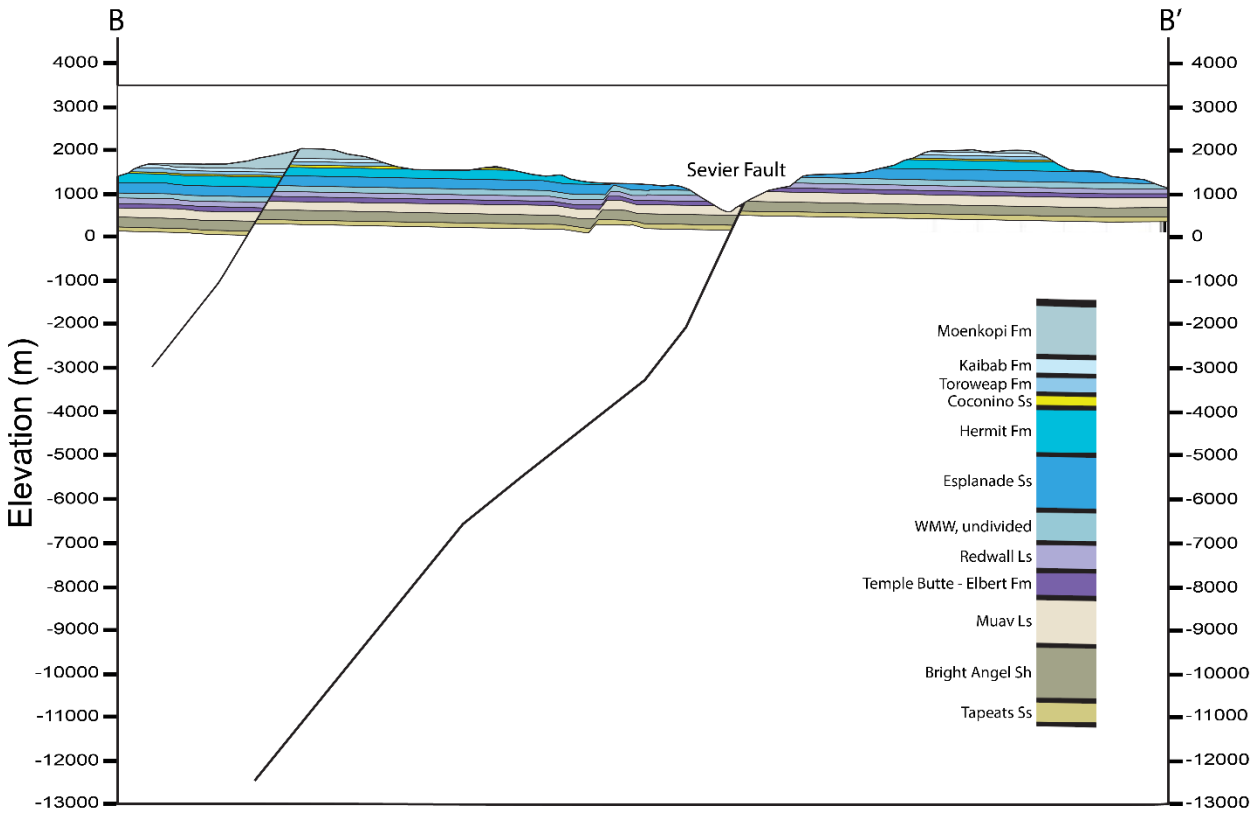

Figure 13: *Cross section B-B' within the Mount Trumbull and Grand Canyon 30' x 60' quadrangles (Billingsley and Wellmeyer, 2004; Billingsley and Hampton, 2000) showing the modeled fault geometry for a single main strand of the Sevier-Toroweap fault system. The fault intersection on this cross section is located at an along strike distance of 56 km . The left fault is a second order fault needed to constrain contacts on the west end of the section. The measured displacement on the Toroweap Fault from this section is 370 m.*

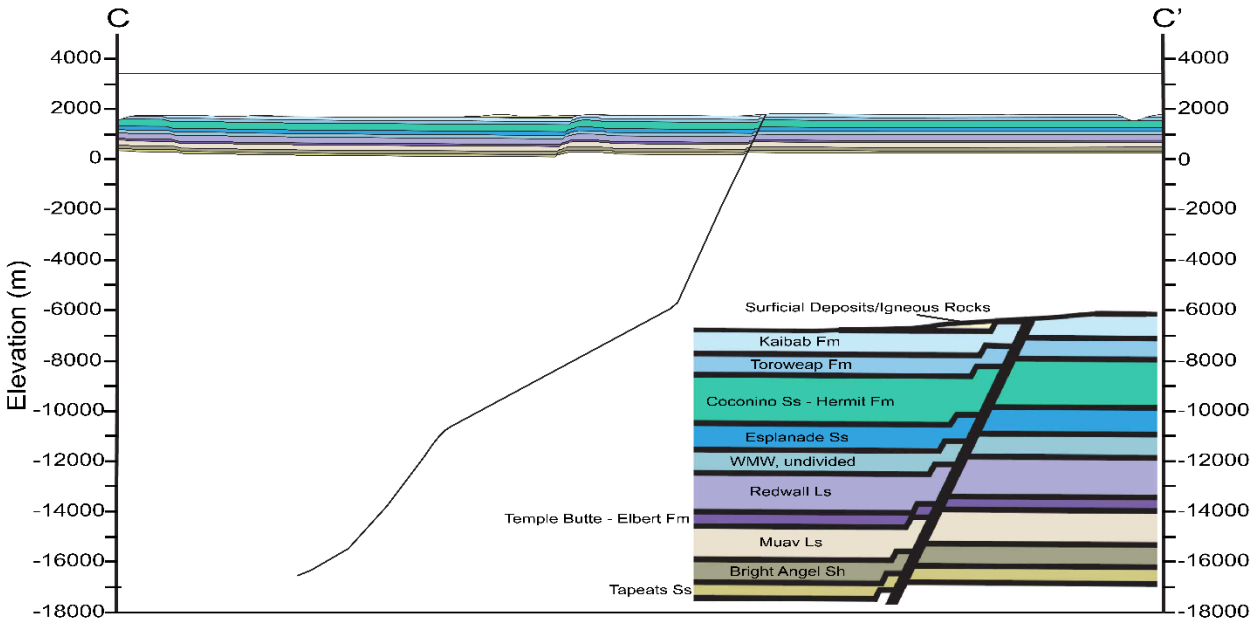

Figure 14: *Cross section C-C' within the Littlefield, Mount Trumbull, and Grand Canyon 30' x 60' quadrangles (Billingsley and Workman, 2000; Billingsley and Wellmeyer 2004; Billingsley and Hampton,2000)) showing the modeled fault geometry for a single main strand of the Sevier-Toroweap fault system. The fault intersection on this cross section is located at an along strike distance of 89 km.The measured displacement on the fault is 67 m.*

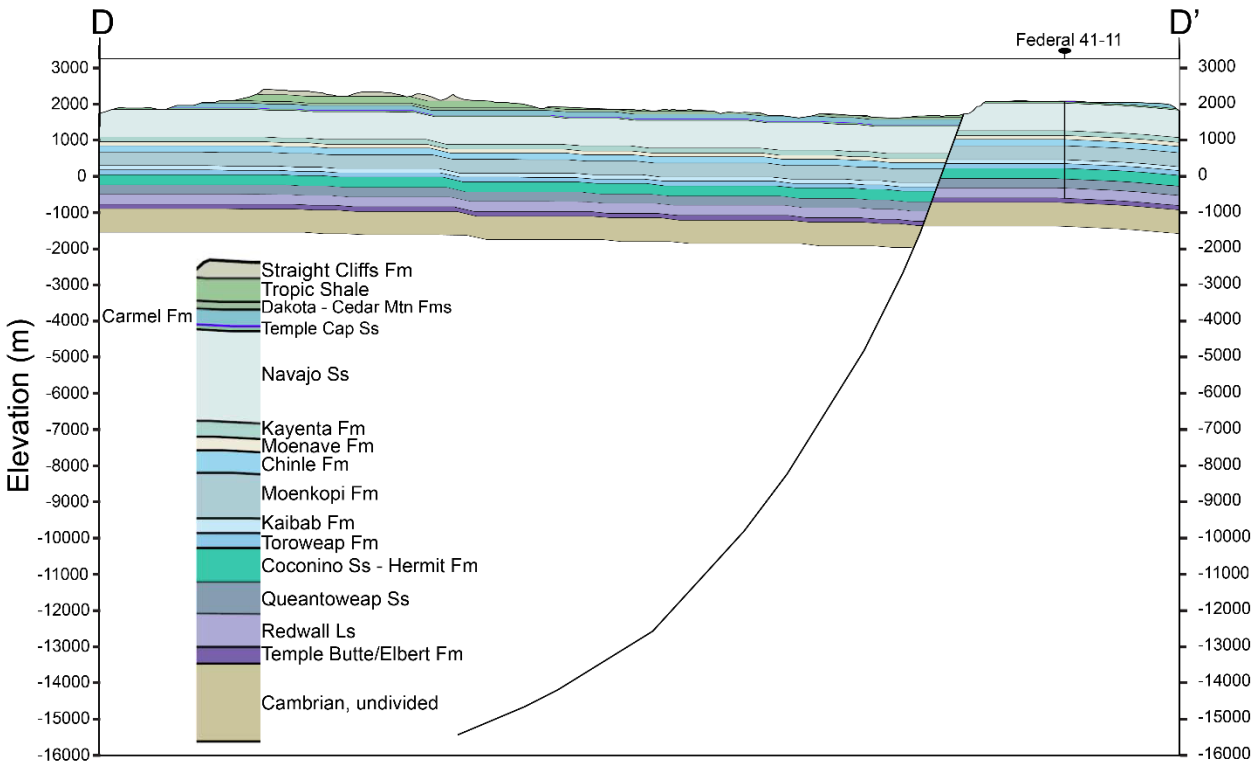

Figure 15: *Cross section D-D' within the Kanab 30' x 60' quadrangle (Doelling, 2008). showing the modeled fault geometry for a single main strand of the Sevier-Toroweap fault system. The fault intersection on this cross section is located at an along strike distance of 186 km. Stratagraphic thicknesses in the footwall are constrained by the Federall 41-11 well. The measured displacement on the fault is 680 m.*

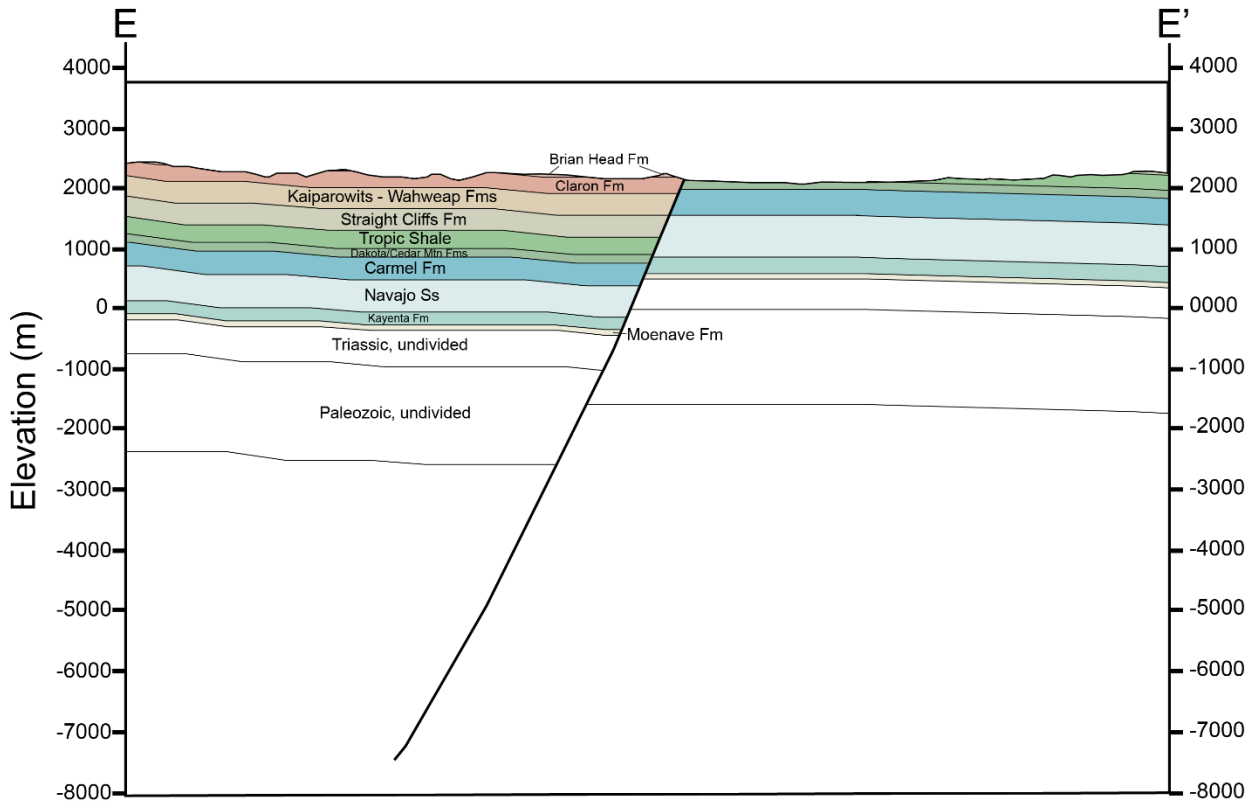

Figure 16: *Cross section E-E' within the Kanab 30' x 60' quadrangle (Doelling, 2008) showing the modeled fault geometry for a single main strand of the Sevier-Toroweap fault system. The fault intersection on this cross section is located at an along strike distance of 210 km . The measured displacement on the fault is 1300 m.*

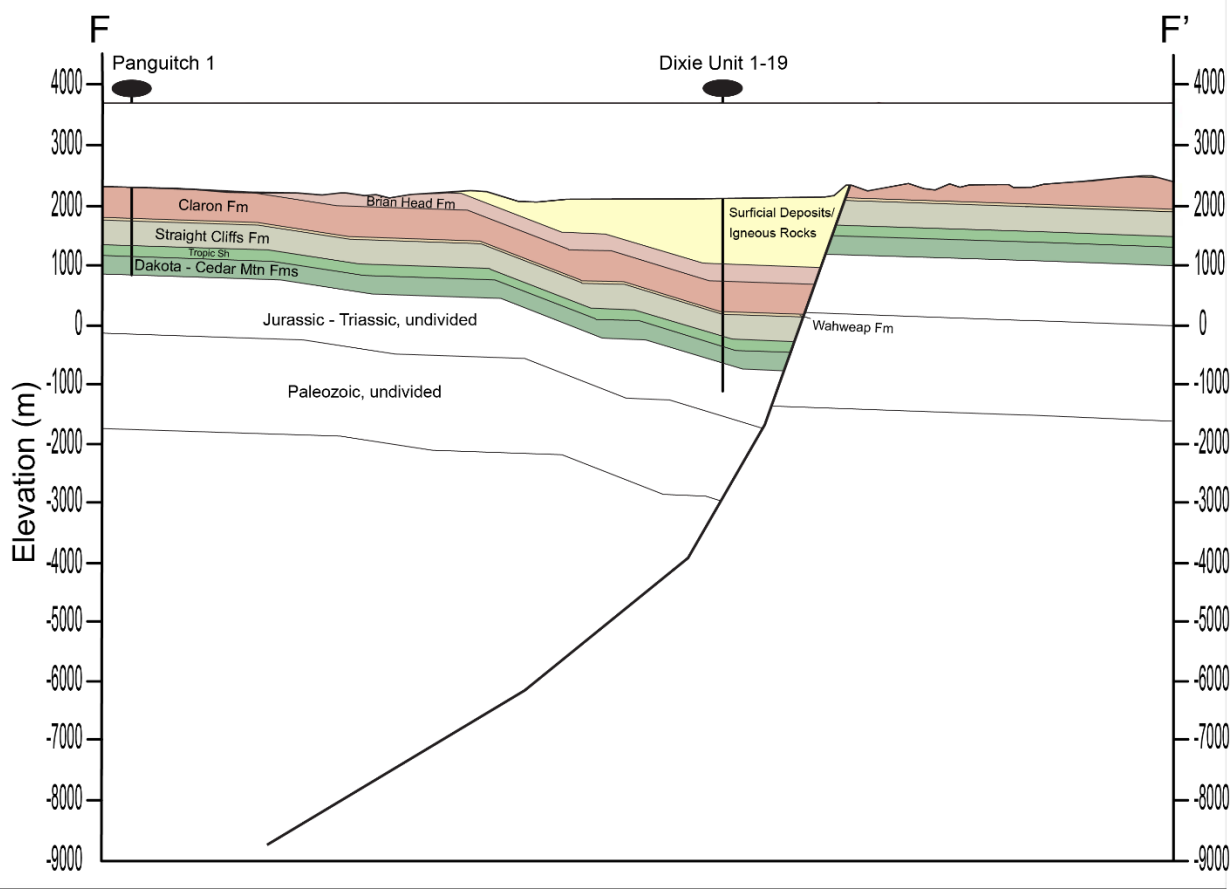

Figure 17: *Cross section F-F' within the Panguitch 30' x 60' quadrangle (Biek and others, 2015) showing the modeled fault geomtry for a single main strand of the Sevier-Toroweap fault system. The fault intersection on this cross section is located at an along strike distance of 252 km . Stratagraphic thicknesses in the footwall and hanginging wall are constrained by the Dixie Unit 1-19 and Panguitch 1 wells,respectively. The measured displacement on the fault is 2100 m.*

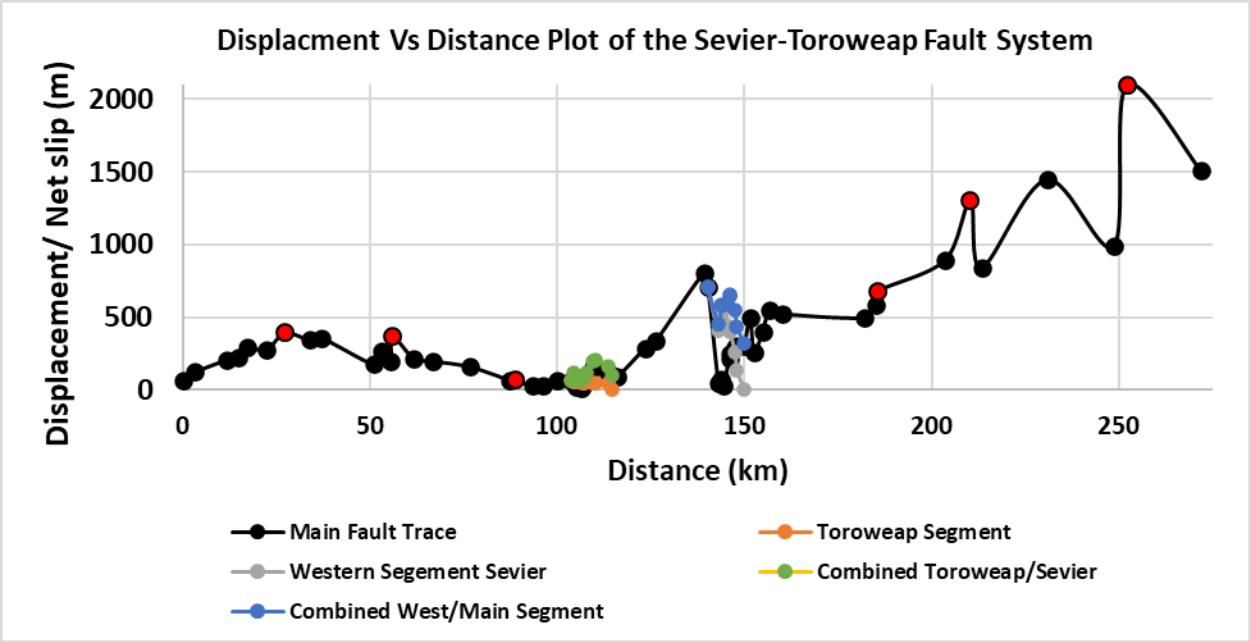

Figure 18: *Displacement vs. distance plot for the Sevier-Toroweap fault system with included displacements fromcross sections in this study (red markers).*

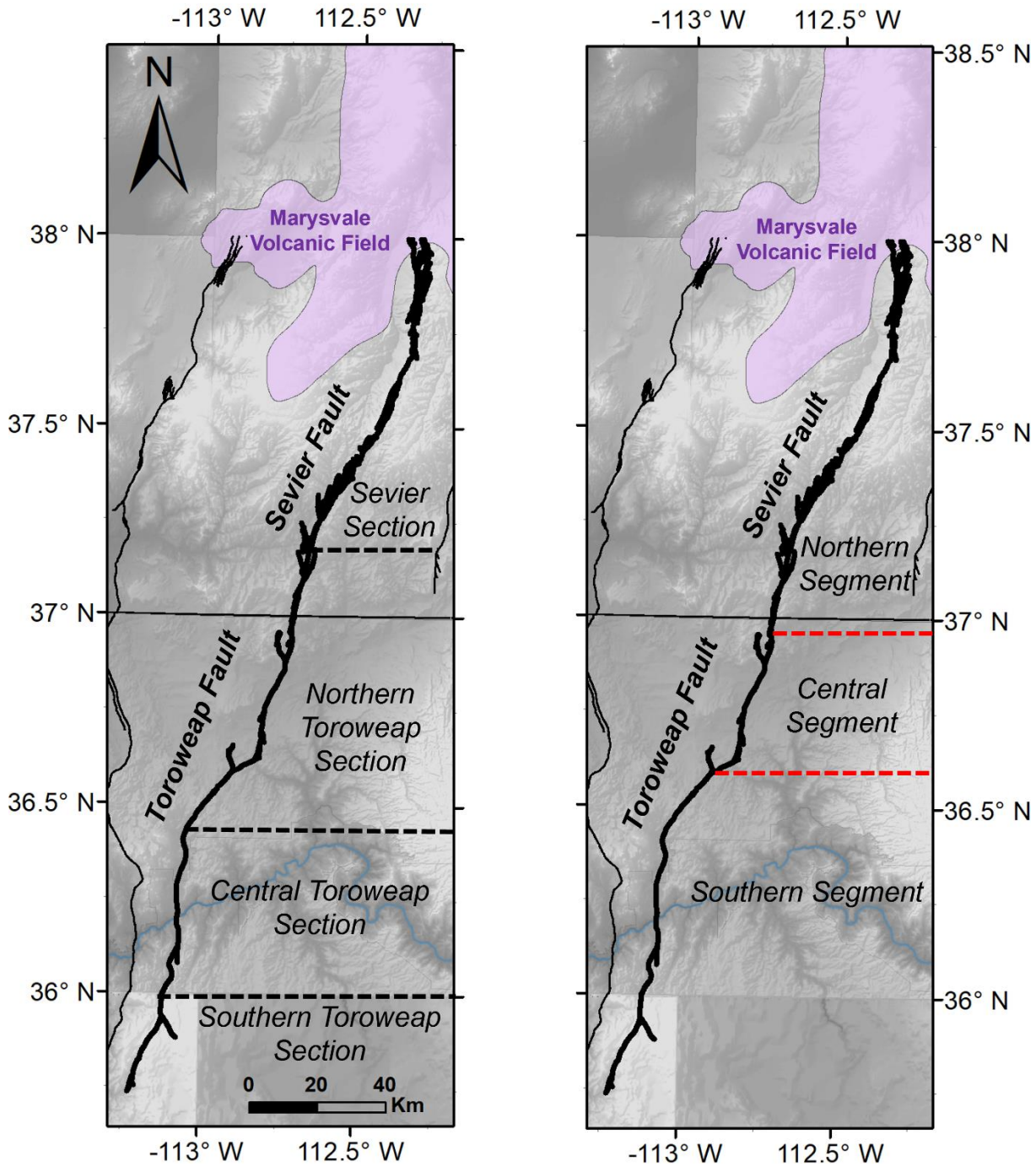

Figure 19: *(Left) Regional map of the Sevier-Toroweap fault system with fault sections characterized in past studies (Pearthree, 1998; Black and others, 2003). (Right) The same regional map but with redefined segments from this study.*

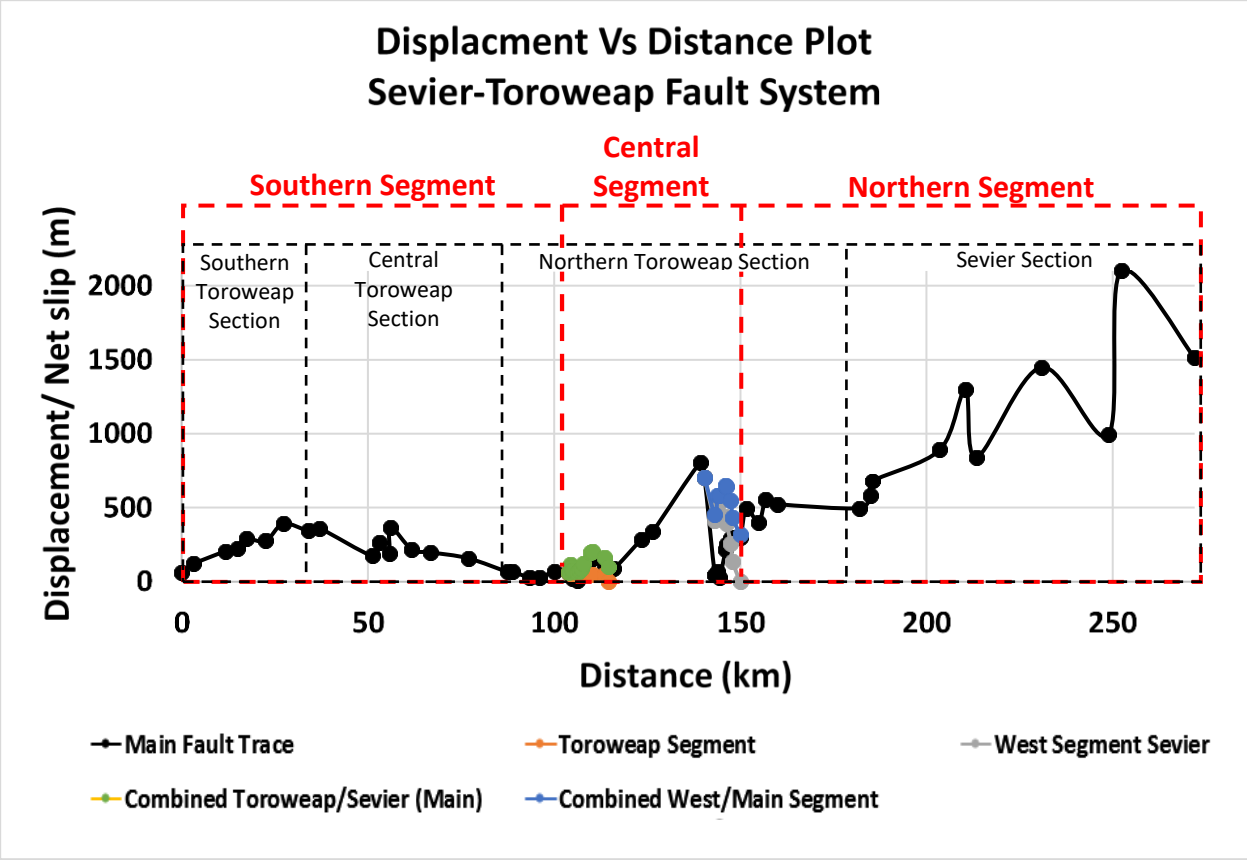

Figure 20: *Displacement vs distance plot for the Sevier-Toroweap fault system indicating the fault sections and their boundaries characterized in past studies (black) (Pearthree, 1998; Black and others, 2003) and the proposed segments and boundaries from this study (red).*

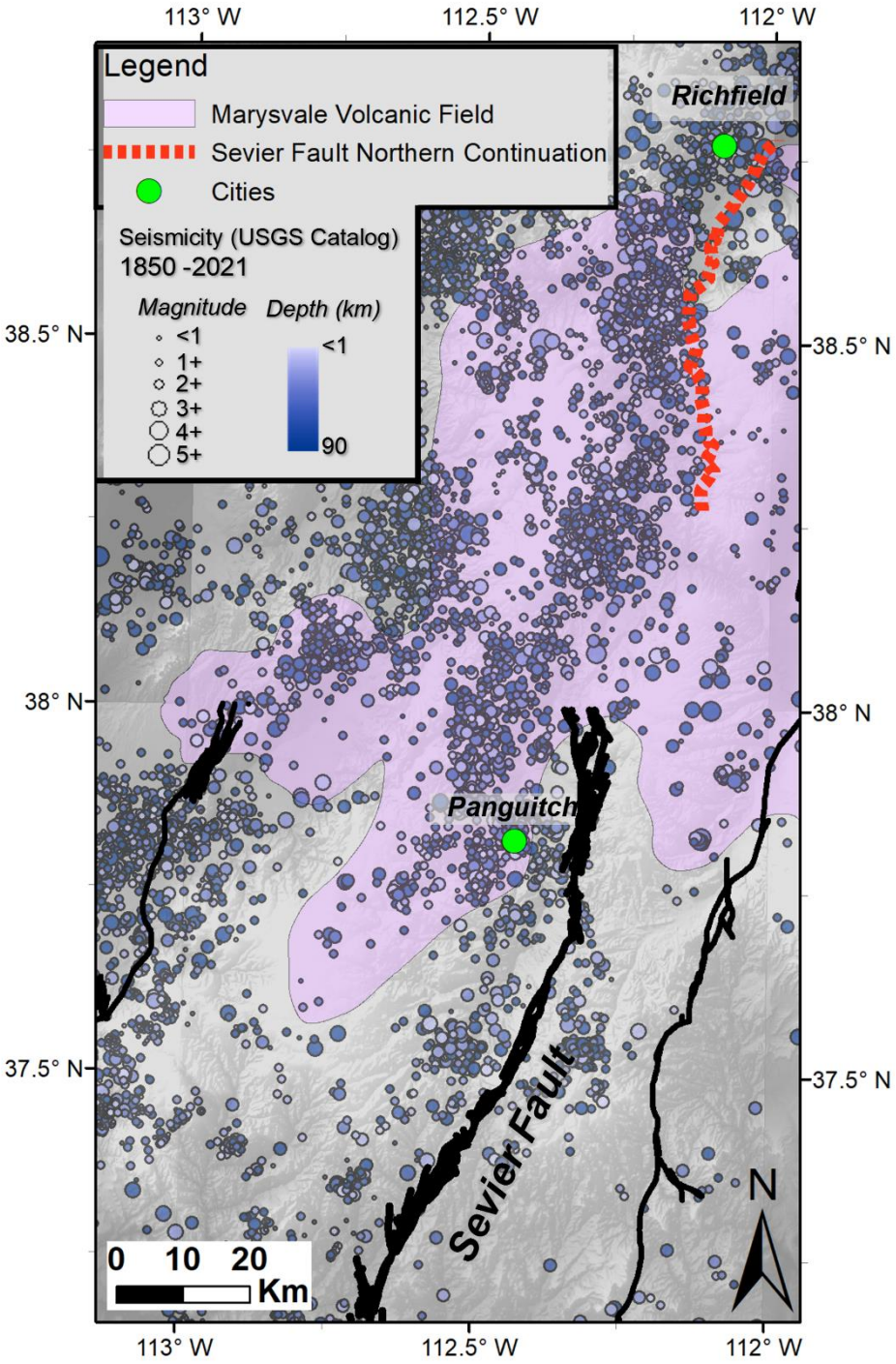

Figure 21: *Regional seismicity map of the northern traced extent of the Sevier-Toroweap fault system to the Marysvale volcanic field and the the mapped speculative northern continuation of the fault. The trace of the northern continuation is after Steven and others (1990). The trend in seismicity suggests that the Sevier fault may continue through the volcanic field and connect with the mapped northern continuation.*

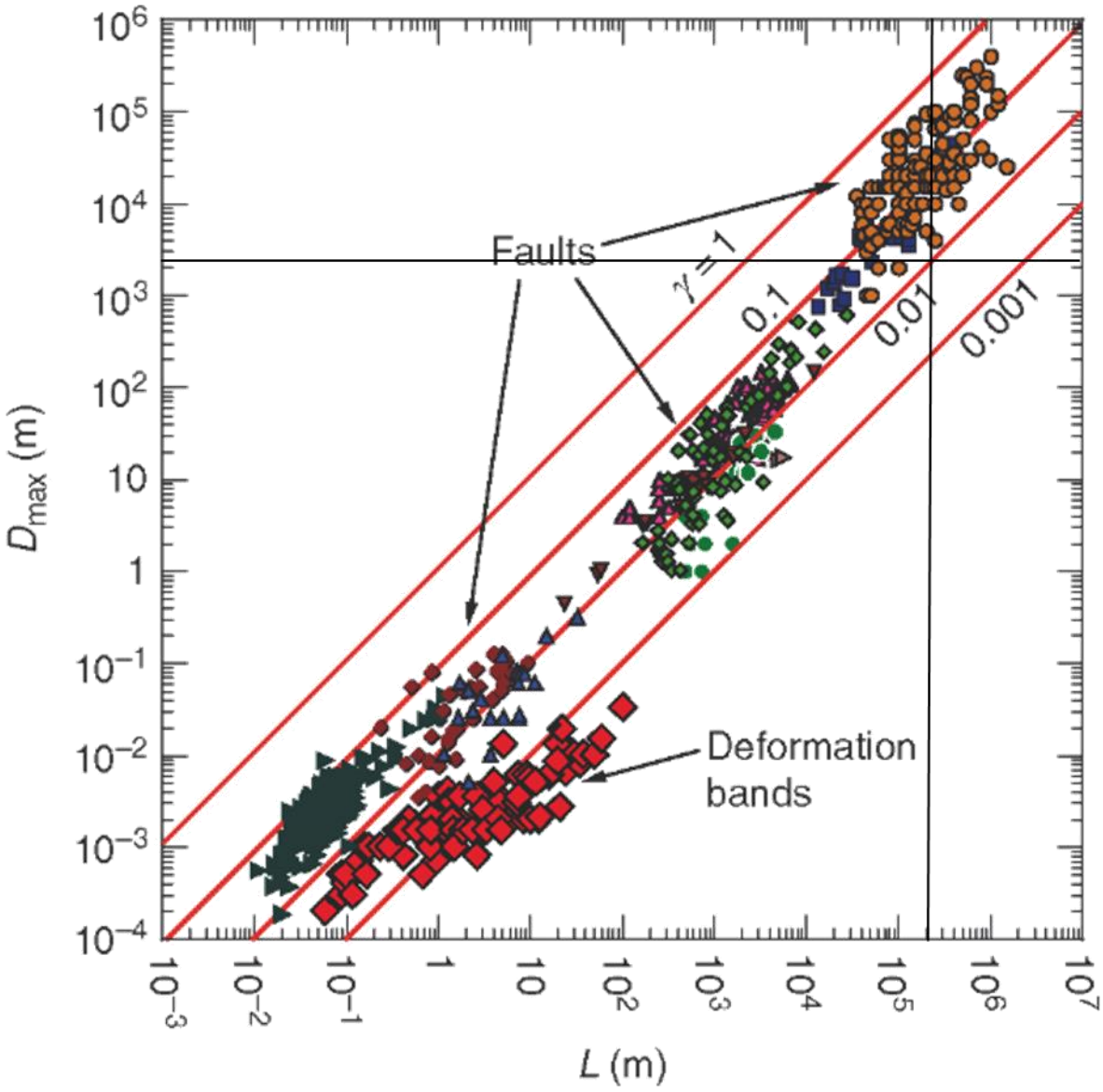

Figure 22: *Displacement vs length digram for studied fault populations with the expected length and displacement maximum plotted for the Northern Segment (indicated with a cross hair). Figure slightly modified from Fossen (2016).*

Table 2: *Possible single- and multisegment rupture scenarios*

Rupture Scenarios				
Fault Segment(s)	**Fault Area (km^2)**	**Magnitude (M_w)**	**Average Displacement (m)**	**Recurrence Interval (years)**
Southern	1944.7	7.46	2.95	29472
Central	796.3	6.94	1.03	25933 - 103732
Northern	1682.1	7.37	2.48	6218 - 49746
Northern + extension	2701.9	7.65	4.33	10824 - 86595
Southern and Central	2741.0	7.65	4.40	44031 - 440312
Central and Northern	2478.5	7.60	3.91	9785 - 391389
Southern, Central, and Northern	4423.1	7.93	7.71	19265 - 770582
Southern, Central, and Northern + extension	5443.0	8.05	9.82	24555 - 982217

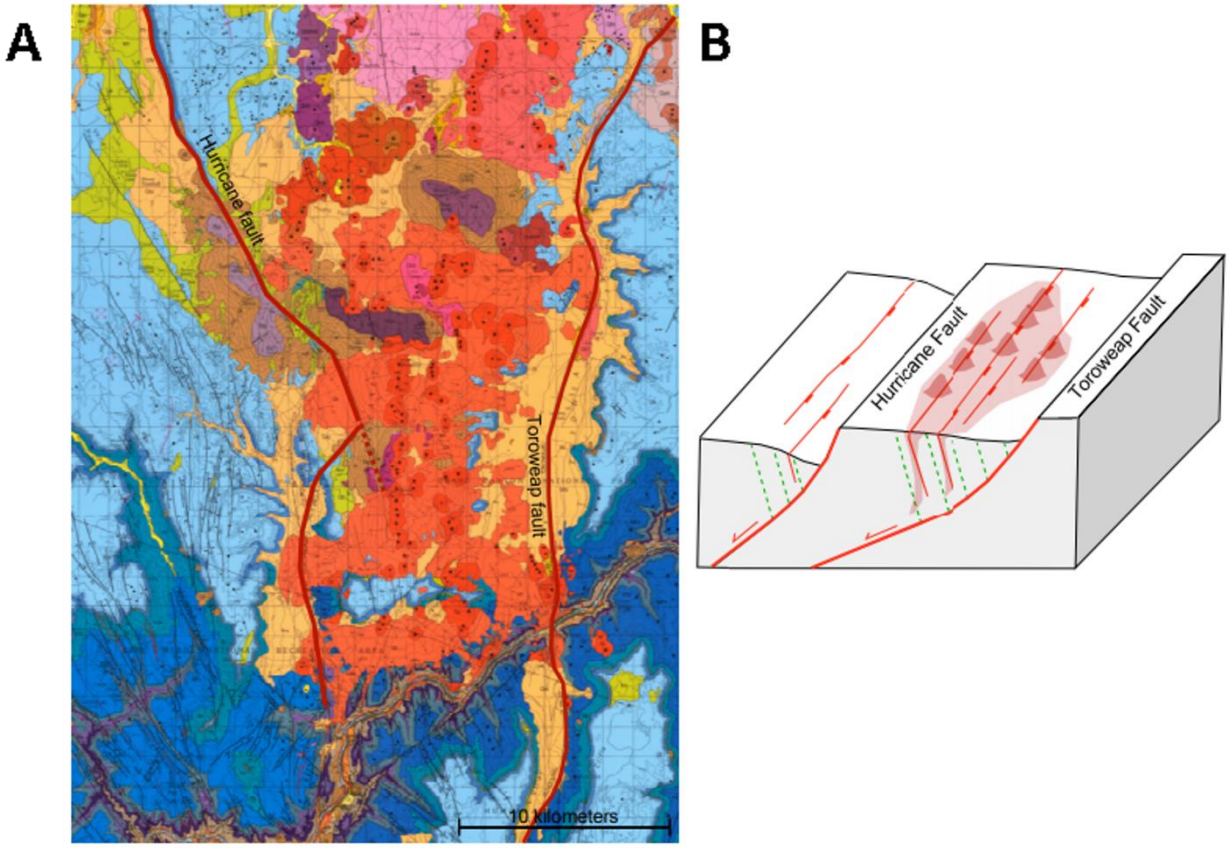

Figure 23: *A) Subsection of the Mt. Turnbull 30'-60' geologic map (Billingsley and Wellmeyer, 2003), with main traces of the Hurricane and Toroweap faults highlighted (dark red), and volcanic vents of the Uinkaret field denoted in black asterisks. B) Conceptual model linking fault-related folding strain in the hanging wall of non-planar normal faults (in the region of green dashed fold axes), associated second order faults (red lines), and volcanic conduits and aligned vents (translucent dark red).*

REFERENCES

Anderson, R. E., & Christenson, G. E. (1989). Quaternary faults, folds, and selected volcanic features in the Cedar City 1 x 2 quadrangle. *Utah: Utah Geological and Mineral Survey Miscellaneous Publication*, 89-6.

Anderson, L. P., & Dinter, D. A. (2010). Deformation and sedimentation in the southern Sevier foreland, Red Hills, southwestern Utah.

Anderson, J. J., & Rowley, P. D. (1975). Cenozoic stratigraphy of southwestern High Plateaus of Utah. *Cenozoic geology of southwestern high plateaus of Utah: Geological Society of America Special Paper*, *160*, 1-51.

Arabasz, W. J., & Julander, D. R. (1986). Geometry of seismically active faults and crustal deformation within the Basin and Range-Colorado Plateau transition in Utah. *Geological Society of America Special Paper*, *208*, 43-74.

Baars, D. L. (1962). Permian system of Colorado plateau. *AAPG Bulletin*, *46*(2), 149-218.

Barnett, J.A.M., Mortimer, J., Rippon, J.H., Walsh, J.J., & Watterson, J. (1987), Displacement geometry in the volume containing a single normal fault, *Bulletin of the American Association of Petroleum Geologists*, 71, p. 925-937.

Bazard, D. R., & Butler, R. F. (1991). Paleomagnetism of the Chinle and Kayenta Formations, New Mexico and Arizona. *Journal of Geophysical Research: Solid Earth*, *96*(B6), 9847-9871.

Best, M. G., Barr, D. L., Christiansen, E. H., Gromme, S., Deino, A. L., & Tingey, D. G. (2009). The Great Basin Altiplano during the middle Cenozoic ignimbrite flareup: Insights from volcanic rocks. *International Geology Review*, *51*(7-8), 589-633.

Best, M.G., & Brimhall, W.H., (1970). Late Cenozoic basalt types in the western Grand Canyon region, *in* Hamblin, W.K., and Best, M.G., eds., *The Western Grand Canyon District, Guidebook to the Geology of Utah*. Utah Geological Society, p. 57-74.

Best, M. G., & Christiansen, E. H. (1991). Limited extension during peak Tertiary volcanism, Great Basin of Nevada and Utah. *Journal of Geophysical Research: Solid Earth*, *96*(B8), 13509-13528.

Best, M. G., Christiansen, E. H., & Gromme, S. (2013). Introduction: The 36–18 Ma southern Great Basin, USA, ignimbrite province and flareup: Swarms of subduction-related supervolcanoes. *Geosphere*, *9*(2), 260-274.

Best, M. G., Christiansen, E. H., Deino, A. L., Grommé, C. S., McKee, E. H., Noble, D. C., ... & Zidek, J. (1989). Eocene through Miocene volcanism in the Great Basin of the western United States. *New Mexico Bureau of Mines and Mineral Resources Memoir*, *47*, 91-133.

Beus, S. S. (1989). Devonian and Mississippian geology of Arizona. *Geologic evolution of Arizona: Arizona Geological Society Digest*, *17*, 287-311.

Biasi, G. P., & Weldon, R. J. (2006). Estimating surface rupture length and magnitude of paleoearthquakes from point measurements of rupture displacement. *Bulletin of the Seismological Society of America*, *96*(5), 1612-1623.

Biek, R.F., 2013, Geologic Map of the George Mountain Quadrangle, Garfield and Kane Counties, Utah: Utah Geological Survey Map 262DM, 11 p., 2 plates, scale 1:24,000.

Biek, R. F., Moore, D. W., & Nealey, L. D. (2007). Interim geologic map of the Henrie Knolls quadrangle.*Garfield, Kane, and Iron Counties, Utah: Utah Geological Survey Open File Report*, *502*(2).Biek, R. F., Rowley, P. D., Hayden, J. M., Willis, G. C., Hintze, L. F., & Brown, K. D. (2010). *Geologic Map of the St. George and East Part of the Clover Mountains 30' X 60' Quadrangles, Washington and Iron Counties, Utah*. Utah Geological Survey.

Biek, R. F., Rowley, P. D., Anderson, J. J., Maldonado, F., Moore, D. W., Hacker, D. B., ... & Matyjasik, B. (2015). Geologic map of the Panguitch 30x 60quadrangle, Garfield, Iron, and Kane Counties, Utah: Utah Geological Survey Map 270DM, scale 1: 62,500, 170 p. booklet, 3 plates, online.

Biek, R. F., Rowley, P. D., Hayden, J. M., Willis, G. C., Hintze, L. F., & Brown, K. D. (2010). *Geologic Map of the St. George and East Part of the Clover Mountains 30′ X 60′ Quadrangles, Washington and Iron Counties, Utah*. Utah Geological Survey.

Billingsley, G. H. (1994).*Geologic Map of the Hat Knoll Quadrangle, Northern Mohave County, Arizona*. US Geological Survey.

Billingsley, G. H. (1997). Geologic map of the Mount Logan quadrangle, northern Mohave County. *Arizona: US Geological Survey Open-File Report*, 97-426.

Billingsley GH, Hampton HM (2000) Geologic map of the Grand Canyon 30' × 60' quadrangle, Coconino and Mohave counties, northwestern Arizona. US Geol Surv Geol Invest Ser Map I-2688

Billingsley, G. H., & Huntoon, P. W. (1983). Geologic map of Vulcan's Throne and vicinity, western Grand Canyon. *Arizona: Grand Canyon Natural History Association, Grand Canyon, Arizona, scale,1*(48,000).

Billingsley, G. H., & Priest, S. S. (2003). *Geologic Map of Upper Clayhole Valley and Vicinity, Mohave County, Northwestern Arizona*. US Geological Survey.

Billingsley, G. H., Priest, S. S., & Felger, T. J. (2004).Geologic Map of Pipe Spring National Monument and the Western Kaibab-Paiute Indian Reservation, Mohave County, Arizona. US Department of the Interior, US Geological Survey.

Billingsley, G. H., Wenrich, K. J., & Huntoon, P. W. (2000). *Breccia-pipe and Geologic Map of the Southeastern Part of the Hualapai Indian Reservation and Vicinity, Arizona*. The Survey.

Billingsley, G. H., & Workman, J. B. (2000).*Geologic Map of the Littlefield 30′ X 60′ Quadrangle, Mohave County, Northwestern Arizona* (p. 25). US Geological Survey.

Billingsley, G. H., & Wellmeyer, J. L. (2003).*Geologic Map of the Mount Trumbull 30'X 60'Quadrangle, Mohave and Coconino Counties, Northwestern Arizona* (No. 2766). US Geological Survey.

Billingsley, G. H., Block, D. L., & Dyer, H. C. (2006a). Geologic Map of the Peach Springs 30′ X 60′ Quadrangle, Mohave and Coconino Counties, Northwestern Arizona.

Billingsley GH, Felger TJ, Priest SS (2006b) Geologic map of the Valle 30′ × 60′ quadrangle, Coconino County, northern Arizona. US Geol Surv Sci Invest Map SIM-2895

Billingsley, G. H., Hamblin, W. K., Wellmeyer, J. L., & Dudash, S. L. (2001). Geologic map of part of the Uinkaret volcanic field, Mohave County, Northwestern Arizona. *US Geol. Surv. Misc. Invest. Ser. Map MF-2368*, 25.

Billingsley, G. H., Priest, S. S., & Felger, T. J. (2008). *Geologic Map of the Fredonia 30'X 60'quadrangle, Mohave and Coconino Counties, Northern Arizona*. USGS.

Bird, P. (1979). Continental delamination and the Colorado Plateau. *Journal of Geophysical Research: Solid Earth*, *84*(B13), 7561-7571.

Black, B. D., Hecker, S., Hylland, M. D., Christenson, G. E., & McDonald, G. N. (2003). Quaternary fault and fold database and map of Utah: Utah Geological Survey Map 193DM, scale 1: 50,000.

Blakey, R. C. (1988). Basin tectonics and erg response. *Sedimentary Geology*, *56*(1-4), 127-151.

Blakey, R. C. (1990). Stratigraphy and geologic history of Pennsylvanian and Permian rocks, Mogollon Rim region, central Arizona and vicinity. *Geological Society of America Bulletin*, *102*(9), 1189-1217.

Blakey, R. C., Jenney, J. P., & Reynolds, S. J. (1989). Triassic and Jurassic geology of the southern Colorado Plateau. *Geologic evolution of Arizona: Arizona Geological Society Digest*, *17*, 369-396.

Blakey, R. C., & Middleton, L. T. (2012). Geologic history and paleogeography of Paleozoic and early Mesozoic sedimentary rocks, eastern Grand Canyon, Arizona. *Spec. Pap., Geol. Soc. Am*, *489*, 81-92.

Blakey, R. C., & Ranney, W. (2008). *Ancient landscapes of the Colorado Plateau*. Grand Canyon Assn.

Bonilla, M.G., (1988), Minimum earthquake magnitude associated with coseismic surface faulting, *Bulletin of the Association of Engineering Geologists* 25(1), 17-29.

Bump, A.P., Davis, G.H. (2003). Late Cretaceous-early Tertiary Laramide deformation of the northern Colorado Plateau, Utah and Colorado. *Journal of Structural geology* 25(3), 421-440.

Brumbaugh, D. S. (2008). Seismicity and tectonics of the Blue Ridge area of the Mogollon plateau, Arizona. *Bulletin of the Seismological Society of America*, *98*(3), 1527-1534.

Cashion, W. B. (1961). *Geology and fuels resources of the Orderville-Glendale area, Kane County, Utah* (No. 49).

Casey, M. C. D. R. F. G., Ebinger, C., Keir, D., Gloaguen, R., & Mohamed, F. (2006). Strain accommodation in transitional rifts: Extension by magma intrusion and faulting in Ethiopian rift magmatic segments. *Geological Society, London, Special Publications*, *259*(1), 143-163.

Christie-Blick, N., Anders, M.H., Wills, S., Walker, C.D., & Renik, B. (2007). Observations from the Basin and Range Province (western United States) pertinent to the interpretation of regional detachment faults. *Geological Society of London Special Publications* 282, p. 421-441.

Clemmensen, L. B., Olsen, H., & Blakey, R. C. (1989). Erg-margin deposits in the Lower Jurassic Moenave Formation and Wingate Sandstone, southern Utah. *Geological Society of America Bulletin*, *101*(6), 759-773.

Darton, N. H. (1910). *A reconnaissance of parts of northwestern New Mexico and northern Arizona* (No. 435). US Government Printing Office.

Connors, C. D., Hughes, A. N., & Ball, S. M. (2021). Forward kinematic modeling of fault-bend folding. *Journal of Structural Geology*, *143*, 104252.

Davis, G.H. (1978), Monocline fold pattern of the Colorado Plateau, in Matthews, V. (ed.) *Laramide Folding Associated with Basement Block Faulting in the Western United States,* GSA Memoir 151, p. 215-234.

Davis, G. H. (1999). *Structural geology of the Colorado Plateau region of southern Utah, with special emphasis on deformation bands* (Vol. 342). Geological Society of America.

DeCelles, P. G. (2004). Late Jurassic to Eocene evolution of the Cordilleran thrust belt and foreland basin system, western USA. *American Journal of Science*, *304*(2), 105-168.

Dickinson, W. R. (2006). Geotectonic evolution of the Great Basin. *Geosphere*, *2*(7), 353-368.

Dickinson, W.R. & Snyder, W.S., (1978), Plate tectonics of the Laramide orogeny, in Matthews, V. (ed.) *Laramide Folding Associated with Basement Block Faulting in the Western United States,* GSA Memoir 151, p. 355-366.

Doelling, H. H. (1975). Geology and mineral resources of Garfield County, Utah. *Utah Geol. Mineral. Surv., Bull.;(United States)*, *107*.

Doelling, H. H. (2008). Geologic map of the Kanab 30'x 60'quadrangle. *Kane and Washington counties, Utah, and Coconino and Mohave counties, Arizona: Utah Geological Survey Miscellaneous Publications*.

Doelling, H. H., Davis, F. D., & Brandt, C. J. (1989).*The geology of Kane County, Utah: Geology, mineral resources, geologic hazards* (Vol. 124). Utah Geological Survey.

Doelling, H. H., Sprinkel, D. A., Kowallis, B. J., & Kuehne, P. A. (2013). Temple Cap and Carmel Formations in the Henry Mountains Basin, Wayne and Garfield Counties, Utah. *The San Rafael Swell and Henry Mountains Basin—geologic centerpiece of Utah: Utah Geological Association Publication*, *42*, 279-318.

Doelling, H.H., Willis, G.C., Solomon, B.J., Sable, E.G., Hamilton, W.L., and Naylor, L.P., II, 2002, Interim geologic map of the Springdale East quadrangle, Washington County, Utah: Utah Geological Survey Open-File Report 393, 20 p., scale 1:24,000.

Dula, W.F. (1991), Geometric models of listric normal faults and rollover folds, *American Association of Petroleum Geologists Bulletin* 75(10), 1609-1625.

DuRoss, C.B., & Hylland, M.D., (2015). Synchronous ruptures along a major graben-forming fault system: Wasatch and West Valley fault zones, Utah. *Bulletin of the Seismological Society of America* 105(1), 14-37.

DuRoss, C.B., Personius, S.F., Crone, A.J., Olig, S.S., Hylland, M.D., Lund, W.R., & Schwartz, D.P. (2016). Fault segmentation: New concepts from the Wasatch fault zone, Utah, USA. *Journal of Geophysical Research: Solid Earth* 121(2), 1131-1157.

Dutton, C.E., (1882). Tertiary history of the Grand Canyon district. *U.S. Geological Survey Monograph* 2, 264 p.

Eaton, J. G., Kirkland, J. I., Gustason, E. R., Nations, J. D., Franczyk, K. J., Ryer, T. A., & Carr, D. A. (1987). Stratigraphy, correlation, and tectonic setting of Late Cretaceous rocks in the Kaiparowits and Black Mesa basins. In *Geologic Diversity of Arizona and its Margins: Excursions to Choice Areas. Geological Society of America 100th Annual Meeting Field-Trip Guidebook and Arizona Bureau of Geology and Mineral Technology Special Paper* (Vol. 5, pp. 113-125).

Eichelberger, N.W., Nunns, A., Perez, N.D., Ball, S., Claroni, D.J., & He, D., (2018). Incorporating simple erosion into structural forward models: The effects of regional erosion on growth strata geometry, *Journal of Structural Geology* 116, 146-158.

Evans, T. (1971). *A stratigraphic study of the Toroweap Formation (Permian) between Sycamore and Oak Creek Canyons, Arizona: Univ. Ariz., Tucson* (Doctoral dissertation, MS thesis, 111 p).

Ferrill, D.A., Morris, A.P., (2001). Displacement gradient and deformation in normal fault systems. *Journal of Structural geology,* 23(4), 619-638.

Fossen, H. (2016). *Structural geology*. Cambridge University Press.

Gilbert, C. M., & Reynolds, M. W. (1973). Character and chronology of basin development, western margin of the Basin and Range province. *Geological Society of America Bulletin*, *84*(8), 2489-2510.

Goldstrand, P. M. (1990). *Stratigraphy and paleogeography of Late Cretaceous and Paleogene rocks of southwest Utah* (p. 58). Utah Geological and Mineral Survey.

Gregory, H. E. (1950). *Geology and geography of the Zion Park region, Utah and Arizona* (No. 220).

Gregory, H. E. (1951). *The geology and geography of the Paunsaugunt region, Utah* (No. 226).

Groshong Jr., R.H., (1994). Area balance, depth to detachment, and strain in extension. *Tectonics* 13(6), 1488-1497.

Haller, K.M., Mochetti, M.P., Mueller, C.S., Rezaeian, S., Petersen, M.D., & Zeng, Y. (2015). Seismic hazard in the Intermountain West. *Earthquake Spectra*, 31, S149-176.

Hamblin, W. K. (1984). Direction of absolute movement along the boundary faults of the Basin and Range–Colorado Plateau margin. *Geology*, *12*(2), 116-119.

Hammond, B. J. (1991). Geologic map of the Jarvis Peak quadrangle. *Washington County, Utah: Utah Geological Survey Open-File Report*, *212*, 63.

Hanks, T. C., & Bakun, W. H. (2008). M-log A observations for recent large earthquakes. *Bulletin of the seismological society of America*, *98*(1), 490-494.

Hawkins, D. P., Bowring, S. A., Ilg, B. R., Karlstrom, K. E., & Williams, M. L. (1996). U-Pb geochronologic constraints on the Paleoproterozoic crustal evolution of the Upper Granite Gorge, Grand Canyon, Arizona. *Geological Society of America Bulletin*, *108*(9), 1167-1181.

Hayden, J. M. (2008). *Interim Geologic Map of the Mount Carmel Quadrangle, Kane County, Utah*. Utah Geological Survey.

Hayden, J. M. (2011).*Geologic Map of the Kanab 7.5 ' Quadrangle, Kane County, Utah and Coconino and Mohave Counties, Arizona*. Utah Geological Survey.

Hayden, J.M. (2013). Geologic Map of the Yellowjacket Canyon Quadrangle, Kane County, Utah, and Mohave County, Arizona: Utah Geological Survey, Map 256DM, doi: 10.1029/2007JB005278.

Heath, B. A., Hooft, E. E. E., Toomey, D. R., Paulatto, M., Papazachos, C. B., Nomikou, P., & Morgan, J. V. (2021). Relationship Between Active Faulting/Fracturing and Magmatism Around Santorini: Seismic Anisotropy from an Active Source Tomography Experiment. *Journal of Geophysical Research: Solid Earth*, e2021JB021898.

Hecker, S. (1993). *Quaternary tectonics of Utah with emphasis on earthquake-hazard characterization* (No. 127). Utah Geological Survey.

Heckert, A. B., & Lucas, S. G. (Eds.). (2005). *Vertebrate Paleontology in Arizona: Bulletin 29* (Vol. 29). New Mexico Museum of Natural History and Science.
Henry, C.D. (2008). Ash-flow tuffs and paleovalleys in northeastern Nevada: Implications for Eocene paleogeography and extension in the Sevier hinterland, northern Great Basin, *Geosphere* 4(1), 1-35.
Hopkins RL, Thompson KL. 2003. Kaibab Formation. In: Beus SS, Morales M, editors. Grand Canyon geology. Oxford: Oxford University Press. p. 196–211.
Hough, S. E., & Hutton, K. (2008). Revisiting the 1872 Owens Valley, California, earthquake. *Bulletin of the Seismological Society of America*, *98*(2), 931-949.
Huntoon, P. W. (1993). Influence of inherited Precambrian basement structure on the localization and form of Laramide monoclines, Grand Canyon, Arizona. *Geological Society of America Special Papers*, *280*, 243-256.
Huntoon, P. W., Beus, S. S., & Morales, M. (2003). Post-Precambrian tectonism in the Grand Canyon region. *Grand Canyon Geology*, 222-259.
Hylland, M. D. (2010). Geologic map of the Clear Creek Mountain quadrangle, Kane County, Utah. *Utah Geological Survey Map*, *245*.
Ilg, B. R., Karlstrom, K. E., Hawkins, D. P., & Williams, M. L. (1996). Tectonic evolution of Paleoproterozoic rocks in the Grand Canyon: Insights into middle-crustal processes. *Geological Society of America Bulletin*, *108*(9), 1149-1166.
Jackson, G. W. (1990). Tectonic geomorphology of the Toroweap fault, western Grand Canyon, Arizona: Karlstrom, K. E., Crow, R. S., Peters, L., McIntosh, W., Raucci, J., Crossey, L. J., ... & Dunbar, N. (2007). 40Ar/39Ar and field studies of Quaternary basalts in Grand Canyon and model for carving Grand Canyon: Quantifying the interaction of river incision and normal faulting across the western edge of the Colorado Plateau. *Geological Society of America Bulletin*, *119*(11-12), 1283-1312.implications for transgression of faulting on the Colorado Plateau.
Karlstrom, K. E., Crow, R. S., Peters, L., McIntosh, W., Raucci, J., Crossey, L. J., ... & Dunbar, N. (2007). 40Ar/39Ar and field studies of Quaternary basalts in Grand Canyon and model for carving Grand Canyon: Quantifying the interaction of river incision and normal faulting across the western edge of the Colorado Plateau. *Geological Society of America Bulletin*, *119*(11-12), 1283-1312.
Karlstrom, K. E., Mohr, M. T., Schmitz, M. D., Sundberg, F. A., Rowland, S. M., Blakey, R., ... & Hagadorn, J. W. (2020). Redefining the Tonto Group of Grand Canyon and recalibrating the Cambrian time scale. *Geology*, *48*(5), 425-430.
Karlstrom, T. N., Swann, G. A., & Eastwood, R. L. (1974). Geology of Northern Arizona: With Notes on Archaeology and Paleoclimate.
Kleber, E. J., McKean, A.P., Hiscock, A.I., Hylland, M.D., Hardwick, C.L., McDonald, G.N., …& Erickson, B.A., (2021). Geologic setting, ground effects and proposed structural model for the 18 March 2020 Mw 5.7 Magna, Utah, earthquake, *Seismological Society of America* 92(2A), 710-724.
Kokkalas, S., & Aydin, A. (2013). Is there a link between faulting and magmatism in the south-central Aegean Sea?. *Geological Magazine*, *150*(2), 193-224.
Koons, E.D., (1945), Geology of the Uinkaret Plateau, northern Arizona, *Geological Society of America Bulletin* 56, 151-180.
Kreemer, C., Hammond, W.C., Blewitt, G., Holland, A.A., Bennett, R.A. (2012), *A geodetic strain rate model for the Pacific-North American plate boundary, western United States*, Nevada Bureau of Mines and Geology Map 178.
Kruger, J.M., Johnson, R.A., Houser, B.B., (1995). Miocene-Pliocene half-graben evolution, detachment faulting and late-stage core complex uplift from reflection seismic data in south-east Arizona, *Basin Research* 7(2), 129-149.
Kurlich III, R. A., & Anderson, J. J. (1997). Geologic map of the Hatch quadrangle. *Garfield County, Utah: Utah Geological Survey Miscellaneous Publications*, 97-5.

Levander, A., Schmandt, B., Miller, M.S., Liu, K., Karlstrom, K.E., Crow, R.S.,…& Humphreys, E.D. (2011). Continuing Colorado plateau uplift by delamination-style convective lithospheric downwelling. *Nature*, 472, 461-465.

Lund, W. R., Knudsen, T. R., & Vice, G. S. (2008). *Paleoseismic reconnaissance of the Sevier fault, Kane and Garfield counties, Utah* (Vol. 122). Utah Geological Survey.

Lundin, E. R. (1989). Thrusting of the Claron formation, the Bryce canyon region, Utah. *Geological Society of America Bulletin*, *101*(8), 1038-1050.

Machette, M.N., Personius, S.F., Nelson, A.R., Schwartz, D.P., & Lund, W.R., (1991). The Wasatch fault zone, Utah—Segmentation and history of Holocene earthquakes. *Journal of Structural Geology* 13(2), 137-149.

MacLeod, N. S., & Sherrod, D. R. (1988). Geologic evidence for a magma chamber beneath Newberry Volcano, Oregon. *Journal of Geophysical Research: Solid Earth*, *93*(B9), 10067-10079.

Mauduit, T., & Brun, J.P., (1998). Growth fault/rollover systems: Birth, growth, and decay. *Journal of Geosphysical Research* 103, 18119-18136.

McClay, K.R., (1990), Extensional fault systems in sedimentary basins: a review of analogue model studies, *Marine and Petroleum Geology* 7(3), 206-233.

McKee, E. D. (1938). The Environment and history of the Toroweap and Kaibab formations on northern Arizona and southern Utah: Publication/Carnegie Institution of Washington.

McKee, E. D. (1954). *Stratigraphy and history of the Moenkopi Formation of Triassic age* (Vol. 61). Geological Society of America.

McKee, E. D. (1982). *The Supai Group of Grand Canyon* (Vol. 1173). US Department of the Interior, Geological Survey.

McKee, E. D., & Resser, C. E. (1945). *Cambrian history of the Grand Canyon region* (Vol. 563). Carnegie Institution.

McKee, E.D., & Schenk, E. T. (1942) The Lower Canyon lavas and related features at Toroweap in Grand Canyon, Jour. Geomorph., vol. 5, p. 243-273.

Merle, O.R., Davis, G.H., Nickelsen, R.P., & Courlay, P.A. (1993). Relation of thin-skinned thrusting to Colorado Plateau strata in southwestern Utah to Cenozoic magmatism, *Geological Society of America Bulletin* 105(3), 387-398.

Metzger, D. G. (1961). *Geology in Relation to Availability of Water Along the South Rim Grand Canyon National Park, Arizona* (pp. 105-138). US Government Printing Office.

Milligan, M. (2012). Sizing up titans-Navajo erg vs. Sahara ergs. *Which was the larger sand box*, 8-9.

Morgan, P., & Swanberg, C. A. (1985). On the Cenozoic uplift and tectonic stability of the Colorado Plateau. *Journal of Geodynamics*, *3*(1-2), 39-63.

Morris, R. H. (1957). *Photogeologic map of the Fredonia NE quadrangle, Coconino and Mohave Counties, Arizona* (No. 247).

Muirhead, J. D., Kattenhorn, S. A., & Le Corvec, N. (2015). Varying styles of magmatic strain accommodation across the E ast A frican R ift. *Geochemistry, Geophysics, Geosystems*, *16*(8), 2775-2795.

Munger, R. D., Greene, J., Peace, F. S., & Liming, J. A. (1965). Pre-Pennsylvanian stratigraphy of the Kaiparowits region, south-central Utah and north-central Arizona.

Murray, K.E., Reiners, P.W., Thomson, S.N. (2016). Rapic Plioene-Pleistocene erosion of the central Colorado Plateau documented by apatite thermochronology from the Henry Mountains, *Geology* 44(6), 483-486.

Noble, L. F. (1923). *A section of the Paleozoic formations of the Grand Canyon at the Bass Trail* (No. 131-B, pp. 23-73).

Norton, A. K. (1990). *Depositional environments, diagenesis, and stratigraphic relationship of the Kaibab and San Andres Formations (Permian) of Navajo and Apache Counties, Arizona* (Doctoral dissertation, Northern Arizona University).

Parsons, T., & Thompson, G. A. (1991). The role of magma overpressure in suppressing earthquakes and topography: Worldwide examples. *Science*, *253*(5026), 1399-1402.

Peacock, D.C.P., & Sanderson, D.J., 1991. Displacements, segment linkage, and relay ramps in normal fault zones, *Journal of Structural Geology*, 13, p. 721-733.
Peacock, D.C.P., & Sanderson, D.J., 1994. Geometry and development of relay ramps in normal fault systems, *American Association of Petroleum Geologists Bulletin*, 78, p. 147-165.
Pearthree, P. A. (1998). Quaternary fault data and map for Arizona.
Reber, S., Taylor, W. J., Stewart, M., & Schiefelbein, I. M. (2001). Linkage and reactivation along the northern Hurricane and Sevier faults, southwestern Utah.
Reiche, P. (1938). An analysis of cross-lamination the Coconino Sandstone. *The Journal of Geology*, *46*(7), 905-932.
Ruch, J., Acocella, V., Storti, F., Neri, M., Pepe, S., Solaro, G., & Sansosti, E., (2010) Detachment depth revealed by rollover deformation: An integrated approach at Mount Etna, *Geophysical Research Letters* 37(16).
Rowley, P.D., Cunningham, C.G., Steven, T.A., Workman, J.B., Anderson, J.J., & Theissen, K.M., (2002), Geologic map of the Central Marysvale Volcanic Field, Southwestern Utah, *Geologic Investigation Series Map* I-2645-A, U.S. Geological Survey.
Sable, E.G., 1995, Geologic map of the Hildale quadrangle, Washington and Kane Counties, Utah, and Mohave County, Arizona: Utah Geological Survey Map 167, 14 p., 2 plates, scale 1:24,000.
Sable, E. G., & Doelling, H. H. (1993). Geologic map of the Barracks quadrangle. *Kane County, Utah: Utah Geological Survey Map*, *147*(11).
Sable, E. G., & Hereford, R. (2004). *Geologic map of the Kanab 30'x 60'quadrangle, Utah and Arizona* (No. 2655).
Sanjuan, J., Eaton, J. G., Rafferty, K. C., & Biek, R. F. (2017). Charophyte flora from the Brian Head Formation, southwestern Utah, and its biostratigraphic implications. *Micropaleontology*, *63*(1), 1-14.
Schiefelbein, I. M. (2002). Fault segmentation, fault linkage, and hazards along the Sevier fault, southwestern Utah.
Schultz, R. A., Soliva, R., Fossen, H., Okubo, C. H., & Reeves, D. M. (2008). Dependence of displacement–length scaling relations for fractures and deformation bands on the volumetric changes across them. *Journal of Structural Geology*, *30*(11), 1405-1411.
Shaw, J.H., Hook, S.C., & Sitohang, E.P., (1997). Extensional fault-bend folding and synrift deposition: An example from the Central Sumatra Basin, Indonesia. *American Association of Petroleum Geologists Bulletin* 81(3), 367-379.
Sieh, K., Jones, L., Hauksson, E., Hudnut, K., Eberhart-Phillips, D., Heaton, T., Hough, S., Hutton, K., Kanamori, H., Lilje, A., & Lindvall, S., (1993). Near-field investigations of the Landers earthquake sequence, April to July 1992. *Science*, 260(5105), 171-176.
Siler, D.L., Faulds, J.E., Hinz, N.H., Dering, G.M., Edwards, J.H., & Mayhew, B., (2019). Three-dimensional geologic mapping to assess geothermal potential: examples from Nevada and Oregon. *Geothermal Energy* 7(1), 1-32.
Smith, R.B., & Sbar, M.L. (1974). Contemporary Tectonics and seismicity of the western United States with emphasis on the Intermountain Seismic Belt, *Geological Society of America Bulletin* 85(8), 1205-1218.
Steven, T. A., Morris, H. T., & Rowley, P. D. (1990). *Geologic map of the Richfield 1 degree by 2 degrees Quadrangle, west-central Utah* (No. 1901).
Steven, T. A., Rowley, P. D., & Cunningham, C. G. (1984). Calderas of the Marysvale volcanic field, west central Utah. *Journal of Geophysical Research: Solid Earth*, *89*(B10), 8751-8764.
Stewart, J. H., Poole, F. G., Wilson, R. F., Cadigan, R. A., Thordarson, W., & Albee, H. F. (1972). *Stratigraphy and origin of the Chinle Formation and related Upper Triassic strata in the Colorado Plateau region* (No. 690). Geological Survey (US).
Suter, M. (2015). The ad 1567 M w 7.2 Ameca, Jalisco, Earthquake (Western Trans-Mexican Volcanic Belt): Surface Rupture Parameters, Seismogeological Effects, and Macroseismic Intensities from Historical Sources. *Bulletin of the Seismological Society of America*, *105*(2A), 646-656.

Taylor, W. J. (1993). *Stratigraphic and lithologic analysis of the Claron Formation in southwestern Utah* (Vol. 93, No. 1). Utah Geological Survey.

Taylor, W. J., Stewart, M. E., & Orndorff, R. L. (2001). Fault segmentation and linkage: Examples from the Hurricane fault, Southwestern USA.

Tilton, T. L., & Sable, E. G. (2001). *Geologic Map of the Alton Quadrangle, Kane County, Utah*. Utah Geological Survey.

Tindall, S.E., & Davis, G.H. (1999). Monocline development by oblique-slip fault-propagation folding: the East Kaibab monocline, Colorado Plateau, Utah, *Journal of Structural Geology* 21(10), p. 1303-1320.

Thompson Jobe, J.A., Philibosian, B., Chupik, C., Dawson, T.K., Benett, S.E., Gold, R., …& Seitz, G., (2020). Evidence of previous earthquake faulting along the 2019 Ridgecrest, California earthquake ruptures, *Bulletin of the Seismological Society of America* 110(4), 1427-1456.

Thorman, C. H., & Peterson, F. (2003, May). The Middle Jurassic Elko orogeny: a major tectonic event in Nevada-Utah. In *Annual Meeting Expanded Abstracts* (Vol. 12, pp. 169-174). Tulsa, Okla.: Am. Assoc. of Pet. Geol..

Valentine, G. A., & Krogh, K. E. (2006). Emplacement of shallow dikes and sills beneath a small basaltic volcanic center–The role of pre-existing structure (Paiute Ridge, southern Nevada, USA). *Earth and Planetary Science Letters*, *246*(3-4), 217-230.

Valentini, A., DuRoss, C.B., Field, E.H., Gold, R.D., Briggs, R.W., Visini, F., & Pace, B., (2020). Relaxing segmentation on the Wasatch fault zone: Impact on seismic hazard. *Bulletin of the Seismological Society of America* 110(1), 83-109.

Velasco, M.S., Bennett, R.A., Johnson, R.A., & Hreinsdottir, S. (2010). Subsurfae fault geometries and crustal extension in the eastern Basin and Range Province, western US. *Tectonophysics*, 488(1-4), 131-142.

Walsh, J. J., & Watterson, J. (1987). Distributions of cumulative displacement and seismic slip on a single normal fault surface. *Journal of Structural Geology*, *9*(8), 1039-1046.

Weaver, C. S., Grant, W. C., & Shemeta, J. E. (1987). Local crustal extension at Mount St. Helens, Washington. *Journal of Geophysical Research: Solid Earth*, *92*(B10), 10170-10178.

West, M.B. (1992). An integrated model for seismogenesis in the Intermountain Seismic Belt, *Bulletin of the Seismological Society of America*, 82(3), p. 1350-1372.

Wells, D., & Youngs, B. (2013). Updated empirical relationships among magnitude, rupture area, rupture length, and surface displacement. *Seismol. Res. Lett.*, *84*, 309.

Wells, D.L., & Coppersmith, K.J. (1994), New empirical relationships among magnitude, rupture length, rupture width, rupture area, and surface displacement, *Bulletin of the Seismological Society of America* 84(4), 974-1002.

Wenrich, K. J., Billingsley, G. H., & Huntoon, P. W. (1996). *Breccia-Pipe and Geologic Map of the Northwestern Part of the Hualapai Indian Reservation and Vicinity, Arizona*. US Geological Survey.

Willis, G. C., Doelling, H. H., Solomon, B. J., & Sable, E. G. (2002). Interim geologic map of the Springdale West quadrangle. *Washington County, Utah: Utah Geological Survey Open-File Report*, *394*, 20.

Xiao, H., & Suppe, J. (1992). Origin of rollover (1). *AAPG bulletin*, *76*(4), 509-529.

Xu, S. S., Nieto-Samaniego, A. F., Alaniz-Álvarez, S. A., & Velasquillo-Martinez, L. G. (2006). Effect of sampling and linkage on fault length and length–displacement relationship. *International Journal of Earth Sciences*, *95*(5), 841-853.

Young, R. A., & Brennan, W. J. (1974). Peach Springs Tuff: Its bearing on structural evolution of the Colorado Plateau and development of Cenozoic drainage in Mohave County, Arizona. *Geological Society of America Bulletin*, *85*(1), 83-90.